Modeling and Control of Brushless Doubly-fed Bar Cage Induction Machines

by

Tainton Hutton

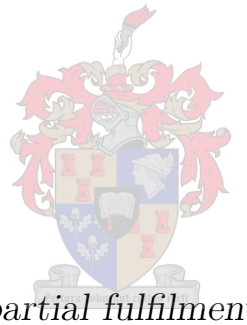

Thesis presented in partial fulfilment of the requirements for the degree of Master of Engineering (Electrical) in the Faculty of Engineering at Stellenbosch University

Supervisor: Dr. N. Gule

April 2022

Stellenbosch University https://scholar.sun.ac.za

Declaration

By submitting this thesis electronically, I declare that the entirety of the work contained therein is my own, original work, that I am the sole author thereof (save to the extent explicitly otherwise stated), that reproduction and publication thereof by Stellenbosch University will not infringe any third party rights and that I have not previously in its entirety or in part submitted it for obtaining any qualification.

Date: .....April 2022.....

Copyright © 2022 Stellenbosch University
All rights reserved.

Stellenbosch University https://scholar.sun.ac.za

Abstract

Modeling and Control of Brushless Doubly-fed Bar Cage Induction Machines

T. Hutton

Department of Electrical and Electronic Engineering,
University of Stellenbosch,
Private Bag X1, Matieland 7602, South Africa.

Thesis: MEng (Electrical)

April 2022

In recent years the requirement for more sustainable sources of energy has increased significantly, with wind energy growing increasingly as a renewable source. Many countries are investing greatly in sustainable growth by going completely renewable. Countries like Iceland had an annual consumption of 60.8 TWh in 2019, of which 79% was produced by renewable energy sources. For this growth to be sustainable, more efficient and economic sources of renewable energy will be required. The Brushless Doubly Fed Induction Generator (BDFIG) has become a focus point due to its variable speed capability and brushless technology.

The direct-current-link (DC-link voltage) in the BDFIG systems' back to back converter allow for bidirectional power flow of the control winding's power. Making effective control of the DC-link voltage a necessity. Due to the presence of switching elements in the back-to-back converter, there are harmonics introduced into the utility network. To mitigate this low pass filters such as inductance capacitance (LCL) and resistive inductive (RL) filters are often used.

Currently, BDFIGs are not used in sizable wind farms. This is mostly due to their complexity when compared to standard doubly fed induction generators (DFIG's) and permanent magnet synchronous generators (PMSGs). Thus far they have mostly been used in islanding applications. In this mode of operation they must be controlled to provide stable voltages at constant frequency with varying load conditions and changing wind speeds. To compete with DFIG's which are already in the market, the BDFIG has a few disadvantages due to its slightly more complex structure, higher cost and larger dimensions.

In this thesis, the power control of the grid-connected BDFIG systems in wind turbine applications are presented. Additionally the control of these machines as motors are also investigated and performed. An experimental machine consisting of a bar cage rotor is modeled in detail and controlled in simulation and by experimentation. DC-link voltage control is analyzed whereby the grid-side converter is controlled as a voltage source converter. Vector control is used in all control solutions, with reductions in control complexity made and analyzed for the control winding side of the machine to reduce cost and improve robustness while maintaining responsiveness and accuracy.

Stellenbosch University https://scholar.sun.ac.za

Uittreksel

Modellering en beheer van Borsellose Dubbel-gevoerde koper-staalhok induksie masjien

("Modeling and Control of Brushless Doubly-fed Bar Cage Induction Machines")

T. Hutton

Departement Elektries en Elektroniese Ingenieurswese,
Universiteit van Stellenbosch,
Privaatsak X1, Matieland 7602, Suid Afrika.

Tesis: MIng (Electrical)

April 2022

In die laaste paar jaar het die aanvraag vir meer volhoubare energiebronne aansienlik toegeneem, veral wanneer daar gekyk word na wind energie as energiebron. Baie lande is al klaar besig om grootliks in hernubare energie te belê. Ysland, byvoorbeeld, het 'n jaarlikse verbruik van 60.8 TWh in 2019 gehad, waarvan 79% van die energie geproduseer was deur hernubare bronne. Vir die groei om volhoubaar te wees word meer effektiewe en ekonomiese hernubare energiebronne benodig. Die Brusellose Dubbel Gevoerde Induksie Generator (BDGIG) het, as gevolg van die masjien se veranderlike spoed vermoë en brusellose tegnologie, n fokus punt in die navorsingsveld geword. Die direkte stroom (DS) skakel spanning in die BDGIG sisteme se rug-aan-rug omskakelaar laat tweerigting krag vloei van die beheer winding se krag toe. Dus is effektiewe beheer van die DS-skakel se spanning nodig. As gevolg van die wisselings elemente wat in rug-aan-rug omskakelaars voorkom, kan daar harmonieke in die krag netwerk geïnduseer word. Om hierdie te versag word laag deurlaat filters, soos LCL en RL filters, gereeld gebruik. Tans word BDGIG nie op groot wind plase gebruik nie. Dit is meestal as gevolg van die kompleksiteit daarvan wanneer dit met standaard DGIGe en permanente magneet sinkroon masjinee (PMSMe) vergelyk word. Tot dusver is dit meestal vir eiland wyse toepassing gebruik. In hierdie wyse van werking moet hulle beheer word om stabiele spanning teen n konstante frekwensie met afwisselende lading kondisies en veranderende wind spoed te kan bied. Dit is moeilik vir die BDGIG om met DGIGe wat klaar in die mark is te kompeteer aangesien dit nadele soos n meer komplekse struktuur, hoër kostes en groter dimensies het. In dié tesis word die krag beheer van die krag-netwerk-gekoppelde BDGIG sisteme in wind turbine toepassing voorgestel. Verder word die beheer van die masjiene as motors nagevors en uitgevoer. n Eksperimentele masjien, wat bestaan uit n staafhok rotor, is in detail ontwerp en beheer in simulasie sowel as deur eksperimentering. DC-skakel spanning beheer is ook geanaliseer waardeur die krag-netwerk omskakelaar as spanning bron beheer word. Vektor beheer word in alle kontrole oplossings gebruik, met vermindering in beheer kompleksiteit wat plaasvind en 'n analise van die beheer winding kant van die masjien

Stellenbosch University https://scholar.sun.ac.za

wat verminderde koste en verbeterde robuustheid vertoon terwyl dit responsiwiteit en akkuraatheid volhou.

Stellenbosch University https://scholar.sun.ac.za

Acknowledgements

I would like to express my sincere gratitude to the following people:

- My wife, Anja for your love, patience unwavering trust and support.
- My parents for their unconditional love, guidance and support.
- My family for never doubting me for pursuing this dream, but instead cheering me on along the way.
- My supervisor Dr N. Gule for his continued trust and guidance throughout.
- All of my friends and colleagues, for their suggestions and comments on this project.
- Murray-beurse, La Grange P, my Mother, Father and Dr N. Gule for their financial support during this en-devour.
- David Marais and Jonathan Olivier at Higeco Africa for allowing me to pursue this opportunity while being their employee.

Stellenbosch University https://scholar.sun.ac.za

To God, my wife and my parents

May the work that I do and the way that I do it bring faith, joy and a smile to all that I come in contact with today

Stellenbosch University https://scholar.sun.ac.za

Contents

Stellenbosch University https://scholar.sun.ac.za

Stellenbosch University https://scholar.sun.ac.za

Stellenbosch University https://scholar.sun.ac.za

List of Publications

International conference proceedings

Hutton, T., and N. Gule. "Simplified Vector Control of a Nested-Loop Rotor Brush-less Doubly Fed Induction Motor." In 2020 International Symposium on Power Electronics, Electrical Drives, Automation and Motion (SPEEDAM), pp. 53-58. IEEE, 2020.

Stellenbosch University https://scholar.sun.ac.za

List of Figures

Stellenbosch University https://scholar.sun.ac.za

Stellenbosch University https://scholar.sun.ac.za

List of Tables

Stellenbosch University https://scholar.sun.ac.za

Notation & Terminology

Notation

Numbers

$\mathbb{R}$	field of real numbers
$\mathbb{C}$	field of complex numbers
$\mathbb{Z}$	set of integers
$\mathbb{N}$	natural numbers (positive integers excluding zero)
j	the imaginary unit, i.e. $\sqrt{-1}$
$\perp$	Perpendicular matrix
T	Transformation Matrix

Terminology

AC	Alternating Current
DC	Direct Current
PF	Power Factor
BDFIM	Brushless Doubly Fed Induction Machine
BDFIG	Brushless Doubly Fed Induction Generator
PMSM	Permanent Magnet Synchronous Machine
VSD	Variable Speed Drive
VFD	Variable Frequency Drive
GSC	Grid Side Converter
CWSC	Control Winding Side Converter
PI	Proportional Integral
DTC	Direct Torque Control
VHz	Volt Hertz
p	Machine Pole Pairs

Variables

V	Voltage	[V]
I	Current	[A]
R	Resistance	[Ω]
L	Inductance	[H]
C	Capacitance	[F]

Stellenbosch University https://scholar.sun.ac.za

P	Active Power	[W]
Q	Reactive Power	[VAr]
S	Apparent Power	[VA]
T	Torque	[N·m]
J	Moment of inertia	[kg.m^2]
ω	Rotation Speed	[rad/s]
θ	Rotation angle	[rad]

Prefix Multipliers

μ	micro	[10^{-6}]
m	milli	[10^{-3}]
k	kilo	[10^{3}]
M	mega	[10^{3}]

Subscripts

$1 \mid p$	Primary stator winding / Power Winding
$2 \mid c$	Secondary stator widing / Control Winding
α	Alpha axis
β	Beta axis
0	Zero axis
d	Direct axis
q	Quadrature axis
abc	Three phase AC reference frames
$\alpha\beta 0$	Stationary reference frame
$dq0$	Rotating synchronous reference frame
s	Stator
r	Rotor

Stellenbosch University https://scholar.sun.ac.za

Chapter 1

Introduction

With electric vehicles and renewable energy becoming major trends in recent years, there has been a growing need for better, more robust, and more efficient machines. Numerous concepts have been developed based on various operational typologies, with many of the unique characteristics proving advantageous for different applications. One major influence on the adoption of these machines into industry has been their feasibility and consequently their ability to operate at various desired operating points within differing conditions and harsh environments [1].

Induction machines are widely known for their wide speed range capabilities. The first few iterations were still fixed-speed machines[2], with limited manual speed control performed by varying the load resistance on the rotor[3]. It would only be with the advancements in power-electronics that more flexible methods for control became more feasible[4].

Doubly fed induction generators (DFIGs) soon followed as a suitable solution to the wind generation industry[5; 6]. However, with its high maintenance due to slip-rings and gearbox wear, induction generators face numerous challenges for off shore application where regular maintenance can be challenging.

Rare earth metals such as the generators used in the Vestas V112 offshore wind turbines are common wind power solutions and widely used in industry[7]. The Siemens Gamesa permanent magnet synchronous generator (PMSG) is another generator which has been commonly used in numerous offshore sites[8]. With the PMSG being widely tested, it has been known to be more cost effective than its wound rotor alternatives. Additionally it is capable of rotating at lower speeds, having larger pole numbers than traditionally wound rotor alternatives. This makes it usable for low speed applications and usable in direct drive applications when a gearbox is not necessary to slow down the rotor speed with incoming wind speed to mitigate potential losses. The brushless doubly-fed induction machine (BDFIM) has been considered another viable solution for these low speed applications. Having a squirrel cage rotor, it is also capable of being used in direct drive applications[9], with the significant advantage of not relying on the scarcity of rare earth metals. However, due to its complicated control philosophy, higher overall machine size due to the extra set of control windings, and slightly lower efficiency, it is yet to be adopted in commercial applications.

Stellenbosch University https://scholar.sun.ac.za

1.1 Problem Statement

One major challenge for the control of BDFIMs is estimating the machine parameters. With accurate vector control being based on the knowledge of the characteristics of the machine, better measurements generally result in a better controller[10]. However, since BDFIMs have a squirrel cage rotor, more traditional mathematical models had to be used to estimate its parameters[11; 12; 13]. More recently, with finite element techniques the parameters could be estimated with even greater accuracy[11].

However, for BDFIM's to be viable for low speed direct drive purposes, they inherently have a large number of rotor nests to match the amount of stator pole pairs. Thus making their modeling increasingly complicated, with the simplest machine requiring at-least 10 system states. It is easy to imagine how full state control of such a machine can become extremely complex to achieve, necessitating development of a simplified model. In most alternating current (AC) controllers, this is achieved by reducing the machine model to a dq-frame equivalent, which allows the machine to be controlled similarly to that of a DC machine[4]. A larger challenge of BDFIM's is the reduction techniques suitable for equivalent circuit models of the rotor. With many different typologies, many require super-positioning or various forms of equivalent circuit analysis in order to be simplified to an equivalently traditional cage rotor, usually a squirrel cage topology. A simple method of summation was presented in [14]. This however could only reliably be applied to nested loop rotors and sometimes lead to erroneous results. A more general technique was required. Soon after such a method was introduced in [15], where a method of mapping is used to get a theoretical reduced state equivalent of all initial states. This is achieved by computing the weighted sum of all loops into a single equivalent loop. This method was however only tested on a nested loop rotor cage design.

As for the control of BDFIM's, various studies with various methods have been proposed. Ranging from sliding mode controllers (SMC) to variable frequency drives (VFD's) to vector controllers, each have their own advantages and disadvantages. One major advantage of the sliding mode controller is its robustness against varying machine parameters during dynamic operation. This however bears minimal insight into the machine and can mask various properties of the machine. Due to the sliding nature of SMC's, unwanted chattering can be introduced into the network, however the signum can reduce this significantly[16]. Flux control on the other hand can be less robust towards varying machine parameters, but in general should have a smoother transient response if, ideal machine measurements, low system noise and perfectly linear control is implemented. This is seldomly the case for practical systems, and as such there is the need for a more robust, responsive vector control system. The control system should offer individual control of all system states while reducing susceptibility to noise, measurement errors and operate without sensor-less control solutions.

1.2 Aims and contributions

In this dissertation, the method proposed in [15] will be used to reduce the experimental bar cage BDFIM down to a dq-equivalent model. This will be simulated and compared to physical measurements using an experimental machine of similar properties.

Throughout the dissertation detailed analysis of the machine will be made, offering simulated bar cage currents, flux and voltages. On a step by step basis all of these estimates will be compared, indicating any loss of accuracy as the transformations go

Stellenbosch University https://scholar.sun.ac.za

along. The full 23-state model will be reduced to an equivalent 8-state synchronous reference frame model, with similar properties of the original. These properties will be compared and it will be shown that throughout the transformation process, minimal loss of accuracy can be achieved.

Accordingly, a control philosophy will be developed whereby a simplified vector controller from the one proposed in [17] will be implemeted. This will be simulated using Matlab Simulink and finally the results of the simulations will be compared with an experimental implementation. The controller will show that all forms of state control can be performed, ranging from stator current control, to active and reactive power control, torque control and finally speed control. Each of the reduction techniques will be simulated and verified experimentally, and compared accordingly to show the benefits or drawbacks of each assumption.
The proposed research will be aimed to achieve the following:

- Accurately model the machine transients during dynamic operations
- Verify the accuracy of the machine parameters through comparison of real measurements to that of the simulations
- Reduce modeling duration's through state reduction techniques
- Retain insight into the machine's physical properties throughout the simplification process
- Provide stable control of the BDFMs' active and reactive power over its entire operating regions
- Be suited for operation in a grid-connected environment. Thus be stable under varying loads or wind speeds
- Provide active and reactive power control in generation mode as well as speed control in motoring modes
- Perform dynamic control under sub and super-synchronous mode of operation
- Confirm, by simulation and experimental implementation of the developed system that the developed controller performs as expected

By achieving the above expectations, the proposed research will enable the BDFIM to be ever more appealing as a robust machine by reduction of the control complexity and reliance on accurate measurements consequently reducing costs of maintenance and hardware development.

A research contribution is shown in [18], where the control simplification process and assumptions are explained, indicating the viability and advantages of such a reduced vector controller for practical BDFIM's.

Stellenbosch University https://scholar.sun.ac.za

1.3 Chapter Summary

To provide a thorough review of the modeling and control of the BDFIM, this dissertation is structured in a manner that allows for a detailed introduction into the machine and control system as a whole, followed by the modeling of the machine, control using the back to back converter, laboratory experiments and conclusions and future recommendations.

An in depth study of current research into the machine modeling and control is done in chapter 2, in the form of a literature review. Here, asynchronous machines are discussed, detailing the history of such machines and how the need for BDFIM's arose. Different types of rotors are shortly reviewed, followed by an overview of the typical topology of BDFIM's used. Here the back to back converter is presented and it is shown that there are significant advantages in having a fractionally rated converter for BDFIM's. A short comparison between the BDFIG and its DFIG companion is done, showing that BDFIG's are generally less efficient, but promise good reliability for harsh environments - such as offshore applications. Additionally, different methods of control is discussed, weighing various advantages and disadvantages of each. An in depth overview of vector control and research into its use for BDFIM's is presented, indicating that vector control theory for BDFIM's are well researched to date, but there is a need for a more forgiving controller.

The BDFIM coupled circuit model is presented in chapter 3. Various aspects regarding the modeling required to develop BDFIM control systems is inspected. For example the aerodynamic conversion of wind for wind energy conversion systems (WECS), where potential wind energy is converted into mechanical input energy on the BDFIM rotor, which is converted into electrical energy and then transmitted over the utility network. For the mechanical energy conversion a mechanical model of induction machines is shown, followed by various different state space representations of the BDFIM. In order to accurately represent the machine dynamics for control purposes, the BDFIM is reduced into a single rotor bar theoretical dq-equivalent model which allows the controls designed to have an in depth representation of the BDFIM transient dynamics. To achieve this a transformation process is followed, whereby graphs are used to represent the machine during the transformation process.

In chapter 4 the back to back converter is briefly discussed. The grid side converter is then discussed and the control theory presented. It is noted that a filter is necessary to reduce the harmonics induced on the grid due to the high frequency switching of the voltage source converter (VSC). A short design of such a filter is shown, followed by a suggested method for tuning the PI gains of the corresponding vector controller. Furthermore it is deemed necessary to implement a phase locked loop in order to properly align the rotating synchronous reference frame with phase voltage of the grid. One such design is accordingly presented and symmetrical optimum is used for the tuning thereof. The control winding side converter is also presented with a short overview of similar schemes and a description of the integration thereof with the switch vector pulse width modulation scheme. An introduction of the vector control to be implemented is presented and the advantages of synchronizing with the stator flux reference frame discussed. An in depth derivation of the vector controller is then performed and followed by a discussion of compensation terms that could be deemed negligible. It is mentioned that the reduction of these terms can enhance the reliability of the controller during sensor / measurement errors. A simulation is accordingly performed indicating the potential advantages and disadvantages of the reduction of various parts of the controller.

For the BDFIM model to be verified reliably as well as the control theory to be confirmed, a practical implementation thereof is necessary. In chapter 5, such a setup is

Stellenbosch University https://scholar.sun.ac.za

presented, where a National Instruments controller is used in addition to Labview to perform real time control of the machine and obtain high speed measurement results. These results are then presented and compared, similarly to that in chapter 4 allowing for a direct comparison into the viability of using the simulations to predict the response of the controller on a theoretical machine. To match the mechanical characteristics of the machine a process of curve fitting is followed, ensuring that the machine dynamics are similar to that of the practical one. Thereafter the output power and currents are analyzed and compared, showing that the derived parameters are within reasonable accuracy. Finally various tests in motoring and generation modes are performed, indicating the stability of the machine controllers while performing speed, active- and reactive-power control. It is also found that minimal gain adjustments are necessary to maintain the expected response of the machine as indicated from the simulations.

Finally in chapter 6 conclusions and recommendations are made, discussing the findings throughout the dissertation and outlining possible improvements to be made.

Stellenbosch University https://scholar.sun.ac.za

Chapter 2

Literature Review

In recent years, the self-cascaded machine or BDFIM has attracted considerable attention, with the robustness of a squirrel cage rotor as well as speed and power factor variability. Having the absence of brushes and slip rings, as well as the possibility of using a fractionally rated converter should small variances in speed be desired, it is easy to imagine that the BDFIM is a potential solution to various limitations seen in conventional machines in industry[19]. That is for low maintenance wind turbines or high power adjustable speed drives where its complex structure, higher development cost and in general larger dimensions when compared to the conventional squirrel cage induction machine can be regarded less prevalent[19; 20; 21]. An in depth overview of machines in practice and both the advantages and disadvantages of each will now be discussed. Wound rotors are briefly mentioned and the necessity of wound rotors in high volume production environments found impractical, especially where brushless control of the rotor is achievable. This leads towards the goal of outlining BDFIM machines as a potential solution towards the impracticality of current high maintenance off-shore wind turbines.

2.1 Asynchronous Machines

In 1879, Walter Baily demonstrated what is effectively known as the first primitive induction motor[22]. This machines' alternating current was induced by manually turning switches on and off. Shortly after this, the first three-phase induction motors were independently invented by Galileo Ferraris and Nikola Tesla between 1885 and 1887[23].

The induction machine is an extremely simple machine design and has the advantage of being able to operate at various frequencies. Consisting of a stator and a squirrel cage rotor, it is simple to run and can be economical to construct.

For the induction machine to induce current, in the rotor winding and produce a counter magnetic field, the induction machine required slip. This implies that the induction machine will never operate at true synchronicity. This is, in fact, a unique advantage of the induction machine. With its reliance on slip around synchronous speed, the induction machine is a perfect solution for wind turbines since it allows for some tolerance in the drive unit. When operating at super-synchronous speed, the induction machine is transformed into a generator without needing any internal modifications.

A basic limitation of induction motors is that they have very low starting torque and high starting currents. This is due to the constant rotor resistance. To achieve high efficiency under normal running conditions a low rotor resistance is required. Counterproductively to produce higher starting torque a higher starting resistance is required[24].

Stellenbosch University https://scholar.sun.ac.za

This can be observed by the torque equation

$$\tau = \frac{3I_r^2 \times R_r}{s\omega_r} \tag{2.1}$$

Another concern of the induction machine is its characteristic to speed up when the load is low, or removed. This can mean that during voltage sags or times of low load requirements the wind turbine can speed up to dangerous speeds, resulting in termination of the machine[25].

2.2 Wound rotor motors

As a solution to the limitations of the squirrel cage rotors' constant resistance, wound rotor motors are constructed of poly-phase windings, similar to that of a stator. The terminals of the rotor windings are connected to slip rings on the rotor shaft which can be connected to external resistors via stationary brushes to control the starting torque and current. As the machine comes up to speed, the resistances can be varied and ultimately short circuited to achieve maximum efficiency at operating speeds[24; 26].

An advantage of the wound rotor is that the machine can be operated in generation mode very easily by reversal of the power flow. However, due to the induced currents in the rotor varying with frequency, direct connection to the grid of the rotor is not recommended.

2.3 The Doubly Fed Induction Machine

This is where the doubly fed induction generator offers optimal power return from the rotor[24]. With the addition of a back-to-back converter connected to the slip-rings of the rotor, the phase AC voltage from the rotor can be converted into DC voltage and then back to AC at the desired grid frequency[27].

This generally requires regular maintenance as the brushes on the slip rings degrade very quickly[28].

2.4 Dual Stator Windings

In 1907 a different kind of induction motor was proposed[29]. The motor described possessed all the characteristics of an ordinary type of slip-ring induction motor, but had differences in the arrangement of its stator windings. These windings are arranged to permit the regulating resistances to be connected to the stator windings instead of to slip rings in the traditional manner, making this machine an improved form of the "cascade" motor which has two magnetic field systems super-imposed upon one another in the same core body. The second field has its origin in the rotor and consequently induces secondary currents in the stator windings.

During the the 20^{th} century major advances in electrical machinery were made, driven by the need to provide a substitute to the steam engine which held its place against the electric motor. Mainly on account of its usefulness as a variable speed machine. It soon became clear that its super-session was dependent entirely on the development of a satisfactory electric motor having somewhat similar characteristics[30].

Stellenbosch University https://scholar.sun.ac.za

As a solution to this, cascaded machines were introduced. Here two machines are physically connected to one another. Additionally, by connecting the primary winding of the induction motor to the secondary winding of the other, they will run at a speed corresponding to the sum of the number of poles in the two machines for a particular direction of relative rotation of the fields, and at a speed corresponding to the difference between these numbers for another direction of relative rotation[29].

The use of cascade machines can be very expensive and result in poor characteristics of the set. As such it was proposed that the two cascade motors be combined into one machine. Here many variations were suggested, but only two typologies are of interest from the stator winding point of view. These are the split wound and self-cascaded machines.

The split-wound dual-winding machine was proposed to improve the power capability of large synchronous generators and to achieve better drive reliability resulting from its inherent redundancy[31].

The self-cascaded machine [32] shows commercial advantages due to the fractionally rated converter and absence of brush gear. However, the special rotor structure significantly increases the complexity of the machine as well as manufacturing costs, whilst producing undesirable spatial harmonics which decreases machine efficiency.

The BDFIM however offers solutions to various of the problems mentioned and will now be discussed.

2.5 BDFIM

With the absence of a brush gear and accompanied by the advantageous of a fractionally rated converter, various methods to mitigate the negative effects of spatial harmonics and to increase the machine efficiency have been suggested for BDFIM's.

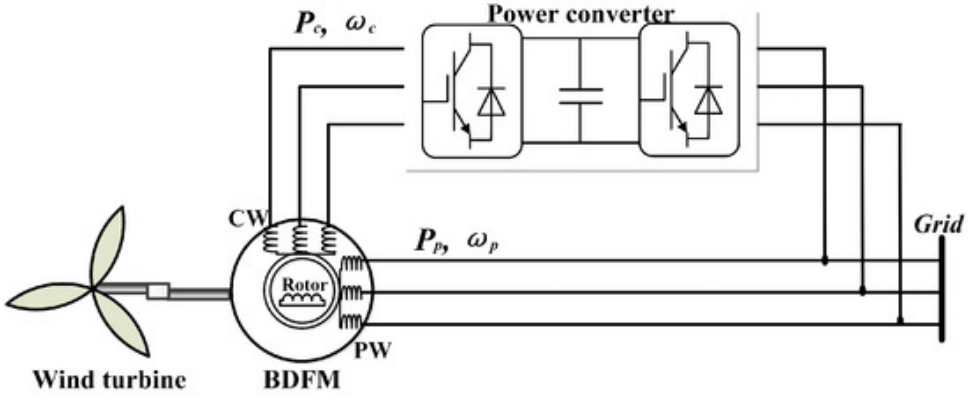

Figure 2.1: BDFIG Implimentation as a wind turbine

As indicated in Figure 2.1 the BDFIG has two balanced three phase windings on its stator. Here one of the windings is the primary winding (also called the power winding) which is directly connected to the grid. The secondary winding (also referred to as the control winding) is also indirectly connected to the grid by means of a fractionally rated frequency bidirectional converter.

Stellenbosch University https://scholar.sun.ac.za

2.5.1 Back-to-back Converter

In some applications, especially in motoring mode, the back-to-back converter is used to control the reactive power, speed and or torque of the motor and as such the control winding focuses mainly on slip power.

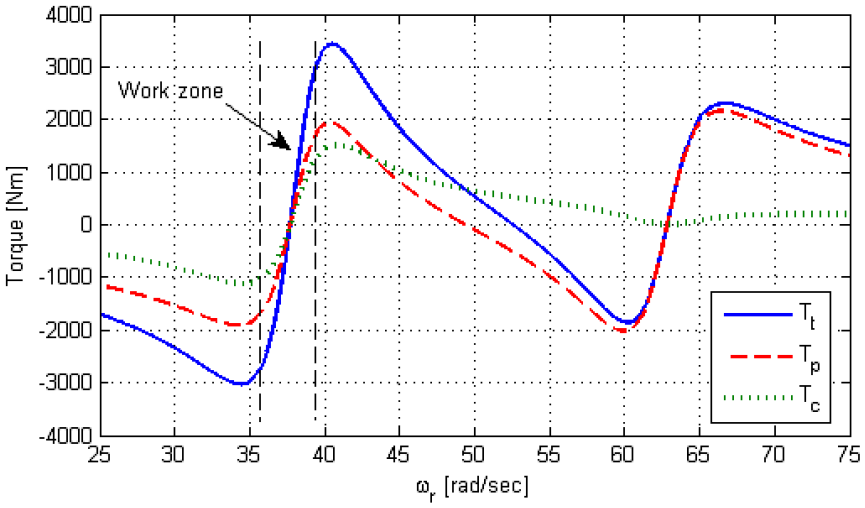

Figure 2.2: BDFIG Torque Operating Regions[33]

Generally the back-to-back converter is only rated at 30% of the rated power, allowing the BDFIG to utilize most of its optimal power curve[34], as shown by the work region in the Figure 2.2, where positive torque represents the machine operating as a generator.

With the slip of a BDFIG for a wind turbine usually being designed from -0.3 to 0.3 of rated speed, corresponding to a ±30% speed range, the highest value of the CW voltage is attained when the machine is running at the highest speed, i.e 130% of the natural speed[35].

2.5.2 Rotor Topographies

There are many variations to the typical squirrel cage rotor suggested for BDFIM machines. There is the double layer design, isolated loop, wound rotor, bar cage and nested loops to name a few. Some of these suggestions are shown in Figure 2.3 and 2.4.

The rotor should be coupled to the magnetic fields of the primary and secondary stator windings in an appropriate manner[36]. Due to its construction simplicity and scalability, the nested loop rotor is often used [37].

To provide indirect cross coupling between the fields of the stator windings, the number of nests should be equal to the summation of the number of primary windings and secondary winding pole pairs $p_r = p_1 + p_2$. One of the major concerns of the rotor cage is that it induces unwanted harmonics. As in the case of squirrel cage induction machines, it can be found that by increasing the number of rotor bars, it decreases the spatial harmonic contents of the rotor flux and its leakage inductance's therefore resulting in better performance characteristics. A study on the comparison of nested-loop rotors in BDFIM's also indicated that the total harmonic distortion of a BDFIG can be significantly reduced by increasing the number of outer loops[38]. This also increases the motor torque. In addition, it is shown that the inner loops have little impact on total harmonic distortion and that the average torque contribution made by an individual loop directly depends on

Stellenbosch University https://scholar.sun.ac.za

its loop span. Thus, the inner loops have less effects on the BDFIM's ability to produce higher torque ratings than the outer loops. It is clear that there are numerous advantages and disadvantages motivating different rotor designs[39], and for the purposes of this study, it was convenient to focus on the bar cage design, as will be further discussed in Chapter 3.

2.5.3 Typical Operation

Due to the BDFIG typically being less efficient than its DFIG alternative, such as the comparison shows in Figure 2.5, the BDFIG is most useful for applications where low maintenance is desired. However, there have been some suggestions for the BDFIG to be used in electric vehicles as a motor.

As for renewable energy, the BDFIG has two methods for operation, grid and stand-alone (also referred to as islanding mode). Another operational use was implemented where the BDFIG is connected to a ship's shaft to generate power for the ship using a sensor-less control scheme[40]. In this particular study, it is investigated whether or not the control scheme is adequate with or without compensation from the negative-sequence power winding voltage. By experimentation it was confirmed that the compensation significantly reduced unbalance of the output voltage and thus improved the output voltage quality under unbalanced loads.

2.5.4 Comparison of DFIG with BDFIG

A DFIG and BDFIG of equal rated power were compared whilst connected to the grid in [41]. It was found that the DFIG had an efficiency advantage of 7% at lower operating speeds, however the BDFIG's performance improved significantly closer to its operating region, where the efficiency difference between the two was reduced to less than 1%. It was also found that even though the DFIG had more losses in the rotor than the BDFIG, the overall increase that was able to be achieved in performance, resulted in much less iron losses and stator losses than the BDFIG.

2.5.5 Faults

In recent years, with the adoption of more independent energy suppliers to the national grid[42; 43], more strenuous regulations have been put in place to ensure sufficient power

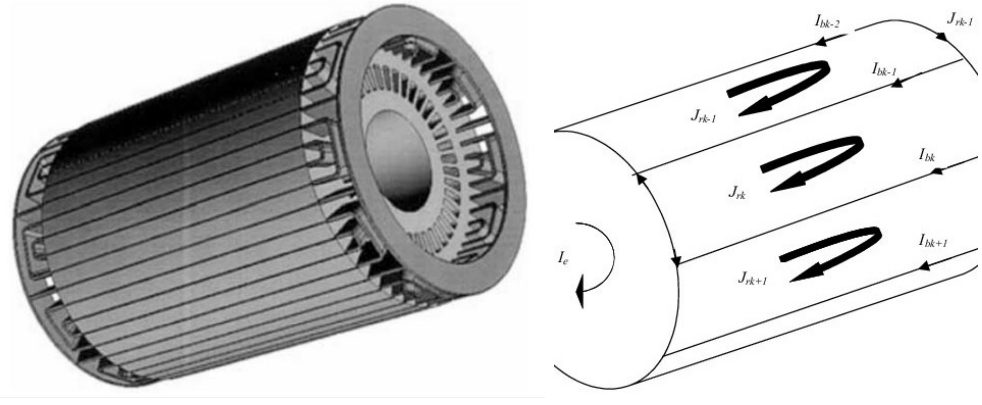

(a) Double Layer Design **(b)** Isolated Loop cage

Figure 2.3: Rotor designs 1 & 2

Stellenbosch University https://scholar.sun.ac.za

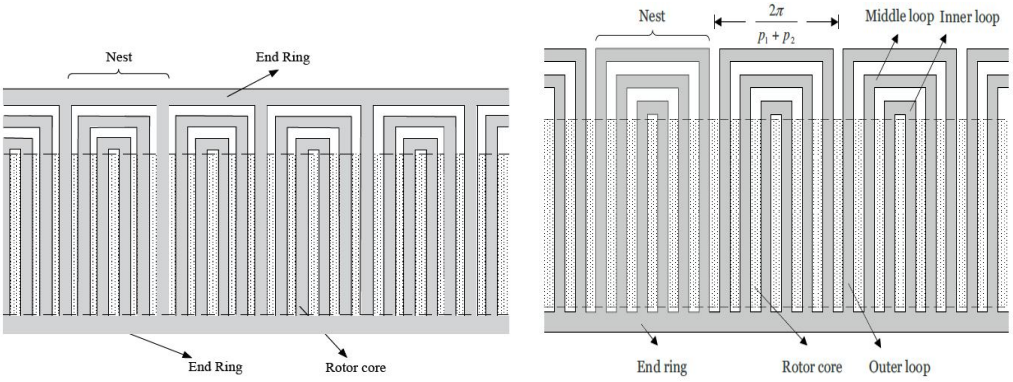

(a) Bar cage **(b)** Nested Loop

Figure 2.4: Rotor designs 3 & 4

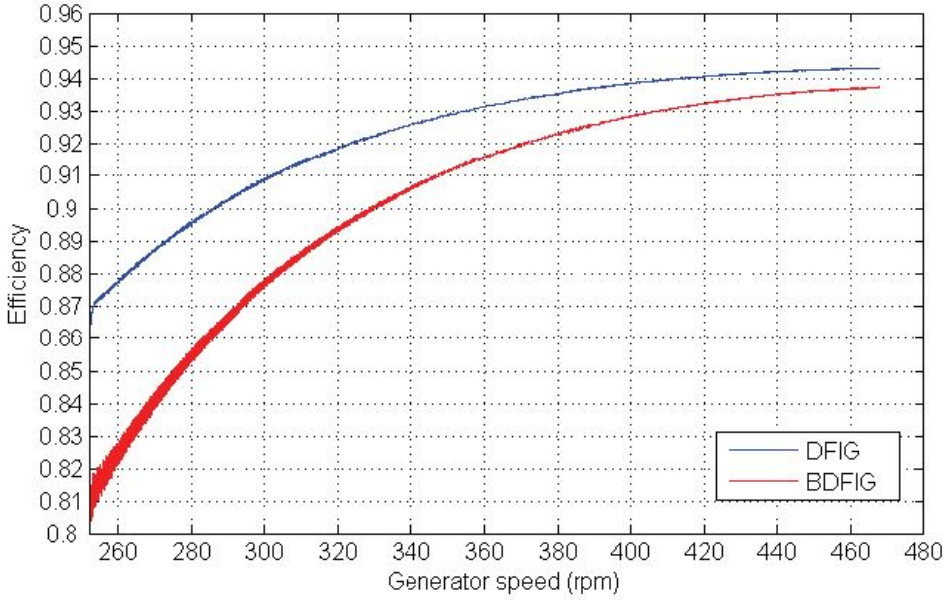

Figure 2.5: DFIG vs BDFIG Efficiencies

quality produced to increase reliability and safety of the networks. One of these regulations implemented, is the requirement of low-voltage fault ride through for generators.

During a low voltage fault, induction machines connected to the grid experience transient over-currents, proportionally increasing the machines rotational speed which can escalate dangerously, potentially resulting in the destruction of the machine[44].
There are varying solutions to this, such as crowbar protection, hardware protective circuits such as stator damping resistor controllers, or a dynamic voltage restorer or a series grid-side converter which all increase the system cost and complexity[45].
A vector control setup was developed to enhance the BDFIG's symmetrical fault ride through capability in[35]. Experimental results showed that the controller which was based on a vector control scheme was able to meet the stringent grid regulations without any additional protective hardware[32].
A further study done on asymmetrical voltage dips in BDFIMs indicated that as a result of negative sequence, induction generators respond differently in asymmetrical faults. Additionally, analysis in this study showed that the major issue for an asymmetrical low voltage fault is from the zero sequence of the control winding current, but not the backward sequence current. Thus, an adapted control strategy was required. It was proposed

Stellenbosch University https://scholar.sun.ac.za

through a novel control strategy for the BDFIM that sufficient ride through could be achieved during these asymmetrical low voltage dips. This solution was shown to offer both high stability and a low cost grid integration[46].

2.6 Control

In recent years, there have been significant amounts of research done regarding the control of BDFIMs. Due to the complexity associated with BDFIMs, the control of BDFIMs is well researched, however improvements can still be made. Additionally, further testing in commercially operational environments is required to increase certainty of reliability in harsh enviornments. Since these machines operate on AC principles, the control is complicated beyond that of DC machines. Various methods exist by which the AC reference characteristics can be converted into a stationary dc-like reference frame[47]. Allowing similar analysis as with DC machines. One example of a well known vector controller used for BDFIMs, makes use of a dq-transformed equivalent circuit model of the BDFIM in order to allow the control of speed, torque, reactive and active power [48]. This study contributes towards the simplification of the BDFIM model for vector control purposes and is further discussed in section 4.4.1.

The general operating mode of the BDFIM is synchronous mode, at which the power- and control windings are cross-coupled through the rotor circuit. As such, an equivalent model for the BDFIM under this order of operation is required.

One of the contributions to the model development of the BDFIM in the synchronous region can be found in [49]. Here an equivalent circuit and performance equations for the BDFIM were presented which are suitable for basic control schemes and performance index optimization.

Further development led to the generalized theory of the brushless doubly-fed machine [50][51]. In these studies, a rigorous mathematical model is developed in the dq synchronous plane, which is suitable for the analysis of the BDFIM. Both electrical and mechanical quantities are derived from first principles and the concept of load angle is discussed. The above derived models form the foundation required to perform most control schemes presented in this paper.

General sensed and senorless control methods such as scalar, volt-frequency (v/f), vector control and direct torque control of the brush-less doubly fed reluctance machine (BDFRM) are analyzed in [52]. These control methods promise to be cost-effective alternatives to existing technological solutions with restricted variable speed capability, such as large pumps and wind turbine generators. It should however be noted that this was based on reluctance BDFIMs. However, the methods explored still provide valuable insight into control solutions for these machines in general.

2.6.1 Speed control solutions

Variable speed drives are typically used to vary a motor's speed based on different models. One such model is the frequency, also referred to as variable frequency drives (VFD's), generally operate by varying the input voltage and frequency fed to the machine. Thus, slowly adjusting the synchronous frequency of the machine to achieve the desired speed.

Stellenbosch University https://scholar.sun.ac.za

For BDFMs, which are desired to operate as a motor, variable frequency drives are very promising solutions, especially with the drive only controlling the secondary winding of the machine.

Furthermore, it has been shown that it is possible to start the BDFIM in cascade mode and make the transition to synchronous mode just below the natural speed[53], and that a simple phase angle controller will stabilize the BDFIM satisfactorily. However, the cascade mode does not offer full starting torque. To achieve this, external resistances will have to be switched in and out, which can be inconvenient and costly. Additionally, the speed ranges and therefore the frequency variations in BDFIMs are usually limited, which mitigates the open-loop stability problems associated with this method in case of sudden step changes in the supply input frequency. A basic V/f control strategy has been proposed in [52] and is shown in figure 2.6 below. It should be noted that the control strategy proposed is by no means optimal and has primarily been developed in cohesion with the conventional IM to illustrate the proof of concept. As such, the V/f control strategy is not very effective at low starting speeds. The control strategy does not compensate for resistive voltage drops, nor does it improve torque production at lower speeds which is normally present in general IM drives.

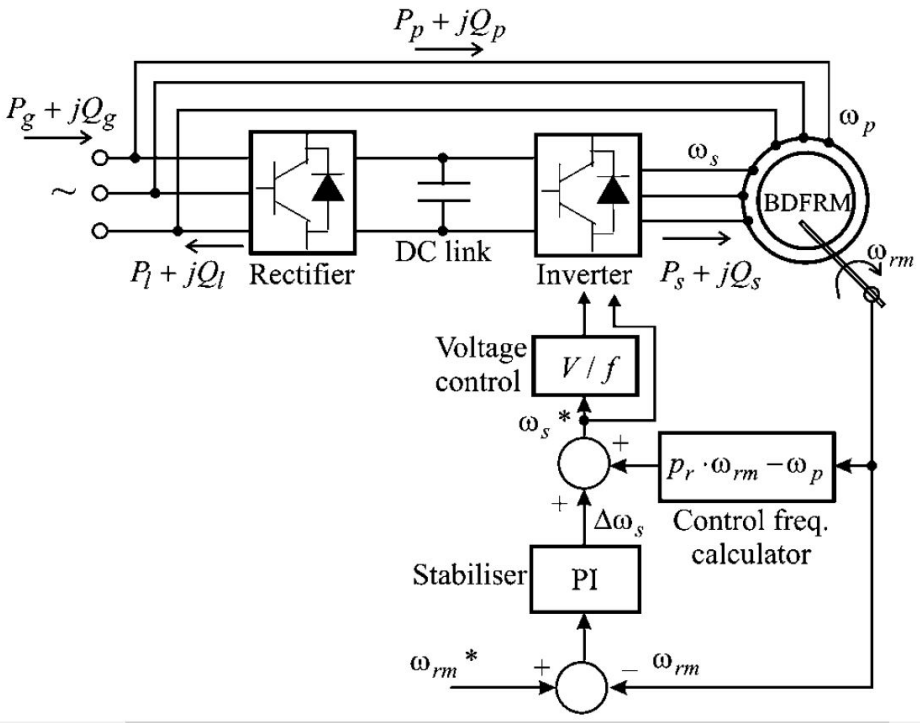

Figure 2.6: Voltage-frequency Control Scheme[52]

These methods are suitable for providing starting torque to operate and or synchronize the machine. However, if the goal is to have stable control at various operating points then further investigation is desired.

2.6.2 Direct Torque Control

The application of direct torque control (DTC) to induction machines can be seen in [54; 55]. Beside its overall simplicity, DTC permits good torque control under both

Stellenbosch University https://scholar.sun.ac.za

steady-state and transient operating conditions[56]. Below is a list of advantages and disadvantages.

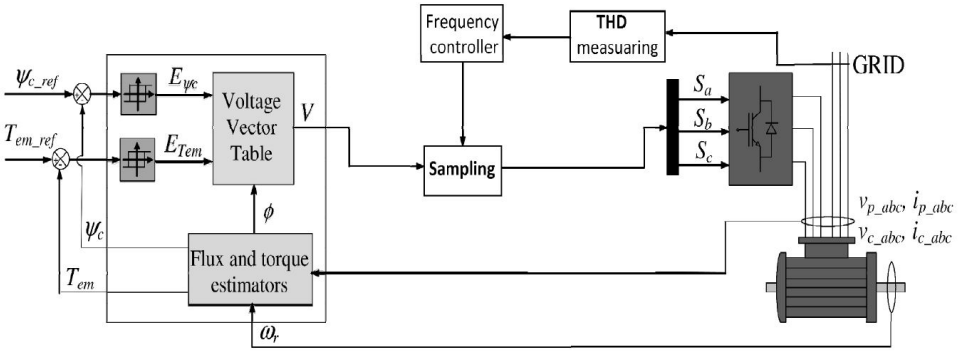

Figure 2.7: Direct Torque Control Scheme[56]

2.6.2.1 Advantages

- Direct torque control does not require coordinate transformations to achieve decoupled control of the flux linkage and torque.
- DTC is not overly sensitive to machine parameters.
- By implementing DTC for unstable grid voltages, the ripples in electromagnetic torque can be significantly decreased through increase of sampling frequency[56].

2.6.2.2 Disadvantages

- It is vulnerable to disruptive harmonics in the power grid which can lead to perturbations in the back-to-back converter.

In a study where the principles of sliding mode control (SMC), direct torque control and space-vector modulation (SVM) were combined, it was shown that this combination of methods yields a simple but robust linear and variable structure controller for torque control of BDFM drives[57]. With a goal of maximum torque per ampere control (MPTA), a sliding mode controller with a linear PI was designed and subsequently it was verified by simulation that the presented control strategy is accurate, quick and robust whilst increasing overall efficiency and reducing copper losses.

Further investigations into the application of DTC on BDFMs in unbalanced situations focused on the presence of turbulence in the voltage grid and the effect thereof on the control scheme[56]. In the proposed controller, a sampler in a specific frequency feeds the output of signals of hysteresis comparators to switches. The sampling frequency controlled, based on the THD level of the grid and by the establishment of boundaries of controller output, spontaneously solved the problem of dead time as well.

2.6.3 Vector Control

Field oriented control (also known as Vector Control) is a well known control method used in electric machines. It has been shown that this method of control shows promising characteristics for the BDFIM to be implemented in a grid or stand-alone operational setup.

Stellenbosch University https://scholar.sun.ac.za

It was shown in this case, the torque of the BDFIM can be controlled very effectively using vector control which lends this control system toward being a high-performance BDFIM shaft speed control system[47].

Research on vector control of BDFMs has mostly been done relatively recently, with papers on the experimental evaluation of a rotor flux oriented control scheme being done in 1997[58].

In 1999, a complex vector model for a dual stator induction machine (DSIM) was developed[59]. The DSIM is very similar to the BDFM, with two three phase windings in the stator, but its rotor is of the squirrel cage type. This study, was soon followed by [31], where a drive was developed for these dual stator winding machines. The proposed drive offered advantages, such as sensor-less operation and more flexibility to manipulate the resultant torque-speed curve of the motor.

Another study was performed on a cascade doubly fed induction machine (CDFM). The CDFM consists of two wound-rotor induction machines which are both mechanically and electrically coupled through the rotor, making its operating characteristics very similar to that of the BDFIM, albeit lacking the compact structure of the BDFIM[59]. In the study, a vector control algorithm was developed to control torque, speed, active and reactive power.

More recently in 2008, a study conducted on the vector control of a BDFM was done to develop control algorithms of the grid-side and control-side converters to regulate the active and reactive power in the machine independently. This method showed soft and fast synchronization at the minimum rotating speeds [60].

With the control of BDFMs based on traditional multiple reference frames, that are very complex, a simplified control scheme was proposed in [48]. The proposed control scheme included a new and simpler derivation of the dq-model of the BDFIM. The results found by this research, offered significant contributions to BDFIM control research to follow.

One limitation of the research done was that the vector model only considered a single-loop per nest rotor. However, it provided guidelines for a multiple-loop per nest rotor as well. Using this approach, the resulting vector model would be based on an approximate equivalent loop for each nest. This grants significant reduction in model complexity, while retaining model accuracy should the reduction techniques followed, be carefully applied to minimize transformation.

In another study by [61], a vector control algorithm was developed with the goal of achieving similar dynamic performance to the DFIM. Here it was confirmed that by exploiting well-known induction motor vector control philosophy, the BDFIM can produce similar dynamic performance under this type of control to that of the DFIM.

A different study developed a vector controller synchronized to the power-winding stator-flux frame which was intended to control both the speed and reactive power [62]. The test results indicated good dynamic performance when changes in speed and reactive power were applied.

In [63] and [60] a vector model was derived for a BDFIM where all the loops in each nest of the rotor were considered. Later in [64], performance simulations and analysis were done. In [47] it is confirmed that the generalized BDFM vector model behaves accurately in predicting the machine performance under different operating conditions. It should be noted that the approaches used above are generalized for a generic BDFIM with p_1/p_2 pole-pair stator windings and N loops per nest.

In [65], a vector control structure is presented for a BDFIM. This structure was further extended in [47] where the vector control system is based on the basic BDFIM equation

Stellenbosch University https://scholar.sun.ac.za

in the synchronous mode accompanied with an appropriate synchronization to the grid. Furthermore an analysis is performed for the generalized vector control system proving the efficacy of the proposed approach.

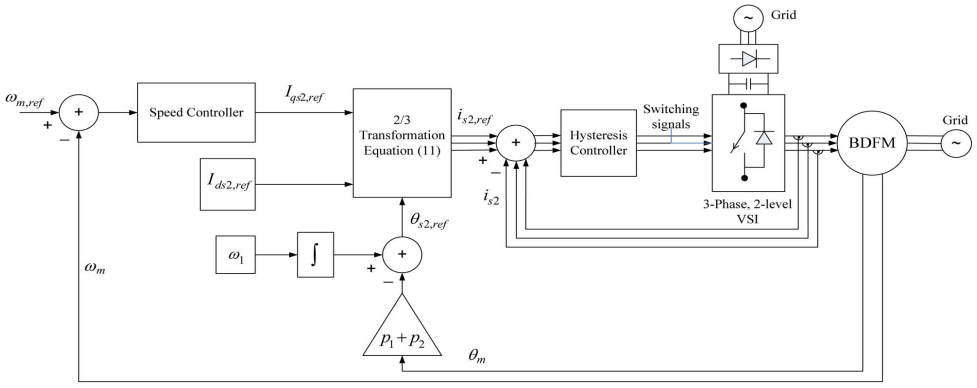

Figure 2.8: Vector Control Algorithm implemented in [47]

Generally, in AC vector controllers the stator currents are identified as two orthogonal components which can be visualized with a vector. One of the vector components defines the motors magnetic flux and the other the motor torque. This control system determines the required currents from the flux and torque reference requirements given by the drives' speed control. In the setup of a generic BDFIM, the vector control system controls the active and reactive powers in the control winding, allowing both speed and torque control for BDFIM's.

2.7 Conclusion

The brushless doubly fed induction machine offers promising dynamics at variable speeds. With its dual wound stator, by adjusting the voltage and frequency in the control winding, accurate control of the active and reactive power in the machine can be established.

By the implementation of a sensored field oriented control strategy with feedback from flux estimation. It is clear that accurate modeling of the BDFIM forms an important role in order to achieve reliable control. From the works presented to date, limited methods to obtain machine parameters for control purposes of the BDFIM are available. One suitable method has been identified and the viabilty thereof with regards to bar cage BDFIM's will now be shown.

Stellenbosch University https://scholar.sun.ac.za

Chapter 3

BDFIM wind energy conversion system modeling

The BDFIG consists of a very similar setup to that of the DFIG, with a back-to-back converter which allows for bi-directional power flow on the secondary 3 phase stator control winding. Typically both VSC's on the back-to-back converter are rated at 30% of the power rating of the BDFIG. In order to optimize the generator output speed with available wind speed, a gearbox with a reduction ratio is generally suggested, however if designed for low speed operation, direct drive solutions can be obtained.

3.1 Aerodynamic model for maximum power point tracking

For wind energy conversion systems such as wind turbines there are various aspects to be considered for wind energy to be utilized. Before reaching the utility supply network the potential energy available to the wind turbine in the form of wind has to be converted to electrical energy.

It is well known that the available energy for wind turbines increases proportionally to the swept area that the blades of the turbine covers. As is shown in equation 3.1 below, the mechanical input power at the blades of the wind turbine can be calculated to be a varying function of the incoming wind speed V and coefficient of power C_p

$$P_m = \frac{1}{2} A \rho V^3 C_p(\lambda, \beta) \tag{3.1}$$

Maintaining an optimal tip-to-wind speed ratio (TSR) is key to reduce wind-spillage and accordingly loss of input power. The TSR is a ratio of the turbine swept area and the incoming wind speed V. The swept area is defined by the rotational speed w_m and the rotor radius R. This is shown by equation 3.2 below

$$\lambda = TSR = \frac{w_m R}{V} \tag{3.2}$$

With a wind turbine that's rotating too fast, turbulent air can significantly reduce power output, and a turbine rotating too slowly results in loss of swept wind energy. Additionally, the torque entering the drive shaft due to the incoming wind on the turbine is a function of the incoming mechanical power against the rotating mechanical shaft speed. By applying

Stellenbosch University https://scholar.sun.ac.za

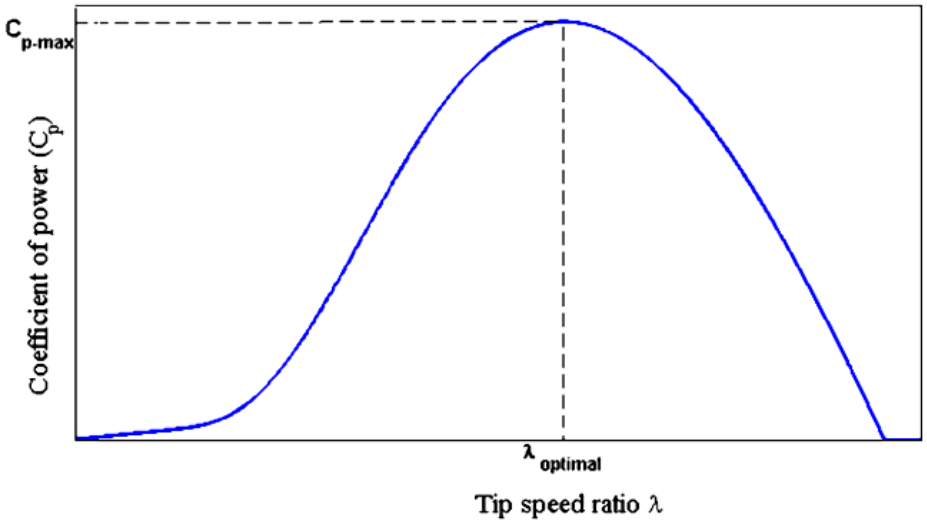

Figure 3.1: Typical coefficient of power curve[66]

equation 3.1 to this, the resulting mechanical torque can be shown to be

$$T_m = \frac{P_m}{\omega_m} = \frac{1}{2} A\rho V^2 C_p(\lambda, \beta)\frac{R}{\lambda} \tag{3.3}$$

The coefficient of power can vary greatly depending on the design of the wind turbine blades. Especially the radius of the blades R and pitch angle β. Numerous studies can be found suggesting suitable approximations of the C_p for different wind turbines[68; 69; 70].A general approximation of the coefficient of power shown below[71; 72]

$$C_p(\lambda, \beta) = 0.5(T - 0.02\beta^2 - 5.6)e^{-0.17T} \tag{3.4}$$

where the constant T is defined as

$$T = \frac{R}{\lambda}\frac{3600}{1609} \tag{3.5}$$

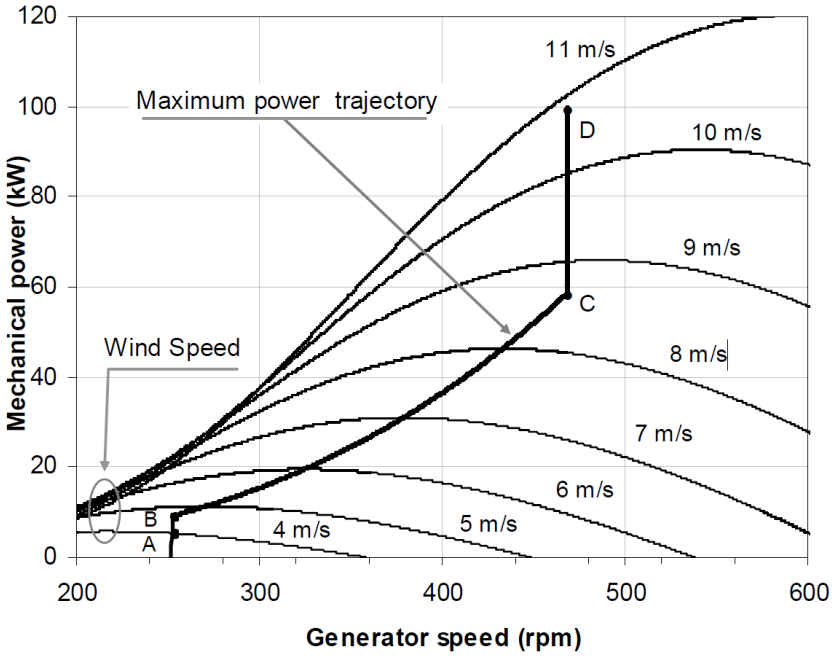

Figure 3.2: Output power vs speed curve[67]

Stellenbosch University https://scholar.sun.ac.za

In Figure 3.1 the curve shows the optimal power coefficient for the corresponding TSR. For this example, the pitch angle is zero. In practice, pitch control is required to ensure that the machine is always pitched optimally, ensuring the desired torque and speed is maintained.

Figure 3.2 shows an example of a maximum power point tracking (MPPT) curve for a wind turbine. To keep the CWSC fractionally rated, the generator is designed to operate around ±30% rated speed. In the case of the example, the natural speed is $n_r = 360$ rotations per minute (rpm). Point A indicates the cut in speed of 252 (rpm) and point D shows the upper speed limit of 468 (rpm). Additionally it can be seen that the maximum power point can only be achieved between points B and C, where the wind speeds range from 4.65 to 8.64 meters per second.

3.2 Working Principle of the Brushless Doubly-fed Induction Machine

To understand the operation of the BDFIM, one can compare it to that of two three-phase rotor-tied electrically connected wound-rotor induction machines with differing pole pairs. Both machines' stators are typically supplied by sources with different frequencies, where the primary machine is supplied by a fixed three phase grid, and the secondary machine by an inverter. Due to the differing pole numbers, both machines have different synchronous speeds for the same supply frequencies. During simple induction mode, both machines can be operated at their own synchronous speeds, defined by their pole pairs p_1 or p_2 respectively. To achieve this, the corresponding machine stator winding can be excited, while leaving the latter machine stator winding open circuited.

During cascade induction mode, the non-supplied stator winding should be short circuited, resulting in a machine with combined characteristics from both machines and the addition of the primary and secondary stator winding pole pairs.

When both stator windings are supplied, this will be referred to as doubly fed mode and this allows for a synchronous mode of operation that the machine can be optimized for based on the user requirements. For synchronous and cascade induction modes of operation to occur, a cross coupling between the stator and rotor is required[50]. Finally, the BDFIM is simply a three-phase induction machine with a secondary pair of three phase windings on the stator. This results in a more compact machine with the exact same characteristics and modes of operation as defined above. Cross coupling will henceforth be implied as the field produced by stator one to stator two and vice-versa. For isolated control of the rotor using the secondary three-phase windings, typical BDFIMs

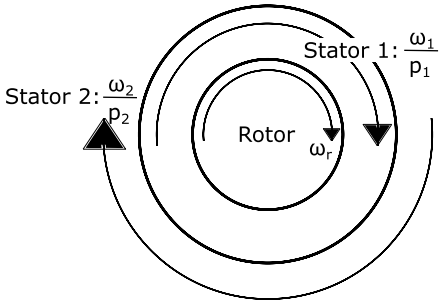

Figure 3.3: Direction of magnetic fields in a BDFIM

Stellenbosch University https://scholar.sun.ac.za

are designed to be non-coupled between the windings of stator one and two. In most cases, this simply means that stator one and two must have different numbers of pole pairs.

When supplying stator one with a three phase supply at w_1 (rad/s) then the air gap magnetic flux will rotate at w_1/p_1 (rad/s), as shown in Figure 3.3. Similarly when supplying stator two with a three phase supply at w_2 (rad/s) then the air gap magnetic flux will rotate at w_2/p_2 (rad/s).

In steady state, the rotor speed is defined as

$$\omega_r = \frac{\omega_1 + \omega_2}{p_1 + p_2} \tag{3.6}$$

where ω indicates the electrical rotational speed, p is the amount of pole pairs and subscripts r, 1 and 2 indicate the rotor, primary stator winding and secondary stator windings respectively. When the secondary winding is supplied by a DC source and thus at $\omega_2 = 0$, the machine will operate at natural speed

$$\omega_n = \frac{\omega_1}{p_1 + p_2} \tag{3.7}$$

3.3 Power Flow in BDFIG WECS Systems

The BDFIG consists of three main components for power flow. Mechanical input power from the rotor, active and reactive power input and output from the utility supply and finally real and reactive power input and output to and from the back-to-back converter. During operation as a wind generation system, the primary winding is synchronized with the grid. In order to keep the back-to-back converter at a reduced power rating, the majority of power supplied from the generator is produced from the primary winding. The secondary winding is then controlled using a control winding side controller (CWSC) through the back-to-back converter. This control is focused on maintaining power output on the primary winding, and can be used to maximize power output by using maximum power point tracking (MPPT) methods. This means that the BDFIG can both draw power to the control winding as well as supply power to the grid using the back to back converter. This occurs at super synchronous operation. The back to back converter uses a dc-bus to ensure that the grid side converter (GSC) and CWSC can operate at varying frequencies, allowing flexible power control on the CWS.

3.4 Modeling of the Brushless Doubly-fed Induction Generator

Various modeling techniques for machines have been developed in recent years. From finite element models to equivalent circuit models, the level of precision ranges according to the needs of the designer.

Finite element modeling provides numerical solutions with very detailed analysis of specific machines based on their physical properties and dimensions. This can be computationally intensive and time consuming [73].

Harmonic analysis has proven itself useful for steady state machine analysis as shown in [51]. By performing harmonic decomposition of the magnetic flux density and coupling between motor circuits, valuable insight can be made for machine design optimization

Stellenbosch University https://scholar.sun.ac.za

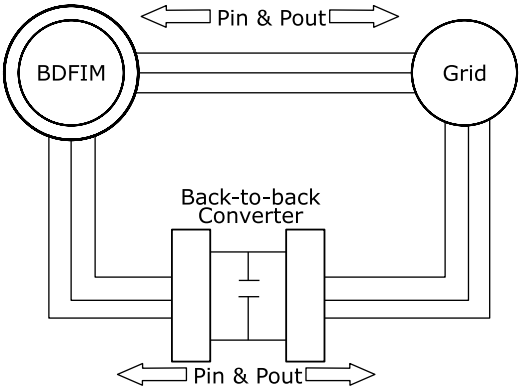

Figure 3.4: Direction of magnetic fields in a BDFIM

[74; 75]. Unfortunately, it is only useful to model stead state and as such is not useful for the dynamic modeling of the machine for the purposes of control[76].

Wallace et. al. and Spée et. al. used a dynamic coupled circuit technique to model a prototype BDFM[34; 77]. A generalized pole number model is presented in [78]. Furthermore the dynamic simulation and two axis (dq-axis) model was also further developed and presented in [79; 80].

In [15] Roberts proposes an extension to the works done by Boger[14]. A method whereby a full state model of the BDFIM is developed and mapped down to an equivalent two-axis model while retaining as much of the machines characteristics as possible, making it suitable for control purposes. Even though it is clear that the technique is suitable for various different rotor types, including bar-cage rotors, no experimental results are shown for the use of the method when applied to a bar-cage rotor.

Thus, using the methods proposed in [15], a dq-equivalent model of an experimental bar-cage rotor will be obtained and compared using simulations and experimental verification.

3.4.1 General Coupled Circuit Model of BDFIM

A BDFIM consists of dual three-phase stator windings and a rotor, where in this particular case a bar-cage topology is considered. The bar-cage can be partitioned into an equivalent circuit as shown in 3.5. Each circuit here has a voltage potential (V) over the span of the circuit, a current (I) flowing through the circuit, and a resulting flux (ϕ) linked to each circuit. Resulting in a combination of Faraday and Ohm's law

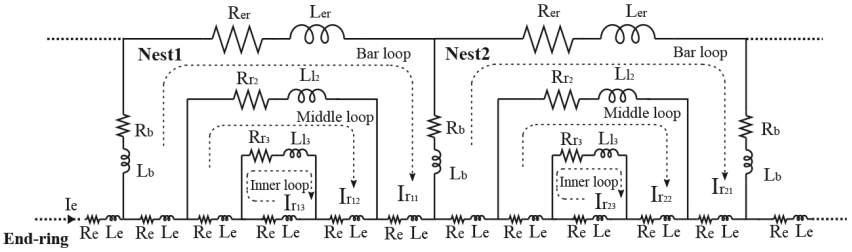

Figure 3.5: BDFIM bar cage rotor equivalent circuit[81]

Stellenbosch University https://scholar.sun.ac.za

$$\mathbf{v} = \mathbf{R}\mathbf{i} + \frac{d\boldsymbol{\phi}}{dt} \tag{3.8}$$

where R represents the individual circuit resistances.

By further noting that magnetic flux in a coil can be expressed as $\phi = Mi$, where M represents the inductance and i the current flowing through the circuit. This allows for (3.8) to be rewritten by use of the chain rule as

$$\mathbf{v} = \mathbf{R}\mathbf{i} + \frac{d\mathbf{M}}{dt}i + \mathbf{M}\frac{d\mathbf{i}}{dt} \tag{3.9}$$

Since the mutual inductance can be assumed to vary with rotational angle θ_r and by defining the rotor mechanical speed ω_r as the rate of change in mechanical rotor shaft position θ_r

$$\omega_r = \frac{d\theta_r}{dt} \tag{3.10}$$

Then (3.9) can be expressed in terms of rotor position

$$\mathbf{v} = \mathbf{R}\mathbf{i} + \omega_r\frac{d\mathbf{M}}{d\theta_r}\mathbf{i} + \mathbf{M}\frac{d\mathbf{i}}{dt} \tag{3.11}$$

By solving according to the differential of the currents, a state space representation of the machine equations can be shown where the currents represent the system states.

$$\mathbf{M}\frac{d\mathbf{i}}{dt} = -\mathbf{R}\mathbf{i} - \omega_r\frac{d\mathbf{M}}{d\theta_r}\mathbf{i} + \mathbf{v} \tag{3.12}$$

3.4.1.1 Mechanical Model

The electrical differential equations of the machine can be coupled to the mechanical differential equations by use of the electro-magnetic torque developed by the machine. With the magnetic co-energy defined as the stored energy in the magnetic field of a coupled circuit network

$$W_{co} = \frac{1}{2}\mathbf{i}^T\mathbf{M}\mathbf{i} \tag{3.13}$$

The instantaneous power transfer from the magnetic field is given by

$$\frac{dW_{co}}{dt} = \frac{1}{2}\frac{d\mathbf{i}^T}{dt}\mathbf{M}\mathbf{i} + \frac{1}{2}\mathbf{i}^T\frac{d\mathbf{M}}{dt}\mathbf{i} + \frac{1}{2}\mathbf{i}^T\mathbf{M}\frac{d\mathbf{i}}{dt} \tag{3.14}$$

As $\frac{dW_{co}}{dt}$ is a scalar and $\mathbf{M} = \mathbf{M}^T$, this simplifies to

$$\frac{dW_{co}}{dt} = \frac{1}{2}\mathbf{i}^T\frac{d\mathbf{M}}{dt}\mathbf{i} + \mathbf{i}^T\mathbf{M}\frac{d\mathbf{i}}{dt} \tag{3.15}$$

By subsitution of (3.10) into (3.11) and multiplying by $\mathbf{i}^T$ results in

$$\mathbf{i}^T\mathbf{v} = \mathbf{i}^T\mathbf{R}\mathbf{i} + \mathbf{i}^T\frac{d\mathbf{M}}{dt}\mathbf{i} + \mathbf{i}^T\mathbf{M}\frac{d\mathbf{i}}{dt} \tag{3.16}$$

$$= \mathbf{i}^T\mathbf{R}\mathbf{i} + \omega_r\frac{1}{2}\mathbf{i}^T\frac{d\mathbf{M}}{d\theta_r}\mathbf{i} + \frac{dW_{co}}{dt} \tag{3.17}$$

Stellenbosch University https://scholar.sun.ac.za

By inspection it can be seen that the theoretical electrical torque generated by the machine can be obtained, noting that the individual components in (3.17) are

$$\underbrace{\mathbf{i}^T\mathbf{v}}_{Input\ Power} = \underbrace{\mathbf{i}^T\mathbf{R}\mathbf{i}}_{Ohmic\ Power\ Loss} + \underbrace{\omega_r \frac{1}{2}\mathbf{i}^T\frac{d\mathbf{M}}{d\theta_r}\mathbf{i}}_{Mechanical\ Power} + \underbrace{\frac{dW_{co}}{dt}}_{Magnetic\ Field\ Power} \tag{3.18}$$

where $\mathbf{i}^T\mathbf{v} = \mathbf{i}^T\mathbf{R}\mathbf{i}$, meaning that the mechanical torque can be defined as

$$T_e = \frac{P_m}{\omega_r} = \frac{1}{2}\mathbf{i}^T\frac{d\mathbf{M}}{dt}\mathbf{i} = \frac{dW_{co}}{d\theta_r} \tag{3.19}$$

3.4.2 BDFIM Modeling in full-state frame

The BDFIM with a cage rotor can be a complex machine to model for purposes of control analysis. Especially when using a cage rotor, measurement of the machine parameters require creative methods since standard RL-meters can no longer be used to provide a phase resistance or inductance. Considering the structure of the BDFIM rotor, an equivalent reduction method is necessary to reduce the rotor frames down to an equivalent ABC frame, and further to a dq-frame for control analysis. This makes it possible to simulate the machine dynamic characteristics with greater mechanical insight and in more reasonable periods of time.

In order to evaluate the effectiveness of the reduced model, a full state model is required. It will also be shown in chapter 6 through experimental verification, that this model is an adequate representation of the BDFIM machine.

In order to reduce the BDFIM states, various models have been proposed. Such as the model for nested loop rotors recommended by Boger[14]. It has further been shown through simulation and experimental verification that certain machine characteristics such as torque harmonics may not always be retained in the method proposed. As such Roberts suggested a method aimed at a wider scope of rotor typologies which should retain as many of the machine characteristics as possible. Including that of a bar cage induction machine. In his works however the method was only applied to a nested loop rotor, and as such it is imperative that an experimental implementation of the proposed method be evaluated[15].

3.4.2.1 BDFIM Coupled Circuit Model

In general, the coupled circuit model of the BDFIM consists of a primary and secondary stator winding, indicated by subscripts 1 and 2. The rotor is referenced to by the subscript r. For a general BDFIM, s_1 and s_2 would be supplied by 4 wires each (3 phases + neutral).

$$v \triangleq \begin{bmatrix} v_{s1} \\ v_{s2} \\ v_r \end{bmatrix}, i \triangleq \begin{bmatrix} i_{s1} \\ i_{s2} \\ i_r \end{bmatrix} \tag{3.20}$$

Thus, the expanded form for the BDFIM components of the stator and rotor, where x can be defined as the voltage v or current i would be:

$$x_{sj} = \begin{bmatrix} x_{sj}^a \\ x_{sj}^b \\ x_{sj}^c \\ x_{sj}^N \end{bmatrix}, x_r = \begin{bmatrix} x_r^1 \\ \dots \\ \dots \\ x_r^n \end{bmatrix} \tag{3.21}$$

Stellenbosch University https://scholar.sun.ac.za

Here phases a, b and c are defined by a, b, c respectively, neutral is N. Furthermore n is defined as the number of circuits in the cage rotor structure and consists of N sets of S rotor circuits.

$$S = p_1 + p_2 \tag{3.22}$$

Finally the full state machine model can be defined as:

$$\begin{bmatrix} v_{s1} \\ v_{s2} \\ v_r \end{bmatrix} = \left(\begin{bmatrix} R_{s1} & 0 & 0 \\ 0 & R_{s2} & 0 \\ 0 & 0 & R_r \end{bmatrix} + \omega_r \begin{bmatrix} 0 & 0 & \frac{dM_{s1r}}{d\theta_r} \\ 0 & 0 & \frac{dM_{s2r}}{d\theta_r} \\ \frac{dM_{s1r}}{d\theta_r} & \frac{dM_{s2r}}{d\theta_r} & 0 \end{bmatrix} \right) \begin{bmatrix} i_{s1} \\ i_{s2} \\ i_r \end{bmatrix} + \begin{bmatrix} M_{s1} & 0 & M_{s1r} \\ 0 & M_{s2} & M_{s2r} \\ M_{s1r}^T & M_{s2r}^T & M_r \end{bmatrix} \begin{bmatrix} i_{s1} \\ i_{s2} \\ i_r \end{bmatrix} \tag{3.23}$$

Where R is the resistance, ω the angular speed in rad/s, θ_r is the position of the rotor, M_{si} and M_r the constant mutual inductance of the stator and rotor respectively, and M_{sir} defines the mutual inductance between the respective stator and rotor, as a function of rotor position.

The electrical torque T_e produced by such a circuit can be derived from 3.19 which results in

$$\begin{aligned} T_e &= \frac{1}{2} \begin{bmatrix} i_{s1}^T & i_{s2}^T & i_r^T \end{bmatrix} \begin{bmatrix} 0 & 0 & \frac{dM_{s1r}}{d\theta_r} \\ 0 & 0 & \frac{dM_{s2r}}{d\theta_r} \\ \frac{dM_{s1r}}{d\theta_r} & \frac{dM_{s2r}}{d\theta_r} & 0 \end{bmatrix} \begin{bmatrix} i_{s1} \\ i_{s2} \\ i_r \end{bmatrix} \\ &= \begin{bmatrix} i_{s1}^T & i_{s2}^T \end{bmatrix} \begin{bmatrix} \frac{dM_{s1r}}{d\theta_r} \\ \frac{dM_{s2r}}{d\theta_r} \end{bmatrix} \begin{bmatrix} i_r \end{bmatrix} \end{aligned} \tag{3.24}$$

Additionally the mechanical equations can be related to the electrical components by:

$$J\frac{d\omega_r}{dt} = T_e - T_l - b\omega_r \tag{3.25}$$

where the machine inertia is represented by J, friction is shown as b and the load torque by T_l.

By combining equations 3.23, 3.24 and 3.25 a complete state-space representation of the dynamics of a BDFIM can be obtained. With the currents of each individual circuit, speed and position forming the state vectors.

$$\frac{d}{dt} \begin{bmatrix} i_{s1} \\ i_{s2} \\ i_r \\ \theta_r \\ \omega_r \end{bmatrix} = \begin{bmatrix} \left[\left\{ - \begin{bmatrix} R_{s1} & 0 & 0 \\ 0 & R_{s2} & 0 \\ 0 & 0 & R_r \end{bmatrix} - \omega_r \begin{bmatrix} 0 & 0 & \frac{dM_{s1r}}{d\theta_r} \\ 0 & 0 & \frac{dM_{s2r}}{d\theta_r} \\ \frac{dM_{s1r}}{d\theta_r} & \frac{dM_{s2r}}{d\theta_r} & 0 \end{bmatrix} \right\} \begin{bmatrix} i_{s1} \\ i_{s2} \\ i_r \end{bmatrix} + \begin{bmatrix} v_{s1} \\ v_{s2} \\ v_r \end{bmatrix} \right] \\ \omega_r \\ \frac{1}{J} \left(\begin{bmatrix} i_{s1}^T & i_{s2}^T \end{bmatrix} \begin{bmatrix} \frac{dM_{s1r}}{d\theta_r} \\ \frac{dM_{s2r}}{d\theta_r} \end{bmatrix} \begin{bmatrix} i_r \end{bmatrix} - T_l \right) \end{bmatrix} \tag{3.26}$$

While equation 3.26 above is a nonlinear state space, where parameters θ_r and ω_r form part of the system states of the full system, while forming dependents of the current

Stellenbosch University https://scholar.sun.ac.za

parameters i_s and i_r in the system parameter. From this it is important to note that the dependence of the system states on the rotor position θ_r can be particularly problematic in order to perform control. As discrete and accurate measurement or estimation of the rotor position is crucial for effective control. Especially when noting that the torque equation is quadratic in currents i which is dependent on rotor speed ω_r and position θ_r, as such it is easy to see how inaccurate measurements / estimations of the machine's position can result in vastly inaccurate state estimations.

3.4.3 BDFIM Modeling in dq0-reference frame

However accurate the model presented in 3.4.2.1 may be, it provides little insight into the machine for control purposes. It is as such necessary to reduce the model to an equivalent dq0-reference frame model. This is done using the methods suggested by Roberts where the original rotor states are reduced to a rotating dq0 reference frame using reduction techniques, effectively mapping the original physical parameters to theoretical equivalent vectors on the new reference axis, while attempting to retain as many of the key characteristics of the full state machine[15].

3.4.3.1 Transformation Matrix

For a stator winding with p pole pairs, the $dq0$-transformation can be derived by the transformation matrix:

$$C_{si} = \sqrt{\frac{2}{3}} \begin{bmatrix} cos(p_i\theta_r) & cos(p_i(\theta_r - \frac{2\pi}{3p_i})) & cos(p_i(\theta_r - \frac{4\pi}{3p_i})) \\ sin(p_i\theta_r) & sin(p_i(\theta_r - \frac{2\pi}{3p_i})) & sin(p_i(\theta_r - \frac{4\pi}{3p_i})) \\ \frac{1}{\sqrt{2}} & \frac{1}{\sqrt{2}} & \frac{1}{\sqrt{2}} \end{bmatrix} \tag{3.27}$$

Where i represents the primary or secondary stator windings 1 or 2.

Due to the rotor matrix not being a square, and thus invertable matrix, it requires a similarity transformation. To achieve this, the transformation matrix has to be square, which allows for the transformation to retain all the machine dynamics. While this does not reduce the system states, further analysis will show that by careful selection of certain state parameters, the dominant characteristics can be retained with minimal loss of accuracy.

As such, the full rank transformation matrix for a single set of loops is defined as:

$$C_r = \begin{bmatrix} C_{r1} \\ C_{\underset{r1}{\perp}} \end{bmatrix} \tag{3.28}$$

Where $C_{\underset{r1}{\perp}}$ is a matrix with rows orthonormal and that span the orthogonal compliment to the row space of C_{r1}. The full rotor $dq0$-transformation can then accordingly be defined as an orthogonal matrix of which the defining rotor has N sets of S rotor circuits as defined in 3.22.

$$C_r^N = \begin{bmatrix} \begin{bmatrix} C_{r1} \\ C_{\underset{r1}{\perp}} \end{bmatrix} & 0 & 0 \\ 0 & \ddots & 0 \\ 0 & 0 & \begin{bmatrix} C_{rN} \\ C_{\underset{rN}{\perp}} \end{bmatrix} \end{bmatrix} \tag{3.29}$$

Stellenbosch University https://scholar.sun.ac.za

Finally the non-square transformation matrix C_{r1} into the equivalent $dq0$-components used in 3.29 above is:

$$C_{r1} = \sqrt{\frac{2}{p_1+p_2}} \begin{bmatrix} cos(0) & cos(\frac{2\pi p_1}{p_1+p_2}) & cos(\frac{2\pi 2p_1}{p_1+p_2}) & \dots & cos(\frac{2\pi(p_1+p_2-1)p_1}{p_1+p_2}) \\ sin(0) & sin(\frac{2\pi p_1}{p_1+p_2}) & sin(\frac{2\pi 2p_1}{p_1+p_2}) & \dots & sin(\frac{2\pi(p_1+p_2-1)p_1}{p_1+p_2}) \\ \frac{1}{\sqrt{2}} & \frac{1}{\sqrt{2}} & \frac{1}{\sqrt{2}} & \dots & \frac{1}{\sqrt{2}} \end{bmatrix} \tag{3.30}$$

By using 3.27 and 3.29 above an overall full state transformation matrix may be defined as

$$C = \begin{bmatrix} C_{s1} & 0 & 0 \\ 0 & C_{s2} & 0 \\ 0 & 0 & C_r^N \end{bmatrix} \tag{3.31}$$

3.4.3.2 Transformation into dq0-space

In order to obtain an equivalent dq0-state-space model, various phases of transformation and reduction techniques are followed. By transforming the full state model as defined in 3.26 to the dq0-equivalent for a machine such as the one considered in this dissertation. Consisting of 2 primary and 3 secondary pole pairs as well as a bar cage rotor with 5 nests, each containing three loops. This model would require a total of 23 system states in order to be an accurate representation of the described machine.
When transformed to its dq0-equivalent representation by using the transformation matrices discussed in chapter 3.4.3.1 above, the new dq0-rotor reference frame model consists of 23-states. However, the unobservable rotor circuits can be removed reducing the rotor states from 15 to 8. If the zero sequence components of the rotor and stator circuits are to be ignored as well - as can be done for balanced circuits such as the ones being considered due to a balanced phase voltage feed. As such the resulting system describing the equivalent full-state dq-model in the rotor reference frame will consist of merely 4 stator, 6 rotor and 2 mechanical circuits, a total of 12 system states. Keeping this in mind, in order to achieve this result, the following derivation is performed as Roberts shows with greater detail in [15].

Considering that the general coupled circuit model defined in 3.23 may also be defined as follows

$$\begin{bmatrix} v_{s1} \\ v_{s2} \\ v_r \end{bmatrix} = \begin{bmatrix} R_{s1} & 0 & 0 \\ 0 & R_{s2} & 0 \\ 0 & 0 & R_r \end{bmatrix} \begin{bmatrix} i_{s1} \\ i_{s2} \\ i_r \end{bmatrix} + \frac{d}{dt} \left(\begin{bmatrix} M_{s1} & 0 & M_{s1r} \\ 0 & M_{s2} & M_{s2r} \\ M_{s1r}^T & M_{s2r}^T & M_r \end{bmatrix} \begin{bmatrix} i_{s1} \\ i_{s2} \\ i_r \end{bmatrix} \right) \tag{3.32}$$

Further noting that the transformation of the currents into the dq0-plane is defined as

$$\begin{bmatrix} i_{s1}^{dq0} \\ i_{s2}^{dq0} \\ i_r^{dq0} \end{bmatrix} \triangleq \begin{bmatrix} C_{s1} & 0 & 0 \\ 0 & C_{s2} & 0 \\ 0 & 0 & C_r^N \end{bmatrix} \begin{bmatrix} i_{s1} \\ i_{s2} \\ i_r \end{bmatrix} \tag{3.33}$$

where i_s with no superscript should be noted as the current in the full state model. This accordingly allows for the transformation from the $dq0$-plane to the full state plane as

$$\begin{bmatrix} i_{s1} \\ i_{s2} \\ i_r \end{bmatrix} \triangleq \begin{bmatrix} C_{s1} & 0 & 0 \\ 0 & C_{s2} & 0 \\ 0 & 0 & C_r^N \end{bmatrix}^T \begin{bmatrix} i_{s1}^{dq0} \\ i_{s2}^{dq0} \\ i_r^{dq0} \end{bmatrix} \tag{3.34}$$

Stellenbosch University https://scholar.sun.ac.za

Similarly the voltage transformations are defined by

$$\begin{bmatrix} v_{s1}^{dq0} \\ v_{s2}^{dq0} \\ v_r^{dq0} \end{bmatrix} \triangleq \begin{bmatrix} C_{s1} & 0 & 0 \\ 0 & C_{s2} & 0 \\ 0 & 0 & C_r^N \end{bmatrix} \begin{bmatrix} v_{s1} \\ v_{s2} \\ v_r \end{bmatrix} \tag{3.35}$$

After applying the transformations of (3.33)-(3.35) to (3.33) as is shown in [15] an equivalent full state dq-model for a general rotor BDFIM may be obtained as

$$\frac{d}{dt} \begin{bmatrix} i_{s1}^{dq0} \\ i_{s2}^{dq0} \\ i_r^{dq0} \end{bmatrix} = (\boldsymbol{M}^{dq0})^{-1} \left((-\boldsymbol{R}^{dq0} - \omega_r \boldsymbol{Q}^{dq0}) \begin{bmatrix} i_{s1}^{dq0} \\ i_{s2}^{dq0} \\ i_r^{dq0} \end{bmatrix} + \begin{bmatrix} v_{s1}^{dq0} \\ v_{s2}^{dq0} \\ 0 \end{bmatrix} \right) \tag{3.36}$$

Where the sub-matrices can be found in the appendix A.2. Accordingly the electrical torque can be shown to be

$$T_e = \begin{bmatrix} i_{s1}^{dq0} \\ i_{s2}^{dq0} \end{bmatrix}^T \begin{bmatrix} Q_{sr1}^{dq0} \\ Q_{sr2}^{dq0} \end{bmatrix} i_r^{dq0} \tag{3.37}$$

In order to visualize the effects that the transformations have on the equivalent model throughout this dissertation, simulations are developed throughout - using parameters of an experimental machine for comparison. Figure 3.6 below is a comparison of the bar currents in the middle loop of a single nest of two different BDFIM models. The first being full 23 state coupled circuit model from equation 3.26 and the second being the equivalent 15 state $dq0-$model. The machine parameters used here is the same as the parameters used in the experimental machine which can be found in appendix B.2.

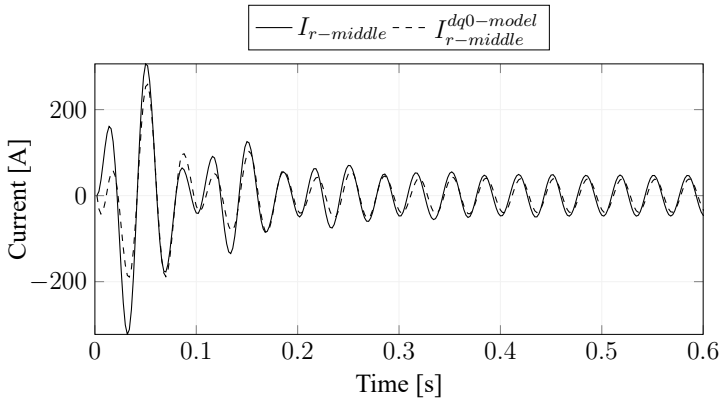

Figure 3.6: BDFIM full state frame middle loop currents compared to the dq0 equivalent model during zero initial current startup natural speed

3.4.3.3 Component selection for reduced order model

For control purposes it is convenient to have a reduced order representation of the BDFIM with a single dq-rotor pair. By simply truncating the model developed in 3.4.3.2 can result in a poor representation of the original model. It is also clear from chapter 3.4.2.1 that the electrical equations for the BDFM are linear. Unfortunately, due to the system not being time invariant in nature, reduction techniques for linear time invariant (LTI) systems such as balanced truncation and optimal Hankel-norm approximation are not suitable for

Stellenbosch University https://scholar.sun.ac.za

transient analysis[15]. Due to the system being dependent on rotational speed ω_r it can be said to be a linear parameter varying system (LPV), for which generalizations of the Hankel-norm or balanced truncation techniques exist as well, however for the physical interpretation of the machine to be maintained, techniques such as balanced truncation will have to be applied to each component individually. For instance the stator is already reduced and as such the technique should only be applied to the rotor. Therefore it is the objective to reduce the states of the rotor currents represented in 3.36 as

$$\frac{di_r}{dt} = -\left((\boldsymbol{M}^{dq})_r^{-1} R_r + \omega_r (\boldsymbol{M}^{\boldsymbol{dq}})_{sr}^{-1} Q_{sr}\right) i_r + u \tag{3.38}$$

where external stator currents and input voltage are represented by u. When applying the suitable reduction techniques, it becomes clear that it can be difficult to represent the balanced system in terms of mutual inductance, resistance and Q terms. As such the designer loses insight into the physical interpretation of the component matrices. As a solution to this, a method of reduction using equivalent circuit mapping is suggested in [15]. The method is suggested to be a good approximation for various rotor types, however it was only applied to nested loop type rotors. As such, it is the aim of this work to verify that the method stays true for different rotor types, such as the bar cage rotor analyzed in this dissertation.
In order to reduce the rotor states to two, a state order is chosen such as to order its eigenvalues in decreasing order from top left. To achieve this the following steps can be performed

1. A matrix $\boldsymbol{T}$ which consists of eigenvectors of $\boldsymbol{M}_r$ must be obtained and ordered such that its eigenvalues decrease from left to right.

2. $\boldsymbol{T}$ must be partitioned into two sub-matrices $\begin{bmatrix}\boldsymbol{T}_1 & \boldsymbol{T}_2\end{bmatrix}$ where T_1 is two columns wide.

3. Reduce the state order of the full state dq0-reference frame BDFIM model by applying the non-square state transformation

$$i^{dq0}_{ReducedState} = \begin{bmatrix}\boldsymbol{I} & 0\\ 0 & \boldsymbol{T}_1^T\end{bmatrix} i^{dq0}_{FullState} \tag{3.39}$$

   where $\boldsymbol{I} \in \mathbb{R}^{6\times 6}$ is an identity matrix

It can be noted that the transformation matrix $\boldsymbol{T}_1$ will always be of the form:

$$\boldsymbol{T}_1^T = \begin{bmatrix}\alpha_1 & 0 & \alpha_2 & 0 & \dots & \alpha_n & 0\\ 0 & \alpha_1 & 0 & \alpha_2 & \dots & 0 & \alpha_n\end{bmatrix} \tag{3.40}$$

From this, it is apparent that the resulting reduced state rotor matrix is merely an equivalently scaled representation of the original matrix. But by careful selection of its eigenvalues, can be reduced to retain as much of the original characteristics as possible. After the transformation has been applied, the final reduced order model can be shown to be:

$$\frac{d}{dt}\begin{bmatrix}i_s\\ \tilde{i_{r1}}\end{bmatrix} = \begin{bmatrix}M_s & \tilde{M_{sr1}}\\ \tilde{M_{sr1}}^T & \tilde{M_{r1}}\end{bmatrix}\left(-\left(\begin{bmatrix}R_s & 0\\ 0 & \tilde{R_{r1}}\end{bmatrix}\begin{bmatrix}Q_s & \tilde{Q_{sr1}}\\ 0 & 0\end{bmatrix}\right)\begin{bmatrix}i_s\\ \tilde{i_{r1}}\end{bmatrix} + \begin{bmatrix}v_s\\ 0\end{bmatrix}\right) \tag{3.41}$$

Here the reduced order matrices are over-set by tilde.

Stellenbosch University https://scholar.sun.ac.za

3.4.3.4 Transformation into the Synchronous Space

For control purposes it is advantageous to analyze the BDFIM in the synchronous reference plane. As will be shown later on the synchronous plane, however dependent on the rotational matrices allows for numerous simplifications, greatly reducing the complexity of the resulting control system.

As it has been shown that a greatly simplified model can be obtained through the methods outlined above in this chapter, it is now convenient to do an equivalent transformation from the rotor reference frame to the stator frame. In order to achieve this a synchronous transformation matrix with reference to the primary stator windings is defined:

$$\boldsymbol{T}_{sync}(\gamma) = \begin{bmatrix} cos(p_1\theta_r - w_1 t + \gamma) & sin(p_1\theta_r - w_1 t + \gamma) & 0 \\ -sin(p_1\theta_r - w_1 t + \gamma) & cos(p_1\theta_r - w_1 t + \gamma) & 0 \\ 0 & 0 & 1 \end{bmatrix} \tag{3.42}$$

For the purposes of this analysis γ is assumed to be zero, as stators 1 and 2 are chosen to be aligned within the synchronous reference frame. This relies on the assumption that stators 1 and 2 are physically aligned, which may not always be an accurate assumption. However the stators were aligned in this implementation.

By applying the transformation matrix to the rotor reference frame model defined. The synchronous reference frame model may now be derived to be:

$$\frac{d}{dt}\begin{bmatrix} i_{s1}^{dq0} \\ i_{s2}^{dq0} \\ i_r^{dqr} \\ \theta_r \\ \\ \omega_r \end{bmatrix} = \begin{bmatrix} \boldsymbol{M}_{sync}^{-1}\left(\left(-\boldsymbol{R}_{sync} - \boldsymbol{Q}_{sync}\right)\begin{bmatrix} i_{s1}^{dq0} \\ i_{s2}^{dq0} \\ i_r^{dqr} \end{bmatrix} + \begin{bmatrix} v_{s1}^{dq0} \\ v_{s2}^{dq0} \\ 0 \end{bmatrix}\right) \\ \omega_r \\ \frac{1}{2J}\begin{bmatrix} i_{s1}^{dq0} \\ i_{s2}^{dq0} \\ i_r^{dqr} \end{bmatrix}^T \boldsymbol{S}_{sync}\begin{bmatrix} i_{s1}^{dq0} \\ i_{s2}^{dq0} \\ i_r^{dqr} \end{bmatrix} - \frac{T_l}{J} \end{bmatrix} \tag{3.43}$$

The equivalent torque and sub-matrices used for the derivation can be found in appendix A.3.

The reduced models are now simulated and compared further. With the full 12-state model in the rotor reference frame, reduced 8 state rotor reference frame model and

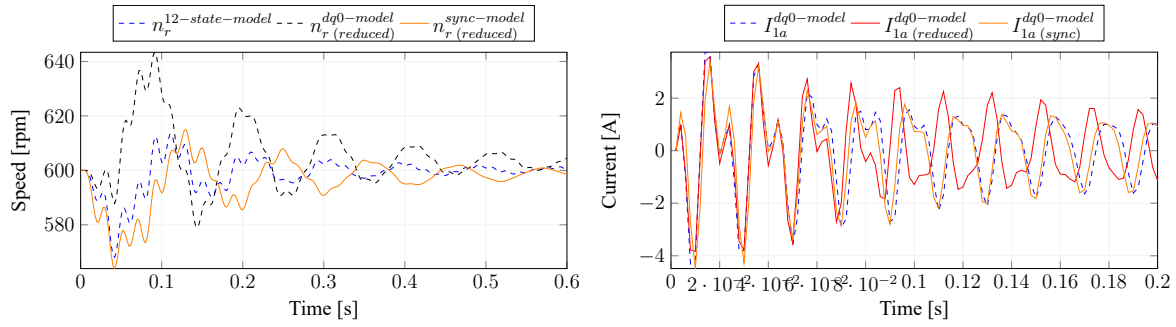

(a) Natural speed response **(b)** Phase a current response

Figure 3.7: BDFIM full state frame compared to dq0-rotor-reference-frame and dq0-reduced equivalent speed response to startup. Initial speed of the machine is 600 rpm with zero currents. Both stators are disconnected before t=0, and closed shortly after, resulting in a current being induced

Stellenbosch University https://scholar.sun.ac.za

equivalent 8 state synchronous frame model, separate simulink simulations are run and compared to show the responses starting at natural speed with zero initial currents. In Figure 3.7(a) it can be seen that all three simulations show responses in similar magnitude and period, with a slight phase offset. The similarities between the simulations are further shown in Figure 3.7(b) indicating very similar transient characteristics.

3.4.4 System equations of BDFIM model in dq-synchronous plane

The result obtained in section 3.4.3.4 is helpful for a state space design approach. However, to maintain insight into the various characteristics of the machine, a root-locus design approach will be followed for the vector control algorithm. As such an equivalent model, representing the various components of the machine is necessary and will be useful for the control design in chapter 4.4.1. Such a model will now be shown.

The brushless doubly fed induction machine equations in the dq reference frame are aligned to the stator flux rotating frame of the power winding. The control winding is transformed to the power winding reference frame through a park transformation where the power winding rotates at an angular speed defined in 3.45

$$x^{dq} = e^{-j[w_p t-(p_p+p_c)\theta_r]}{}^{*}x^{\alpha_c\beta_c} \tag{3.44}$$

$$w_p = 2\pi f_p \tag{3.45}$$

Here f_p is the feed frequency of the grid. The system equations are shown to be[48]

$$v_p = R_{sp}i_p + \frac{d\phi_p}{dt} + j\omega_p\phi_p \tag{3.46}$$

$$v_c = R_{sc}i_c + \frac{d\phi_c}{dt} + j\omega_c\phi_c \tag{3.47}$$

$$v_r = R_r i_r + \frac{d\phi_r}{dt} + j\omega_{Rp}\phi_r \tag{3.48}$$

$$\phi_p = L_{sp}i_p + L_{mp}i_r \tag{3.49}$$

$$\phi_c = L_{sc}i_c + L_{mc}i_r \tag{3.50}$$

$$\phi_r = L_r i_r + L_{mc}i_c + L_{mp}i_p \tag{3.51}$$

where v refers to voltage, i to current, L to inductance, ϕ is machine flux, ω is the angular speed of the power, control and rotor windings respectively and subscripts p, c, s and r represent the power winding, control winding, stator and rotor cage respectively and subscript m implies the mutual coupling between two windings. The angular frequency of the control winding as well as the angular slip frequency of the rotor to stator power winding is defined by

$$\omega_c = \omega_p - (p_p + p_c)\omega_r \tag{3.52}$$

$$\omega_{Rp} = \omega_p - p_p\omega_r \tag{3.53}$$

Stellenbosch University https://scholar.sun.ac.za

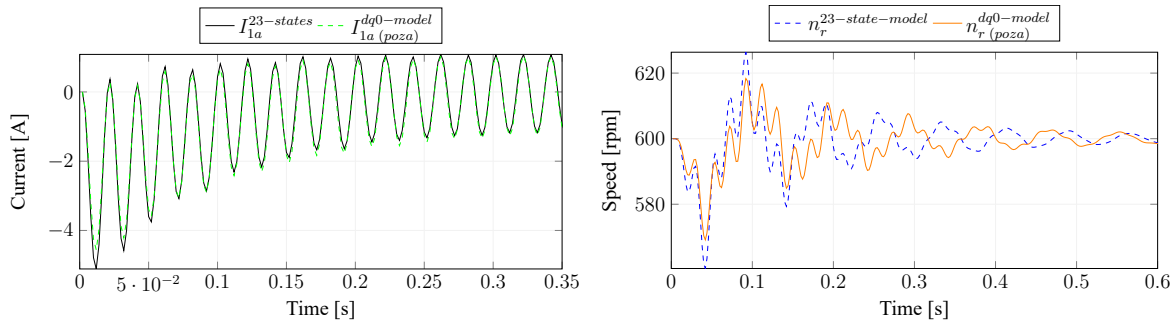

(a) Phase a current response **(b)** Speed response

Figure 3.8: BDFIM full state frame compared to dq0-synchronous reference frame at natural speeds and zero initial currents

The electro-mechanical equations can be stated as follows,

$$T_p = \frac{3}{2} p_p Im\{\overset{*}{\phi}_p i_p\} \tag{3.54}$$

$$T_c = \frac{3}{2} p_c Im\{\phi_c \overset{*}{i}_c\} \tag{3.55}$$

$$T_e = T_p + T_c \tag{3.56}$$

$$= \frac{3}{2}\left[p_p(\phi_p^d i_p^q - \phi_p^q i_p^d) + p_c L_{mc}(i_c^d i_r^q - i_c^q i_r^d)\right] \tag{3.57}$$

$$\frac{d\omega_r}{dt} = \frac{1}{J}(T_e - T_l - b\omega_r) \tag{3.58}$$

where J is the moment of inertia, b is the rotational friction coefficient, T_p and T_c is the torque produced by the primary and secondary winding respectively, ω is angular speed, T_e is the total electrical torque and T_l is the load torque. Superscripts ^{d} and ^{q} refer to the direct and quadrature axis respectively as will be discussed later in this synopsis.

To ensure the accuracy of the system equations, a Simulink model comparison is done. As is shown in Figure 3.8 it results in a very narrow approximation of the original expanded form response, indicating near identical transient responses.

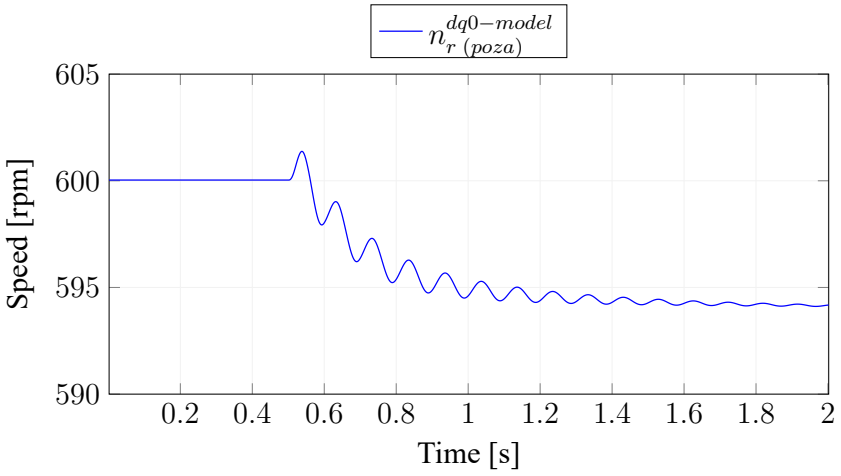

Figure 3.9: BDFIM control model response to V/Hz control

Stellenbosch University https://scholar.sun.ac.za

3.5 V/Hz Control

A simple method of speed control of the BDFIM can be performed using V/Hz control. During such control, a voltage varying at a proportional frequency is applied to the control winding while keeping the grid feed constant. In doing so the motor can be accelerated and decelerated within small stability margins. For the simulation speed response shown in Figure 3.9 the speed is changed from natural speed (600 rpm) to 594 rpm by applying a control winding voltage with frequency $f_c = -0.5$ Hz which correspondingly requires a voltage magnitude of

$$V_c = 0.7w_c = 3.14V, \tag{3.59}$$

$$w_c = 2\pi f_c \tag{3.60}$$

The a-phase voltages applied to the primary and secondary windings of the BDFIM stator can be seen in 3.10. The a-phase primary voltage here is $311V_{LN}$ in magnitude and rotates at a grid supply frequency of 50 Hz.

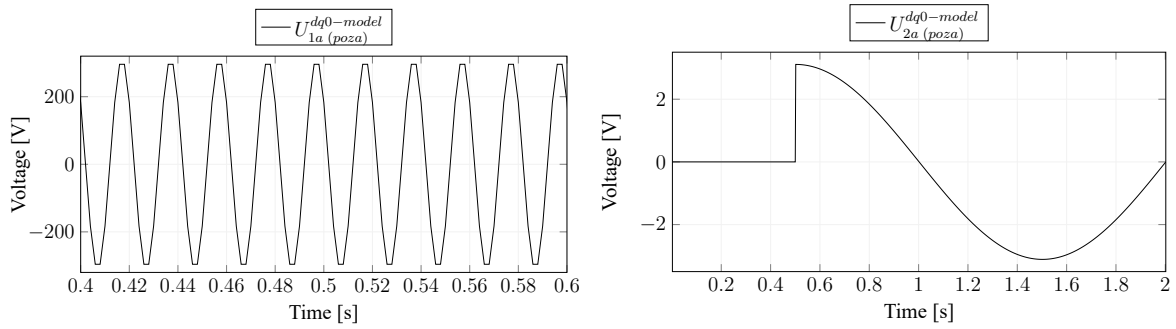

(a) Primary winding a-phase voltage **(b)** Secondary winding a-phase voltage

Figure 3.10: BDFIM control model input voltages for VHz control

3.6 Conclusion

To perform vector control on the BDFIM, an accurate model representation of the system is required. In this chapter, the energy flow starting at the potential energy in the wind, traveling through the mechanical rotor and being converted to electrical energy was discussed. Theoretical models of all of the states of energy flow were presented, starting at the aerodynamic model where wind energy is transformed into mechanical energy. This was followed by the mechanical model of the machine where input torque is converted to stator current, which flows directly to the grid for the primary winding and through the back to back converter to the grid for the secondary winding.

Furthermore a detailed couple circuit model of the BDFIM was presented. It was found that the presented model can be increasingly complex, and that a reduced order model is required. Accordingly an example of such a transformation process was presented, showing that a reduced order model for a bar cage rotor BDFIM could be achieved. Throughout the transformation simulation comparisons were shown, indicating the validity of the transformations. Finally a synchronous reference frame model was presented, and it was decided that this model be used for the vector control analysis to be performed in chapter 4.

Stellenbosch University https://scholar.sun.ac.za

Chapter 4

Back to back converter Control

The fractionally rated back-to-back converter, can be a major advantage for DFIG systems and in many aspects, is the heart of the control system. With a dc-bridge used to transform the asynchronous secondary winding frequencies for the BDFIM stator to synchronous grid frequencies, allowing power flow to and from the stator to the grid. To achieve this a two-part control system is required. The first being grid side control, where the AC grid currents are converted into DC currents and vice versa. The second portion is the control winding side controller (CWSC). The control thereof is significantly more complex, requiring an in depth knowledge of the BDFIM's transient behavior. To ensure that the output voltages of the controllers are as expected, a switching technique called space vector pulse width modulation (SVPWM) is used. This method of modulation is briefly discussed. For all of these control systems a design analysis will be shown throughout this chapter, as well as simulation test results of the CWSC. In doing insight can be gained into the experimental controller. As well as the viability of the assumptions made for the reduction techniques in chapter 3.

4.1 Grid/Load Side Converter Control

To give a thorough overview of the control of the BDFIM it is necessary to fully cover the workings of the back-to-back converter. To achieve this, a conventional control method

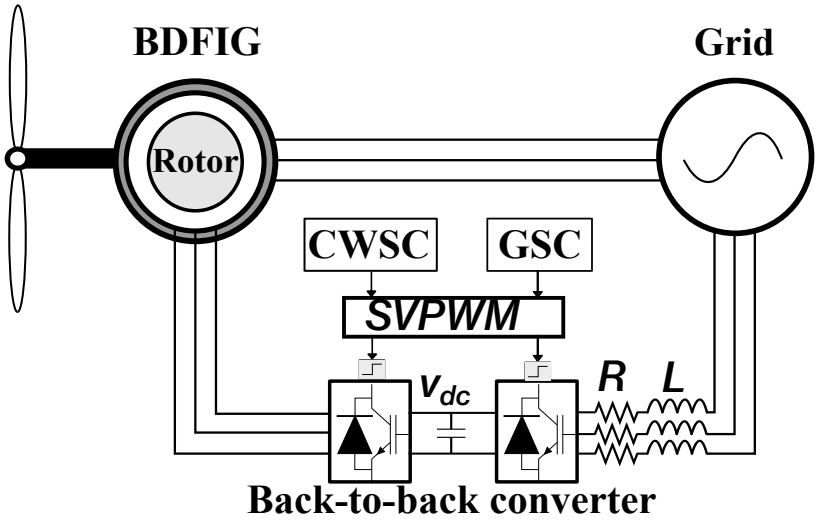

Figure 4.1: Back to back converter

Stellenbosch University https://scholar.sun.ac.za

for the GSC will be shown. Since there is no difference in the operation of the GSC for BDFIM's when compared to DFIG's or other applications where a stable dc-link voltage is required for AC-power conversion purposes. It is beyond the scope of the works in this dissertation to show the practical operation thereof. As such, a stable DC supply is adequate for the operation of the CWSC.

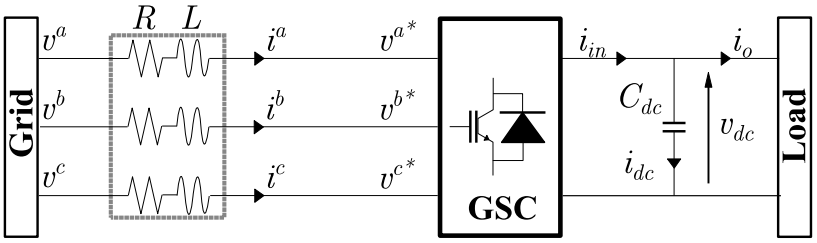

Figure 4.2: Inverter ac to dc power transfer

4.2 GSC Configuration

The grid side controller's purpose is to ensure that 3-phase AC power can be converted to single phase DC power and vice versa. This allows bidirectional power flow through the inverter. To achieve this, vector control is used to monitor the DC-link voltage, drawing current in to charge the DC capacitor when its' voltage is too low and equivalently discharging power to the AC side when the DC voltage is too high.

As the inverter output typically consists of a bridge of insulated gate bipolar transistors (IGBT's) or thyristors and the grid is considered purely sinusoidal without internal impedance, it is important that the inverter switching AC-output be filtered to reduce unwanted harmonics to the grid. These filters need to comply with the IEEE standard 519-2014 for grid-integration purposes, which states that the total harmonic distortion produced from the voltage source converter (VSC) may only inject a sinusoidal wave with less than 8% total harmonic distortion (THD). Usually manufacturers use passive filters with their VSC's for this purpose[82].

4.2.1 Filter Types

Various types of filters are used on the output of inverters. Ranging from L-filters to LC-filters to LCL-filters, each have their own advantages and disadvantages. Crucially for LCL-filters their costs for production are generally lower, having a smaller inductor size when compared to an L-filter of the same performance.

Different design approaches have also been developed for LCL-filters. Studies show approaches to design these filters based on the power rating of the VSC with frequency ranges ten times that of the line frequency and one-half of the switching frequency. Another approach aims to implement the design with a multi-objective optimization approach. Further methods to minimize the physical filter size are also suggested. Whereas another design is based on a LCL filter with a resonant frequency higher than the Nyquist frequency[83; 84; 85; 86].

All of the designs above show good performance, however, focus on switching frequencies ranging between 5 kHz and 15 kHz. For the inverter used in this dissertation, a

Stellenbosch University https://scholar.sun.ac.za

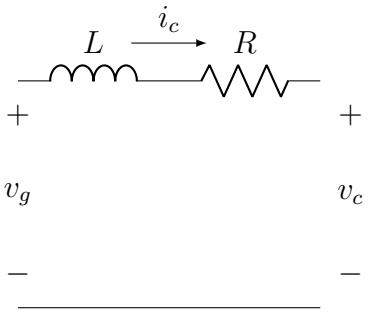

Figure 4.3: RL Filter open circuit

maximum switching frequency of 5 kHz is achievable. As such, a filter designed for less than this frequency is necessary. In [87], an analysis of the design for such a filter has been thoroughly reviewed and analyzed. In the study, a design for an L filter as well as LCL filter with switching frequencies well below 5 kHz was presented and compared. The LCL filter was shown to perform slightly better than the L filter. Additionally a dc-link controller for a VSC with a filter of this type was presented, showing good performance under various dynamic conditions. For this research, the design of such filters are inconsequential. As such an L-filter will be sufficient for the purposes of this control and one such design is now presented.

4.2.2 L Filter Modeling

The mathematical model for an L filter can be derived from the single phase circuit in Figure 4.3, which results in the following voltage equation

$$v_g = Ri_g + L\frac{di_c}{dt} + v_c \tag{4.1}$$

where v_g and v_c depict the grid and converter voltages respectively. The line resistance is shown by R and line inductance by L. When assuming that only the converter is a source of harmonic components in the system, the system transfer function can be derived from 4.1 above as

$$H_l(s) = \frac{i_c}{v_c} = \frac{1}{Ls + R} \tag{4.2}$$

where $H_l(s)$ is the transfer function of the filter and the frequency domain is indicated by using s-plane notation. Furthermore by assuming a higher frequency $L_T^2\omega_h^2 >> R_T^2$ the

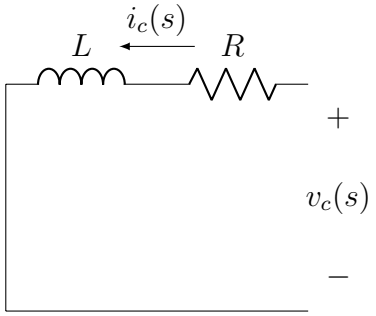

Figure 4.4: RL Filter circuit

Stellenbosch University https://scholar.sun.ac.za

filter attenuation is given by

$$|H_l(j\omega_h)| \approx \frac{1}{\sqrt{L_T^2\omega_h^2}} \tag{4.3}$$

where $H_l(j\omega_h)$ denotes the L filter attenuation and w_h is the angular speed at the harmonic frequency

4.2.3 Grid Side Converter

To maintain a constant dc-link voltage for the control side controller (CSC) the grid side controller (GSC) needs to be adequately sized. For general applications, wind turbines experience speed fluctuations of up to ±30% of their synchronous speed. Thus it is chosen that the converter should be one third the rating of the generator, allowing speed variations of ±33% [88]. To further perform decoupled control of the reactive power and maintain a constant dc-link voltage, the model used to develop the vector controller is now discussed.

The whole converter circuit including the final controller block diagram is shown in Fig. 4.2. From this circuit the voltage equations can be derived using KVL,

$$\begin{bmatrix} v^a \\ v^b \\ v^c \end{bmatrix} = (R + L\frac{d}{dt}) \begin{bmatrix} i^a \\ i^b \\ i^c \end{bmatrix} + \begin{bmatrix} v^{a*} \\ v^{b*} \\ v^{c*} \end{bmatrix} \tag{4.4}$$

Converting to the dq-reference frame and aligning with the direct axis of the grid voltage space vector, the following equations are obtained in the synchronous reference frame[89]

$$\begin{bmatrix} v^d \\ v^q \end{bmatrix} = \underbrace{(R + L\frac{d}{dt}) \begin{bmatrix} i^d \\ i^q \end{bmatrix}}_{v^{dq'}} + \omega_p L \begin{bmatrix} -i^q \\ i^d \end{bmatrix} + \begin{bmatrix} v^{d*} \\ v^{q*} \end{bmatrix} \tag{4.5}$$

where w_p is the electrical frequency of the power winding. By rearranging (4.5), the command signals for the GSC are obtained

$$v^{d*} = -v^{d'} + (w_p L i^q + v^d)$$
$$v^{q*} = -v^{q'} - w_p L i^d$$

The equivalent control strategy is shown in Fig.4.6. Furthermore the transfer function for the current control loops are obtained as

$$H_i(s) = \frac{i^{dq}(s)}{v^{dq'}(s)} = \frac{1}{Ls + R} \tag{4.6}$$

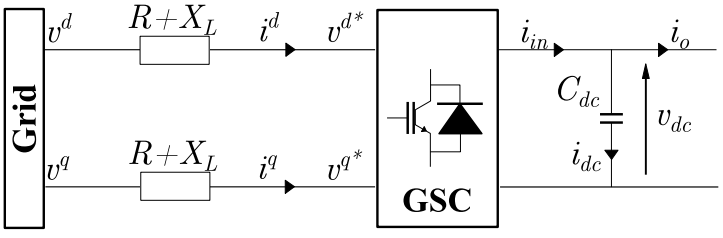

Figure 4.5: Inverter ac to dc power transfer dq

Stellenbosch University https://scholar.sun.ac.za

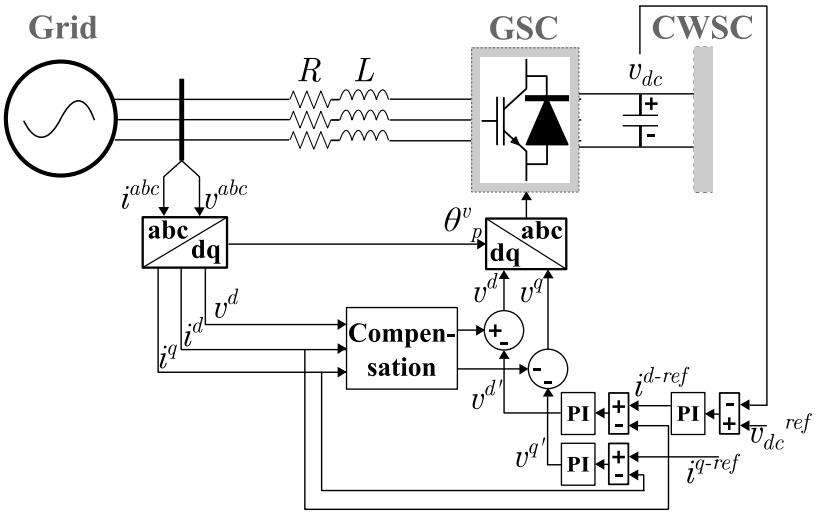

Figure 4.6: Grid side converter block diagram

If the synchronous reference frame is aligned with the d-axis of the grid supply voltage vector, the active (P) and reactive (Q) power of the system is

$$P = \frac{3}{2} v^d i^d \tag{4.7}$$

$$Q = -\frac{3}{2} v^d i^q \tag{4.8}$$

Further, from the law of conservation of energy, the dc power can be shown to be proportionally equal to the magnitude of the voltage and currents on the ac side

$$v_{dc} i_{in} = \frac{3}{2} v^d i^d \tag{4.9}$$

Additionally the input voltage into the converter is proportional to the DC output-voltage with a modulation index constant m_a, where

$$v^d = \frac{m_a}{2\sqrt{2}} v_{dc} \tag{4.10}$$

It follows that a relation between the ac-side input current and dc-side output current can be derived

$$i_{in} = \frac{3 m_a}{4\sqrt{2}} i^d \tag{4.11}$$

$$i_{dc} = i_{in} - i_o = C \frac{dv_{dc}}{dt} \tag{4.12}$$

This is shown in an equivalent circuit in Figure 4.5. By treating the output current i_o as a negligible disturbance, a transfer function for the voltage loop is derived

$$H_v = \frac{v_{dc}(s)}{i^d(s)} = \frac{3 m_a}{4\sqrt{2} C s} \tag{4.13}$$

4.2.4 Utility flux reference frame synchronization using a phase locked loop

For the alignment of the BDFIG with the utility a form of synchronization is necessary. Phase locked loops are well known solutions for this problem as are widely used in applications where frequency matching is required, such as telecommunications, radio and

Stellenbosch University https://scholar.sun.ac.za

motor control[90]. There are conventionally three different types of PLL's used in phase synchronization:

- Zero crossing
- Stationary reference frame
- Synchronous reference frame

Furthermore there are more elaborate methods continually developed for sensitive tracking purposes as well as quicker tracking. These methods also allow the PLL to track both positive and negative frequencies thus providing even more stable phase extraction under unbalanced conditions, as well as under grid faults[91]. For this dissertation, a stable grid supply can be assumed and such elaborate methods are not required. However, since there are still minor imperfections in the grid and the phases are not spaced perfectly 120 deg and their voltage amplitudes are not perfectly equal, some versatility is still required. The synchronous reference frame PLL (SRF-PLL) provides such versatility. Based on the principle to control the angular position of the dq-reference frame in using a feedback loop, driving the q-component to zero, ensuring that only the direct axis carries the magnitude of the voltage frame. Thus, when synchronicity is achieved, the d-axis component carries the amplitude of the sinusoidal positive sequence vector and its angle determined by the output of the PLL feedback loop[91]. A great advantage of this is the PLL's ability to attenuate harmonic distortions in the grid voltage, with high order harmonic effects almost completely rejected on the PLL output signals[91].

Since the exact transfer function for a PLL can be complicated to model, conventional tuning methods such as symmetrical optimum criterion are used. This maximizes the phase margin at a given crossover frequency, in this case the utility frequency of 50 Hz[92; 93]. Accordingly the gain selection is described by

$$\alpha = \frac{1}{\omega_c T_s} \tag{4.14}$$

$$T_{n,PLL} = \alpha^2 T_s \tag{4.15}$$

$$V_{r,PLL} = \frac{1}{\alpha U_0 T_s} \tag{4.16}$$

where U_0 is the peak grid phase voltage (311 V_{LN}) and ω_c is the crossover frequency equal to the grid frequency (314 rad/s). Lastly T_s represents the control system sampling time (200μ seconds).

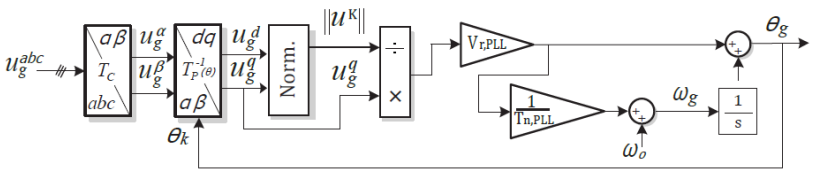

Figure 4.7: Block diagram for a basic structure of SRF-PLL[93]

Stellenbosch University https://scholar.sun.ac.za

4.3 Simulation of GSC

While the work presented in this dissertation is focused on control simplification for the machine side of the back-to-back converter, for completion a simple design for a GSC is now shown. In order to showcase a response to voltage change for the grid side converter, a simulation is performed according to the following design criteria.

$$V_r = \frac{T_g R}{2T_{vsc}} \tag{4.17}$$

$$T_n = 4T_g \tag{4.18}$$

where T_g is the filter time constant defined by

$$T_g := \frac{L}{R} \tag{4.19}$$

T_{vsc} is defined as the averaged time constant of the voltage side converter. The control response of the DC bus with a step change in reference voltage from 540V to 700V is shown in figure. The RL filter in the simulation shown has a resistance of $100\mu\Omega$ and inductance of 20μH. The switching frequency is the same as that used on the inverters in the experiments of $5k$Hz. The dc-bus consists of a 0.15F capacitor.

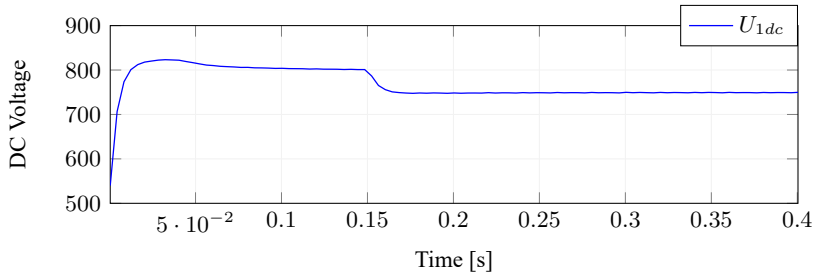

Figure 4.8: DC Voltage response to reference voltage changes from 540V to 800V at t=0 and 800V to 750V at t=0.15

4.4 Control-Winding Side Converter Control

Various methods for control of the BDFIM exist. For most cases, the aim of these controllers are to produce a similar end result - whether it be speed, active or reactive power, torque or even current control. These control methods allow us to use these machines with optimal performance for their implementation purposes. These methods can be further extended for sensor-less purposes, by allowing state estimations or observations. One such method which is already well researched is sliding mode control (SMC). This method of control is well known for its robustness to parameter variations and load disturbances, as well as its simple design[16].

It has thus been shown in numerous findings that SMC can effectively and suitably be used to control the BDFIM[94; 95; 96]. Due to its' robustness against parameter variations, SMC would overshadow the goal of obtaining reasonable machine parameters suitable for further control development purposes.

As such, flux control (also referred to as vector control) has been chosen for its' notoriously sensitive nature to machine parameters and complex nature. For this method

Stellenbosch University https://scholar.sun.ac.za

of control a complex cascade of PI controllers are required with compensation terms to keep the model linearized. However it will be shown that many of these parameters can be considered insignificant for the PI controllers and as such can be significantly reduced. It is still however necessary to show that a full controller is achievable using the parameter estimations applied in chapter 2, and accordingly these reductions are merely suggestions to increase robustness to inaccurate measurements and sensor noise, without significantly reducing the control accuracy nor stability in any way.

For the control to be applied to the control winding (CW) side of the machine, an space vector pulse width modulation (SV-PWM) scheme is used[97; 98]. This requires a reference input voltage from the controller, which is then optimally converted using a pulse width modulation scheme to ensure that the inverter gates produces the same voltage on the output gates allowing for the correct currents to be injected into the corresponding phases of the control winding of the machine. This method of current injection is well known and will not be discussed further throughout this dissertation[99].

Due to vector control requiring accurate model representations and linearizations of the plant for optimal proportional and integrator (PI) control, complex systems such as the BDFIM can require a complicated vector control solution, as cross compensation and disturbance rejection terms are required to linearize the plant as far as possible. It has also been noted in chapter 2 that although the steady state of the BDFIM can be linearly approximated, it is still a parameter varying system. Meaning that during transient operation the machine cannot be considered linear and considerations must take into account for these variations. Whether it be designing the PI gains in a way as to ensure stability throughout these variations or by approximation of these changes.

4.4.1 Control-Winding Side Controller

In order to obtain the required dc-equivalent transfer functions to adequately describe the BDFIM, we start with the BDFIM model defined in section 3.4.4. This model is chosen for its' dc-like transient characteristics, thus reducing computational intensity for the controller. Additionally reductions to the controller will be suggested to reduce cross compensation where possible. In doing so decoupled control between speed and reactive power in the power winding is maintained and performance loss is negligible. The control system derived here is similar to that derived in [17; 36], however after some derivations it will be shown that the complexity of the control can reduced even further.

For alignment with the synchronous reference frame of the primary winding a PLL will be used, and is discussed later on in this chapter. In doing so, the alternating current characteristics of the BDFIM can be greatly simplified, with the stator operating in a dc-machine-like fashion. Accordingly, reference frames for the rotor and control winding stator can be obtained, allowing for dc-analysis of these components as well. The resulting synchronous reference frame axis is defined as the rotating dq-reference plane.

When considering three phase machines they are typically framed in a 3-phase axis referred to as the abc-axis. In this case, all three voltage vectors can be converted into a single vector with a certain magnitude and frequency. These three axis can equivalently be transformed into another stationary reference plane referred to as the alpha-beta-0 ($\alpha\beta0$) reference plane by application of a Clarke transformation, equally capable of representing the $\alpha\beta0$-components of the same voltage and magnitude vector. The advantage of this transformation is that for balanced circuits, the zero component can be removed, allowing for the original 3 phase vector components to be represented by two equivalent alpha-beta vectors. Both of these vector components however will still be rotating in magnitude

Stellenbosch University https://scholar.sun.ac.za

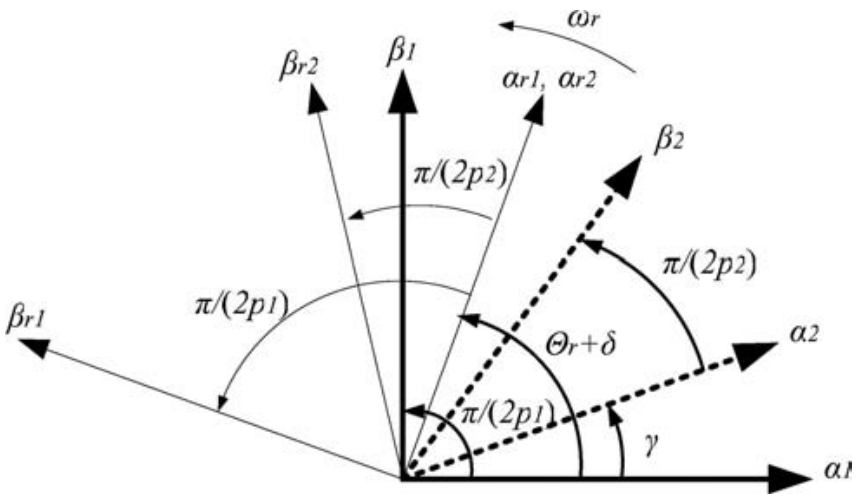

Figure 4.9: Park Transformation Reference Frames[61]

with the fixed grid frequency. Finally, by further application of a Park transformation, the stationary reference frame can be converted to a rotating equivalent reference frame. Accordingly, the individual rotating dq-vectors can be fixed in relation to a reference vector of constant magnitude. When a perfect alignment of either of the axis is made with the rotating vector, the magnitude of the orthogonal axis will be zero, greatly simplifying control components. This process of transformation is shown in Figure 4.9 above. This process of transformation has also been discussed and used in chapter 2 and was applied in great detail in order to obtain the equivalent circuit parameters of the BDFIM in this frame of rotation.

The fundamental target of the control to be performed edges on the ability to control active and reactive power. For torque and speed control, further derivations can follow based upon these fundamentals, as will be shown. The real and reactive power in the primary winding within the rotating stator reference frame is now defined

$$P_p = \frac{3}{2} v_p^d i_p^d + v_p^q i_p^q, \quad Q_p = \frac{3}{2} v_p^q i_p^d - i_p^q v_p^d \tag{4.20}$$

By aligning the stationary reference frame with the d-axis of the power winding stator flux vector ϕ_s^d, these power equations simplify to[99; 100]

$$P_p = \frac{3}{2} v_p^q i_p^q, \quad Q_p = \frac{3}{2} v_p^q i_p^d. \tag{4.21}$$

By substituting the flux of the rotor cage (3.51) and power winding (3.49) into the control winding flux relation (3.50) the following control flux equation is produced

$$\phi_c^{dq} = -d_1 \phi_p^{dq} + d_2 \phi_r^{dq} + d_3 i_c^{dq}, \tag{4.22}$$

$$d_1 = \frac{L_{mp} L_{mc}}{L_r L_{sp} - L_{mp}^2} \tag{4.23}$$

$$d_2 = \frac{L_{sp} L_{mc}}{L_r L_{sp} - L_{mp}^2} \tag{4.24}$$

$$d_3 = L_{sc} - \frac{L_{sp} L_{mc}^2}{L_r L_{sp} - L_{mp}^2} \tag{4.25}$$

Furthermore, by substituting the control flux equation (4.22) into the dynamic control

Stellenbosch University https://scholar.sun.ac.za

winding voltage equation (3.47), the voltage command signals can be expressed as

$$v_c^{d*} = R_{sc}i_c^d + \frac{d}{dt}(-d_1\phi_p^d + d_2\phi_r^d + d_3 i_c^d) - \underbrace{\omega_c(d_2\phi_r^q + d_3 i_c^q)}_{v_{c-comp}^d} \tag{4.26}$$

$$v_c^{q*} = R_{sc}i_c^q + \frac{d}{dt}(d_2\phi_r^q + d_3 i_c^q) + \underbrace{\omega_c(-d_1\phi_p^d + d_2\phi_r^d + d_3 i_c^d)}_{v_{c-comp}^q} \tag{4.27}$$

The dynamic disturbances caused by the rotor flux and the power-winding are considered negligible for steady state to low transient behavior and therefore, they are omitted from the inner loop transfer function. As such the voltage control function in the s-domain becomes,

$$v_c^{d*}(s) = (R_{sc} + d_3 s)i_c^d - \underbrace{\omega_c(d_2\phi_r^q + d_3 i_c^q)}_{v_{c-comp}^d} \tag{4.28}$$

$$v_c^{q*}(s) = (R_{sc} + d_3 s)i_c^q + \underbrace{\omega_c(-d_1\phi_p^d + d_2\phi_r^d + d_3 i_c^d)}_{v_{c-comp}^q} \tag{4.29}$$

It can be seen that the transfer function for the plant can be approximated as,

$$H_{ic}(s) = \frac{i_c^{dq}}{v_c^{dq}} = \frac{\frac{1}{R_{sc}}}{1 + \frac{d_3}{R_{sc}}s} \tag{4.30}$$

Remembering that the dq-axis is aligned with flux vector ϕ_p^d and assuming that $R_{sp}i_p << j\omega_p\phi_p$, the power winding flux can be approximated as

$$\phi_p^d \approx \frac{v_p^q}{\omega_p} \tag{4.31}$$

By considering (3.46) and (3.49) an expression relating the rotor currents and flux can be obtained, allowing the rotor flux to be estimated as,

$$i_r = \frac{1}{L_{mp}}\phi_p - \frac{L_{sp}}{L_{mp}}i_p \tag{4.32}$$

$$\phi_r = \frac{L_{mp}^2 - L_r L_{sp}}{L_{mp}}i_p + L_{mc}i_c + \frac{L_r}{L_{mp}}\phi_p \tag{4.33}$$

Now by substituting the rotor flux and rotor current into the rotor voltage equation (3.48) and regarding the disturbances caused by the dynamic current changes to be negligible, the relation between the power and control-winding currents is

$$\begin{aligned} i_c = &\left[\frac{L_r L_{sp}}{L_{mc}L_{mp}} - \frac{L_{mp}}{L_{mc}} - j\frac{L_{sp}R_r}{\omega_{rp}L_{mc}L_{mp}}\right]i_p \\ &+ \left[-\frac{L_r}{L_{mc}L_{mp}} + j\frac{R_r}{\omega_{rp}L_{mc}L_{mp}}\right]\phi_p \end{aligned} \tag{4.34}$$

Stellenbosch University https://scholar.sun.ac.za

It can be noted that the rotor to power-winding slip speed only becomes small enough to have a significant influence at a maximum rotor speed of four times the natural operating speed.

$$w_{r(max)} = \frac{w_p}{p_p} \tag{4.35}$$

$$w_n = \frac{60 f_p}{p_p + p_c} \tag{4.36}$$

Thus, for machines with poles in the power winding less than the amount of poles in the control winding - to ensure that the rotor to power-winding slip only becomes considerable at twice the natural operating speed, the imaginary terms above can be regarded as negligible. Additionally, due to the dq-axis alignment, the quadrature reference current ϕ_p^q is zero and ϕ_p^d remains near constant.

$$\phi_p^d = \frac{v_p^q}{w_p} \tag{4.37}$$

This results in the complete removal of cross compensation between the winding currents, for the power winding control loop. There is still however flux compensation (U_{p-comp}^{dq}) to be added to the direct current control loop.

$$i_c^d \approx \frac{L_r L_{sp} - L_{mp}^2}{L_{mc} L_{mp}} i_p^d - \underbrace{\frac{L_r}{L_{mc} L_{mp}} \phi_p}_{U_{p-comp}^{dq}} \tag{4.38}$$

$$i_c^q \approx \frac{L_r L_{sp} - L_{mp}^2}{L_{mc} L_{mp}} i_p^q \tag{4.39}$$

The resulting transfer function used for PI control parameter sizing is approximated as the following

$$H_{ip}(s) = \frac{i_p^{dq}}{i_c^{dq}} \approx \frac{L_{mc} L_{mp}}{L_r L_{sp} - L_{mp}^2} \tag{4.40}$$

Due to the linearity of the zero-order function above, it is recommended to remove the PI control for the power winding loop, since it can be compensated for by the PI controllers up-stream, should the objective of the control not to be to directly control the power winding currents.
Similarly to [17] the torque and rotor speed transfer functions can be obtained to be

$$\frac{T_e}{i_p^q} \approx \frac{3}{2}(p_p + p_c)\phi_p^d \tag{4.41}$$

$$\frac{\omega_r}{T_e} = \frac{1/J}{s + b/J} \tag{4.42}$$

In order to control the reactive power in the power winding, it is necessary to determine the reference reactive power as a function of the reference current i_p^d. By substituting the estimated power winding flux into the reactive power equation (4.21), the transfer function for the control of reactive power is

$$\frac{Q_p}{i_p^d} = \frac{3}{2}\omega_p \phi_p^d \tag{4.43}$$

Stellenbosch University https://scholar.sun.ac.za

In order to tune the gains for the controller the Ziegler Nichols approach was used with a controller sampling time of 5000 Hz and a desired settling time on a ramp of 100 rpm of less than 2 seconds with a maximum overshoot of 5%. The tuning parameters obtained are[101]

Table 4.1: cwsc gains for practical machine parameters

	Kp	***Ki***
CW Current Loop	9.64	268
PW Current Loop	15.51	164
Reactive Power Loop	0.12	0.25
Speed Loop	0.15	0.2

In order to maintain stability in the controller, the cascaded PIs have to be tuned in such a fashion that the leading PI has a faster response than the controller feeding into it. An example of the pole-zero equivalent circuit for this plant is shown in appendix A.1. Note that the parameters used in the specific plot is that of the machine used in [100] and not the practical model used here.

4.5 Analysis and Simulation of a BDFIG System as a WECS

The BDFIG model developed in chapter 2 is now used further in simulation software Matlab Simulink to give an indication of the viability of the developed control algorithm. The process of transformation and reduction was merely done in order to find accurate equivalent parameters for control purposes. As such to maintain accuracy and viability, the full state BDFIM model is now used as this is the closest representation of the real machine with similar transient behavior.

4.5.1 Simulation Control Simplification

We now present in Figure 4.10 the equivalent CWS control scheme, with circuits in red indicating definite reducible terms, and orange optionals - depending on the application of the machine. As for the reasoning behind these reductions see section 4.4.1. Furthermore tables describing the control circuits used for simulation and experimental results later on can be found in appendix A.1 It will be shown that the gain parameters were set to target performance rather than stability. The reason is that for the control reduction techniques to be apparent, the controller has to be operating on the border of its' capabilities. In doing so indicating that the reduced control methods are not entirely unsuitable if instability is shown, and with some tuning could likely perform with great results. However, instability is necessary to show the importance of certain compensation terms, but also the flexibility of ignoring others.

In all of the simulations to follow PI gains were kept constant, designed for the full controller. Re-designing the gains for each controller would change the stability of the

Stellenbosch University https://scholar.sun.ac.za

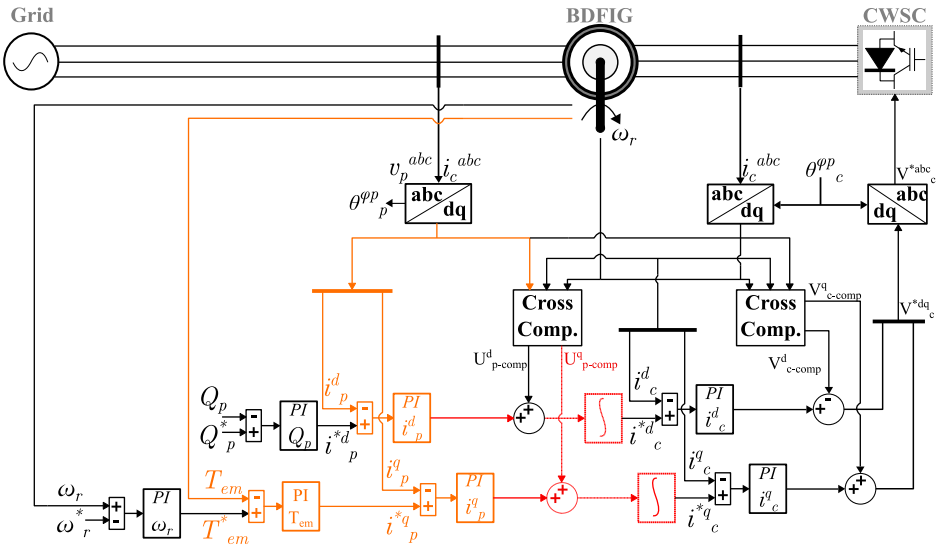

Figure 4.10: Control Side Controller Schematic. Red indicates objects removed by the simplified control whilst optional simplifications are indicated in orange.

machine, reduce the impact that various portions of the controller have during the simplification process. Using key parts of the control of table A.3 a comparison of the reduction techniques for the experimental controller is obtained.

With the motor operating at its natural speed of 600 rpm, the response of the controller to ±50 rpm and 100 rpm step input speed references as well as reactive power step reference changes of 100 VAr and 200 VAr respectively is shown. In Figure 4.11 the subscripts $3b, 4a, 4c$ and $5c$ refer to the simplified single PI with compensation followed by the dual PIs with no compensation, dual PIs with compensation and the full controller with three PIs and compensation respectively. In doing so, a direct comparison of the effects of removing voltage and current compensation as well as cascading the PIs in the control response is possible. It can be seen from the speed response that the reduction of voltage compensation terms in addition to the reduced PI structure results in instability at super-synchronous speeds.

The following controller with voltage cross compensation shows a smoother and quicker

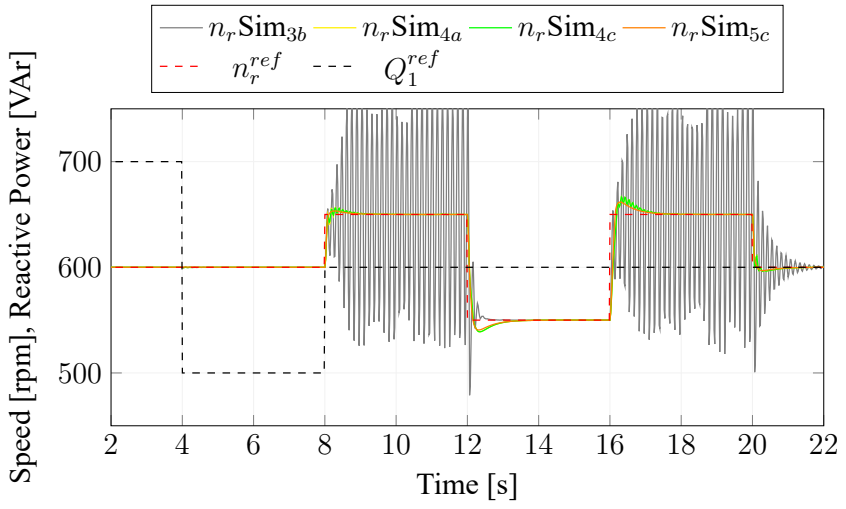

Figure 4.11: Comparison of different controllers applied to the simulated machine while applying a varying amplitude step input to the speed reference

Stellenbosch University https://scholar.sun.ac.za

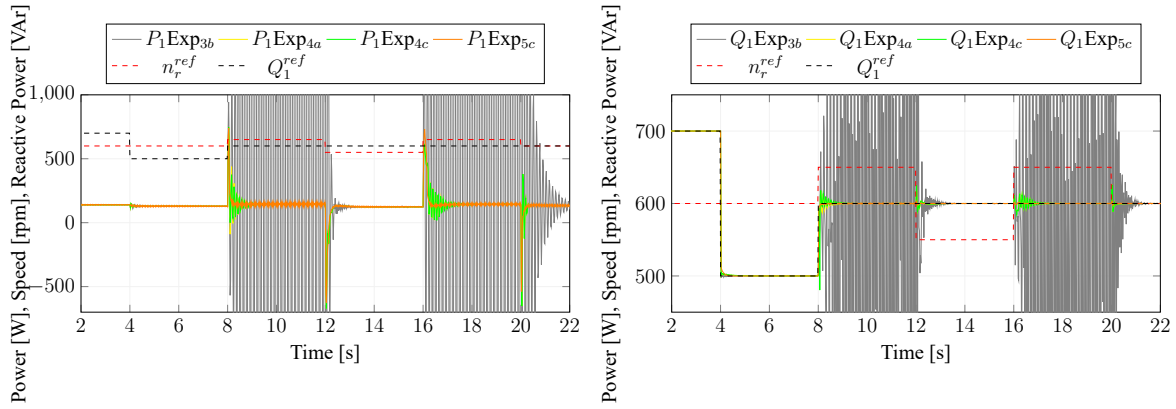

(a) **(b)**

Figure 4.12: Comparison of different controllers applied to the experimental machine while applying a varying amplitude step input to the speed reference.

response, with much less instability. The controller settles in less than two seconds with an overshoot of 15%, which is higher than the target of 5% achieved by the full controller. It is apparent from 4*a* and 4*c* that the current compensation terms have little impact on the speed loop, both showing near identical results. The controller with two PIs respond very similarly to the full controller, with slightly more overshoot and marginal harmonics present during the super-synchronous response.

From Figure 4.12(a) the power output of the machine is shown. It can be seen that the machine is drawing around 130 Watt of active power at synchronous speeds. Controller 4*a* and 4*c* shows great oscillations during step changes in speed and reactive power, which are largely removed in 5*c* where the current of the primary winding is being controlled as well. At time step 4 controller 3*b* shows small disturbances in Figure 4.12(b) due to the reactive power step change. The effect hereof is largely removed in the rest of the controllers, indicating that the cross compensation terms or cascaded PIs are capable of correcting the cross disturbances of the orthogonal axis for the machine. The reactive power of all three controllers indicate similar responses, with the expanded controller 5*c* indicating an overall transition curve which is less susceptible to unwanted harmonics.
To clearly indicate the advantages of the cascaded PI controllers, the $q-$axis (speed control loop) of the current loops are now shown using Figure 4.13. The current response to speed and reactive power step changes at time step 8 can be seen to reduce in Figure 4.13(a), where the response overshoot reduces with an increase in cascaded PIs. This is shown

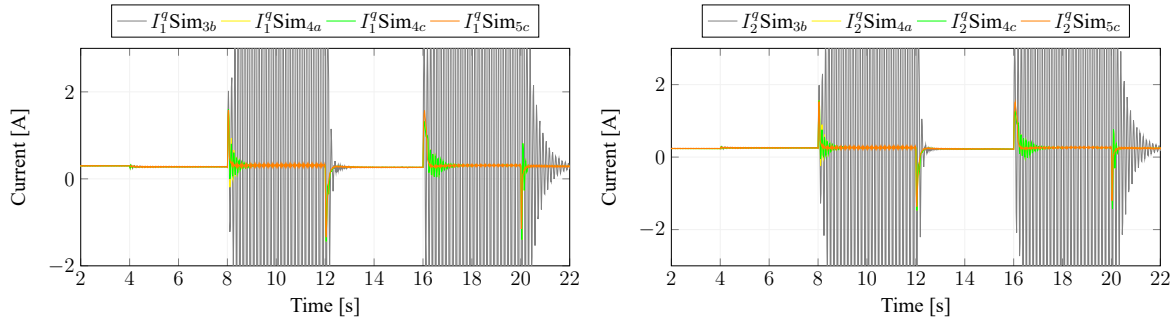

(a) **(b)**

Figure 4.13: Comparison of different controllers applied to the experimental machine while applying a varying amplitude step input to the speed reference.

Stellenbosch University https://scholar.sun.ac.za

again in Figure 4.13(b). The effect of the addition of voltage compensation is again clearly visible here, indicating great improvements in stability in all operating regions of the machine.

4.6 Conclusion

For full control of the back-to-back converter various aspects were reviewed. It was noted that a filter is necessary, to reduce the harmonics induced on the grid due to the high frequency switching of the voltage source converter (VSC). A short discussion regarding the choice of suitable filters and the design thereof was then discussed. The control theory regarding the GSC was then mentioned and it was noted that there is a need to implement a phase locked loop in order to properly align the rotating synchronous reference frame with phase voltage of the grid. One such design was presented and symmetrical optimum used for the tuning thereof. The control winding side converter was also presented with a short review of similar schemes and a description of the integration thereof with the SV-PWM scheme. An introduction of the vector control to be implemented is presented. Followed by an in depth derivation of the vector controller used and a discussion of compensation terms that could be regarded negligible. It is mentioned that the reduction of these terms can enhance the reliability of the controller during sensor / measurement errors. A simulation was done, accordingly indicating the potential advantages and disadvantages of the reduction of various parts of the controller.

Stellenbosch University https://scholar.sun.ac.za

Chapter 5

Laboratory Experiments of the Grid-Connected CWSC

5.1 Introduction

An experimental setup is used to verify the theoretical predictions in this dissertation. The goal is to show that the designed controller is able to respond similarly on the experimental machine. This allows for both the validation the motor parameter estimation using the proposed method in section 3.4.3.4 as well as the suggested control simplification of section 4.5.1.

5.2 BDFIG Test Bench Description

The BDFIG test bench consists of a custom designed three phase 3.4 kW bar cage BDFIG directly coupled to a 22 kW driver induction motor. This allows for testing in both motoring and generation modes. Furthermore the controller used is a National Instrument (NI) PXIe-8115 embedded real-time controller. The proposed control strategies designed in Simulink are implemented for the experimental test bench using LabVIEW. Additionally the test-bench also includes two NI 7841R FPGA expansion modules that allows for both input and output signals to or from the PXIe-8115 controller. Furthermore the back to back converter consists of two 8.7 kVA custom-modified with a switching frequency of 5 kHz commercially available SEW power converters. For the purpose of this setup however, only the CWSC is connected as a stable GSC is already assumed and the DC bus is powered using the onboard rectifier bridge. The measurement of the three-phase voltages are gathered using LEM LV25-P sensors and that of the three-phase currents are measured using LA55-P sensors. A GI341 BAUMER incremental encoder, mounted on the rotor shaft is used to measure the rotor speed and angle.

The BDFIG electrical and mechanical parameters can be found in table A.1.

5.3 Start-up procedure

Before the control system can be engaged, it is important to ensure that the machine is at a stable operating point to allow for a seemless transition into vector control mode. For the purposes of the control system designed there are two scenarios for this, motoring mode and generation.

Stellenbosch University https://scholar.sun.ac.za

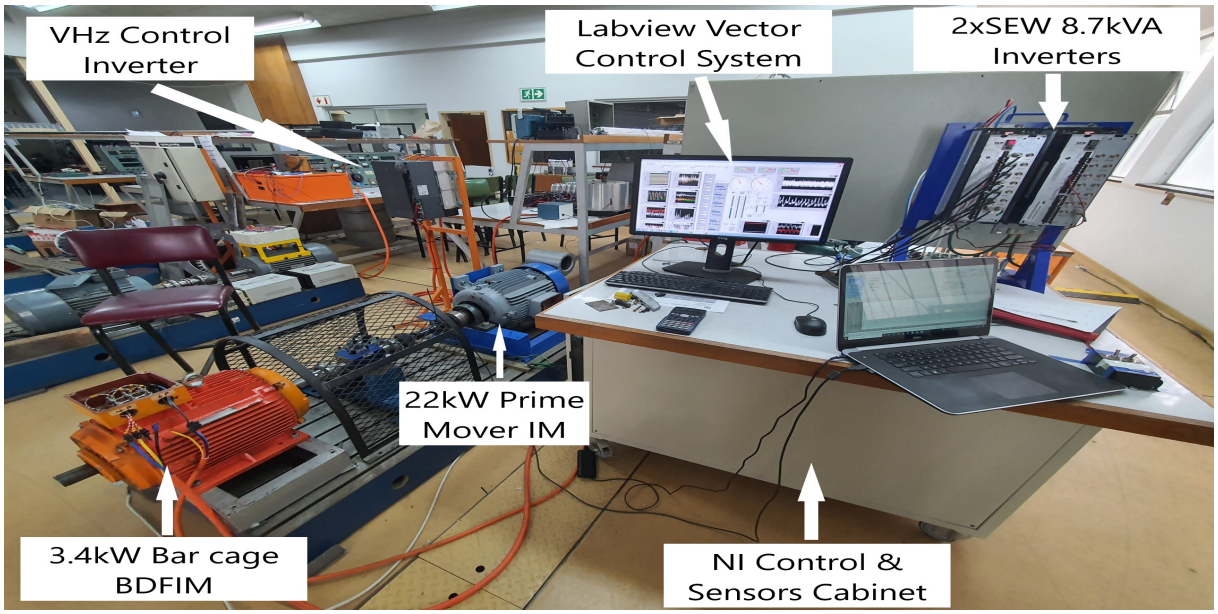

Figure 5.1: Test Bench Setup

5.3.1 Motoring

When controlling the machine in motoring mode, independent speed and reactive power control will be performed. However, before the control can be engaged, a constant reference frequency from the grid winding is necessary for a constant reference frame to align the flux control. As such the startup procedure is as follows:

1. Activate the control winding side inverter with all outputs set to 0. This allows current to flow through the IGBT's of the inverter, acting as a short circuit on the control winding side.

2. Ramp the machine up using a 3 phase variac, connected to the primary side of the BDFIM, thus operating in cascade induction mode.

3. Ensure that there are output limits set on all PIs in the control loop, setpoint bounding could also be used to allow for this.

4. Once at natural speed, the PI output to the CWSC can be increased allowing for the controller ot take over.

5.3.2 Generation

When controlling the machine in generator mode, independent active and reactive power control will be performed. However, before the control can be fully engaged a constant reference from the grid winding is necessary to have a constant reference frame to perform the flux control to accordingly. As such the startup procedure is as follows:

1. With the control winding side open circuited and a breaker between the primary winding and the grid open, ramp the BDFIG up to natural speed using the 22 kW primary mover while monitoring the phase rotation between the grid and the primary winding.

Stellenbosch University https://scholar.sun.ac.za

2. Once at natural speed, activate the controller and perform current control of the control winding, increasing the current until the voltage on the grid side matches the voltage on the power winding. In order to match the phases, the generator speed should be ramped up or down as necessary.

3. Once the phases are aligned and voltage amplitudes equal, the breaker between the primary winding and the grid can be closed. The generator is now locked in and synced with the grid.

4. The control winding current can be reduced and the desired control can be engaged.

5.4 Experimental machine mechanical parameter identification

In order to verify that the developed model using chapter 2 is as accurate possible, curve fitting is performed on the ramp curve of the experimental machine during cascade induction mode. To achieve this, the machine is operated in motoring mode and a 3-phase grid voltage of 220 V_{LN} applied to the primary winding while short circuiting the control winding. The same is done in simulation using the full state model as developed in 3.4.2.1 and then compared as shown in Figure 5.2 below. The full state dq-model is suggested here as it is the most accurate dynamic model of the models suggested in the dissertation. As such can it is the best representation of the machine during the curve fitting process.

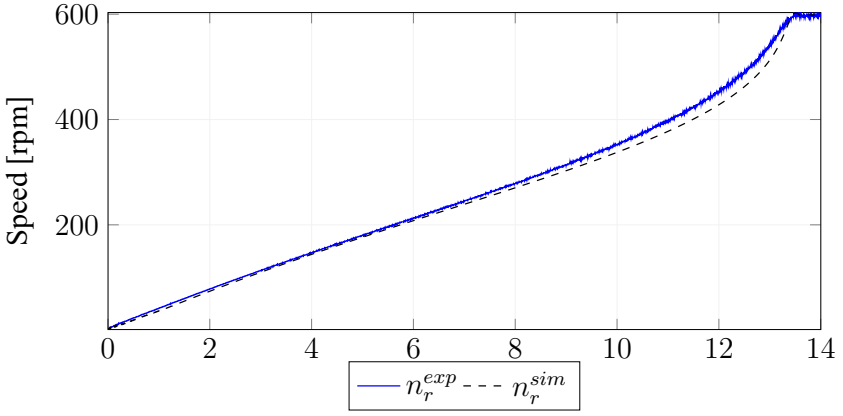

Figure 5.2: Comparison of Experimental Machine versus Full state simulated machine with the secondary stator windings short circuited

The electrical and mechanical parameters of the machine can be found in table B.1. The machine friction and inertia is accordingly determined to be:

Table 5.1: Machine Mechanical Parameters

Parameter	Symbol	Unit	Value
Moment of inertia	J	$kg.m^2$	0.154
Rotor friction coefficient	b	-	0.022

Stellenbosch University https://scholar.sun.ac.za

5.5 Experimental machine compared to simulations

In order to gain insight into the validity of the experimental model compared to the ideal simulated model, a few measurements are taken and compared. The first experiment is a comparison during natural startup of the BDFIM in cascade induction mode. Hereby a visual comparison can be made of the stator winding constants as well as the rotor constants. Due to the physical limitations of accessibility to the rotor, measurements of the rotor bar currents are impractical, and thus the induced currents into the secondary stator windings are used for comparison, essentially visualizing the machine as a black box with the primary winding as input and secondary winding currents as output.

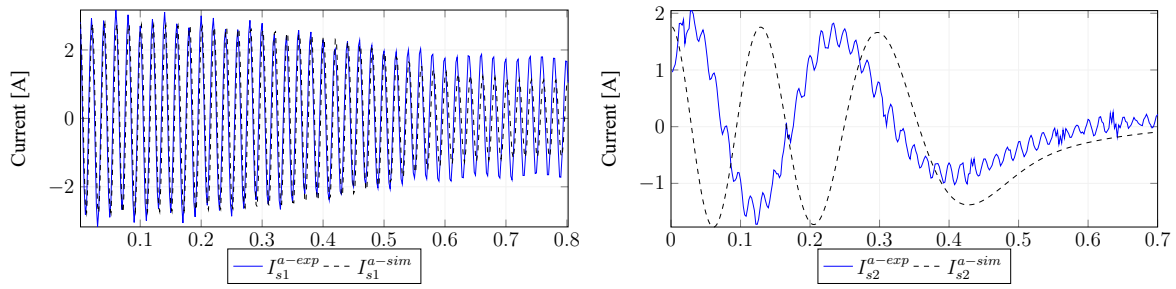

(a) Machine Primary winding currents during startup

(b) Machine Secondary winding currents during startup

Figure 5.3: Machine Stator currents during startup

From Figure 5.3(a) a comparison between the simulated and experimental bar cage motor primary stator phase a current is shown. It is noteworthy that the currents are oscillating as expected at the grid feed frequency of 50 Hz. The currents start out with very similar amplitudes of ≈ 2.5 A and soon-after the simulated currents reduce to a peak amplitude of 1.2 A compared to the peak of 1.7 A in the primary stator. It is important to note that there are likely significant differences in the winding manufacturing of the primary stator winding compared to the design estimates, obtained using finite element modeling (FEM) software. It should also be noted that the stator windings of the particular BDFIM have been skewed, as it greatly reduces manufacturing difficulty compared to the skewing of the rotor. It is likely that the deviation from the expected measurements are due to the skewing as this was difficult to model using the FEM software in the design phase. It is standard practice to skew the rotor of induction machines as this helps the machines self starting capability by reducing magnetic logging whilst also reducing torque ripple[102; 103].

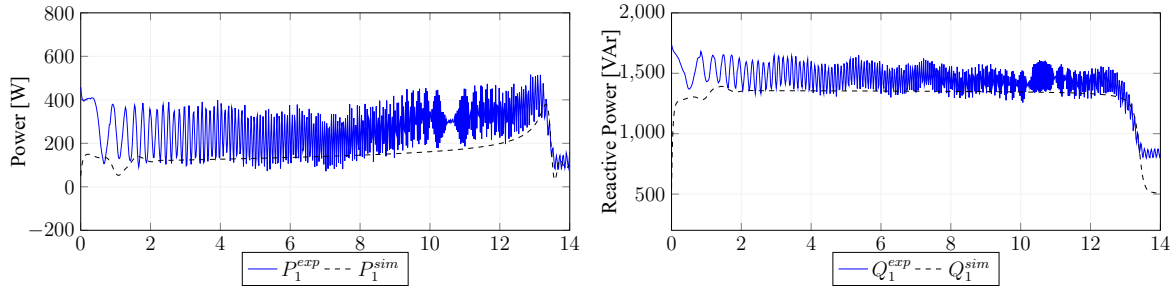

(a) Machine Active Power during startup

(b) Machine Reactive Power during startup

Figure 5.4: Machine active and reactive power during startup

Stellenbosch University https://scholar.sun.ac.za

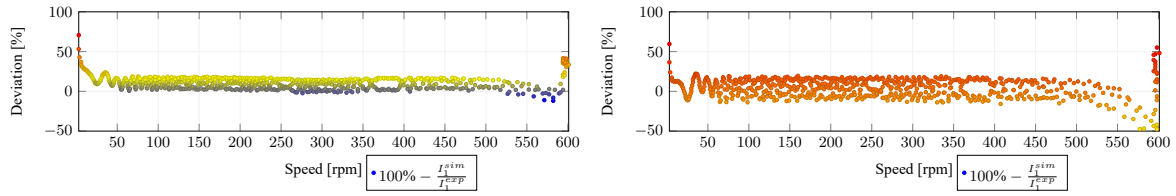

(a) Current deviation stator 1 **(b)** Current deviation stator 2

Figure 5.5: Deviation of predicted current compared to measured current over the transient operating region of the machine

The secondary winding induced phase a currents are shown in Figure 5.3(b) below. With very similar current peaks and periods, a small phase shift is notable, likely due to the difference in rotor speed causing a drift in angular position during startup. The active power output of the primary winding is indicated in Figure 5.4(a). With an actual input power starting at 220 W and peaking at 400 W compared to the simulated starting power of 150 W peaking at 400 W it can be seen that the simulated machine has a larger transient region for input power during startup, however settles at roughly the same steady state power of 100 W active power.

A similar behaviour can be seen for the reactive power in Figure 5.4(b), however there is a notable difference in the steady state reactive power, indicating slight differences in the inductance of the stator windings. These losses are likely largely attributed to leakage inductance not being accounted for in the initial model.

To easily visualize the measurements above, Figure **??** indicates the distribution in simulated versus actual measurements over the sub-synchronous speed range of the motor. With a mean deviation of 11.32% to the estimated readings for the primary stator winding and 3.06% for the secondary stator windings. Additionally the standard deviation for the primary winding was determined to be 8.71 and 16.34 for the secondary winding. Indicating that although the model estimates for the primary winding currents are slightly offset from the real values, the surety of the estimates are more reliable than for the secondary windings as can be seen in Figure 5.6. To increase the accuracy of the reading, the standard deviation can be greatly reduced by the addition of low pass filters. LPF were not implemented on the control measurements performed in this dissertation as the robustness of the controller would be increased with filtered measurements.

5.6 Current Control

Current control of the primary and secondary windings are first performed individually to show that stable control using these measurements can be achieved. To ensure that

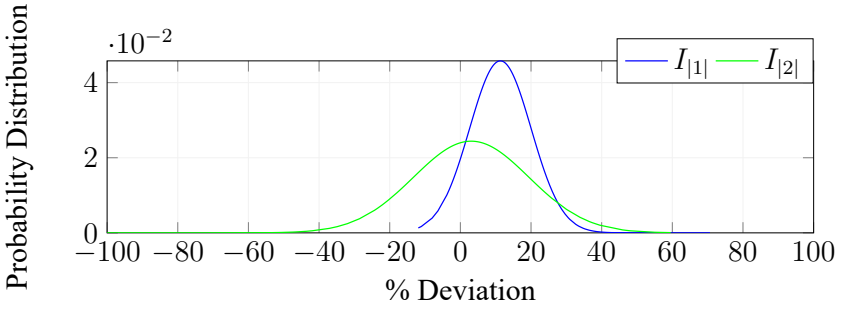

Figure 5.6: Spread of deviation of simulated currents compared to experimental currents

Stellenbosch University https://scholar.sun.ac.za

the machine does not accelerate / decelerate this test is conducted in generation mode, i.e with the BDFIM being driven by the IM driver, fixing the BDFIM to its' natural speed of 600 rpm. Firstly control of the primary winding is performed. In this test a dual cascaded

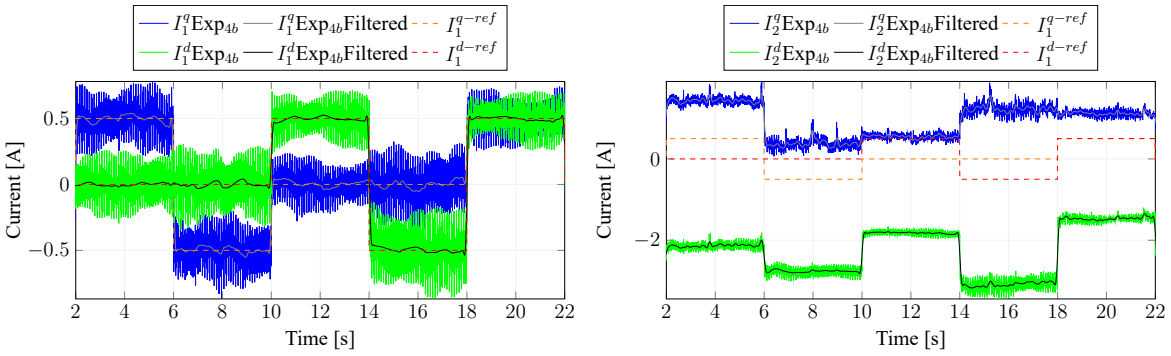

(a) **(b)**

Figure 5.7: Current Control of primary winding fixed at natural speed 600 rpm

PI setup is used without current compensation, as it will later be shown that this can be considered negligible. For the input reference decoupled dq-axis currents are selected individually. The responses are shown in Figure 5.7, where the measured currents track the input references with little overshoot and cross disturbances and very quick response.

As for the secondary winding a single PI is needed. The response of this control with voltage compensation is shown in Figure 5.8 where the control winding current quickly tracks the reference with good accuracy. The PI response shows little to no overshoot with a settling time well below 100 milli-seconds which was the chosen design criteria as it is important that the secondary winding responds in less time when compared to the primary winding.

5.7 Speed and reactive power control

Using key parts of the control of table A.3 a comparison of the reduction techniques for the experimental controller is obtained. In this way a comparison of the stability of parts of the controller can be shown, while showing that the removable components in chapter 4 are negligible for certain purposes.

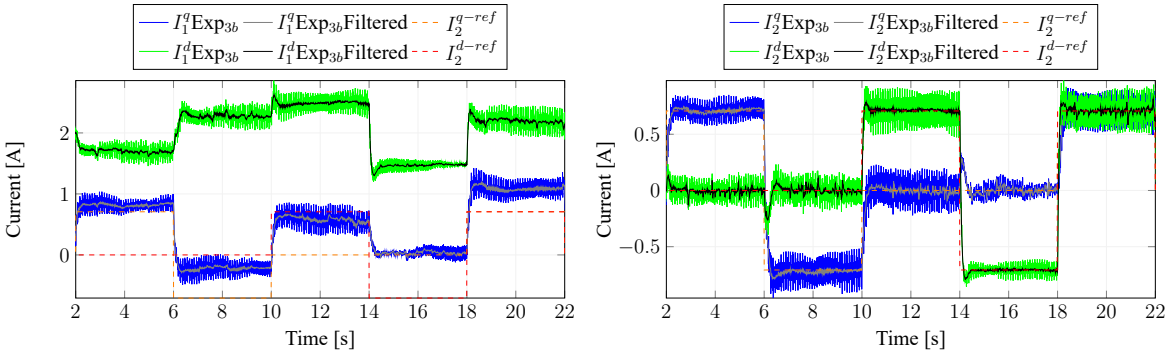

(a) **(b)**

Figure 5.8: Current Control of secondary winding fixed at natural speed 600 rpm

Stellenbosch University https://scholar.sun.ac.za

In all of the tests to follow PID gains were kept constant, designed for the full controller. Re-designing the gains for each controller would change the stability of the machine and muffle the impact that various portions of the controller have during the simplification process. The gains used for the practical BDFIM are fine tuned from the theoretical gains for the machine and found to be:

Table 5.2: cwsc gains for practical machine parameters

	Kp	***Ki***
CW Current Loop	9.75	203.47
PW Current Loop	11.31	109.7
Reactive Power Loop	0.15	0.24
Speed Loop	0.12	0.253

With the motor operating at natural speed, the stability of the controller according to ±50 rpm and 100 rpm step input speed references as well as reactive power step references of 142 VAr and 244 VAr respectively is shown. In Figure 5.9 the subscripts $3a, 3b, 4c$ and $5d$ refer to the completely simplified single PI followed by the simplified single PI with compensation, simplified dual PIs with compensation and the full controller with three PIs and compensation respectively. This allows for direct comparison of the effects of removing voltage compensation, current compensation and cascading PIs in the control response. It can be seen from the speed response that the reduction of voltage compensation terms results in instability at sub-synchronous speeds - which is to be expected. The response is quicker overall, with less overshoot.

The following controller with voltage cross compensation results in a very smooth and quick response, with much less instability and little overshoot. It is worth noting that the original PI response for the speed loop was designed and tuned for an overshoot of less than 5% on a step of 100 rpm at natural speed. The settling time target was 2 seconds. The controller with two PIs responds very similarly to the full controller, with

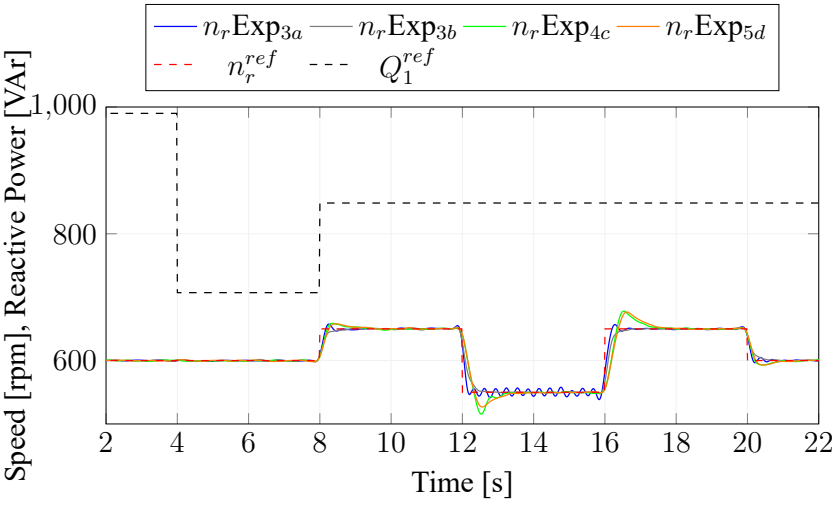

Figure 5.9: Comparison of different controllers applied to the experimental machine while applying a varying amplitude step input to the speed reference

Stellenbosch University https://scholar.sun.ac.za

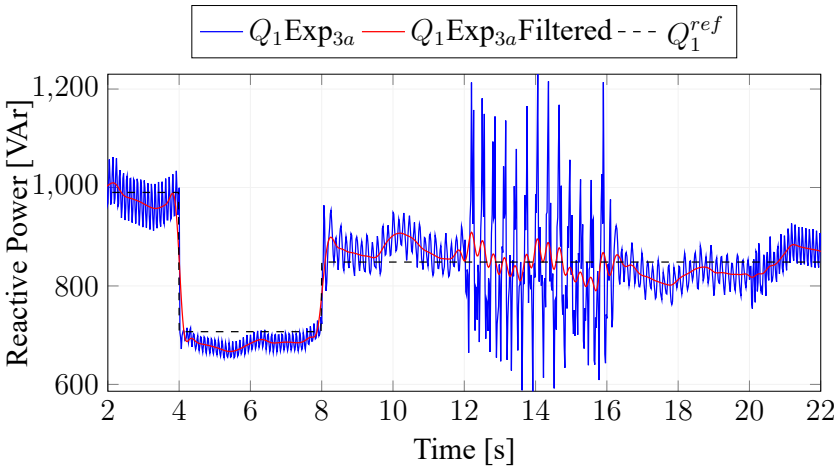

Figure 5.10: Raw reactive power data compared to filtered reactive power data

slightly more overshoot and marginal non-linearities present during the sub-synchronous response.

For analysis of measurements with high harmonic components, where the component of interest is at lower frequencies a low pass filter (LPF) is applied. As an example for the power measurements a LPF with a cutoff frequency of 5 Hz and a sampling frequency of 500 Hz was applied to the measurement results in order to compare the results more intuitively . An example of the actual measurements compared to the filtered measurements is shown in Figure 5.10.

The power output of the machine is shown in Figure 5.11 where the machine is drawing around 80 W of active at synchronous speeds. at time step 4 controller $3a$ shows small disturbances in Figure 5.11(a) due to the reactive power step change. The effect is largely removed in the rest of the controllers, indicating that the cross compensation terms or cascaded PIs are capable of correcting the cross disturbances of the orthogonal axis for the machine. The reactive power of all three controllers indicate similar responses, with the expanded controller $5d$ indicating an overall transition curve which is smoother, however the filtered response of the controller does indicate a lot of disturbance and noise. In order to further evaluate this the unfiltered response is shown for comparison. In Figure 5.12 it can be seen that controller $4c$ shows a quicker step response whereas the settling time for

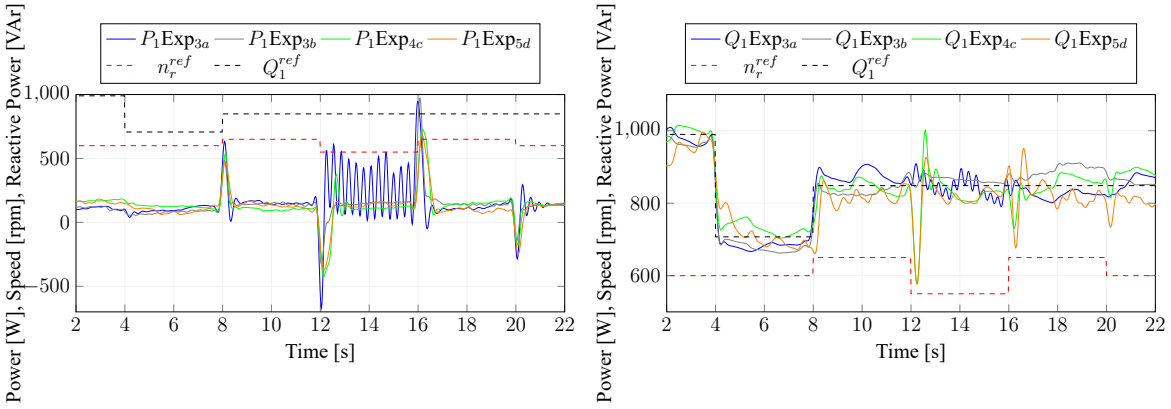

(a) **(b)**

Figure 5.11: Comparison of different controllers applied to the experimental machine while applying a varying amplitude step input to the speed reference.

Stellenbosch University https://scholar.sun.ac.za

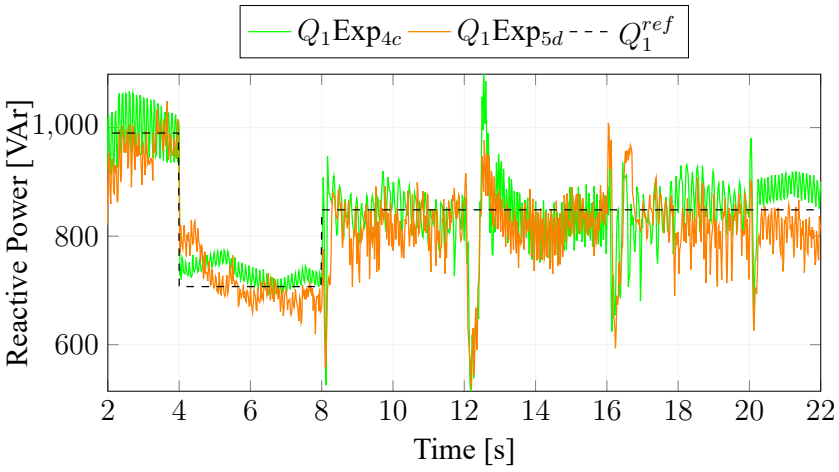

Figure 5.12: Comparison of raw reactive power data

5d is slightly quicker. The expanded controller 5d does indicate more disturbances with larger steady state oscillations, which is an important side effect of greater response to disturbances. It is clear that measurement noise carry through to the cross compensation components, indicating that over-compensation can become detrimental to a control system and actually reduce robustness, making a system more vulnerable to sensor failures as well as incorrect machine parameters. At time step 12 it is clear however that the expanded controller 5d as well as the reduced controller show similar immediate responses to the speed reference step input, however the expanded controller shows less overshoot and a quicker settling time during the disturbance.
To clearly indicate the advantages of the cascaded PI controllers, the $q-$axis (speed control loop) of the current loops are now analyzed using Figure 5.13. The current response to speed and reactive power step changes at time step 8 can be seen to decline in Figure 5.13(a), where the response overshoot reduces with an increase in cascaded PIs. This is shown again in Figure 5.13(b). The effect of the addition of voltage compensation is again clearly visible here, indicating great improvements in stability in all operating regions of the machine.

As for the current cross compensation terms between controllers 4c and 5d it is reasonable to conclude that the terms don't carry any significant impact in the speed control loop, nor in the reactive power control loops and as such the assumptions in 4.4.1 are confirmed that their influence is negligible for stable control purposes.

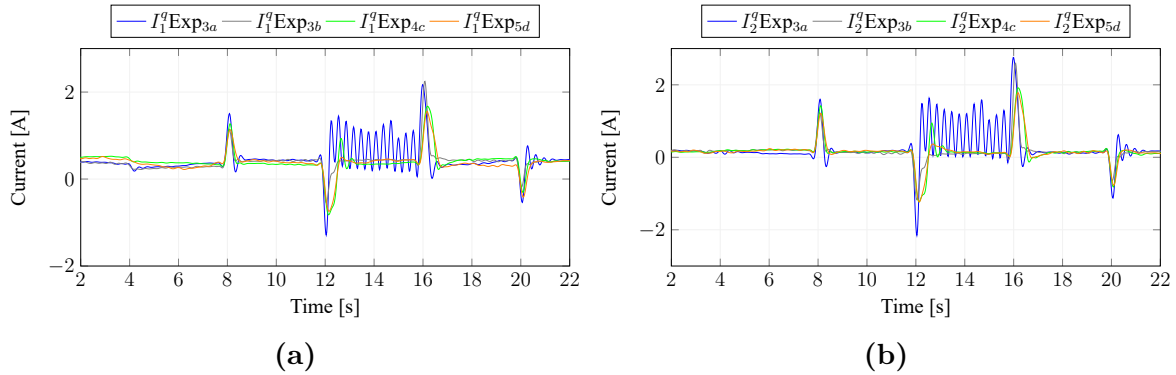

(a) **(b)**

Figure 5.13: Comparison of different controllers applied to the experimental machine while applying a varying amplitude step input to the speed reference.

Stellenbosch University https://scholar.sun.ac.za

5.8 Fixed speed, active- and reactive-power control

The machine is now operated in generation mode in order to show the stability of the various controllers using active and reactive power control loops. During this mode of operation the prime mover is operated using a V/Hz frequency inverter.

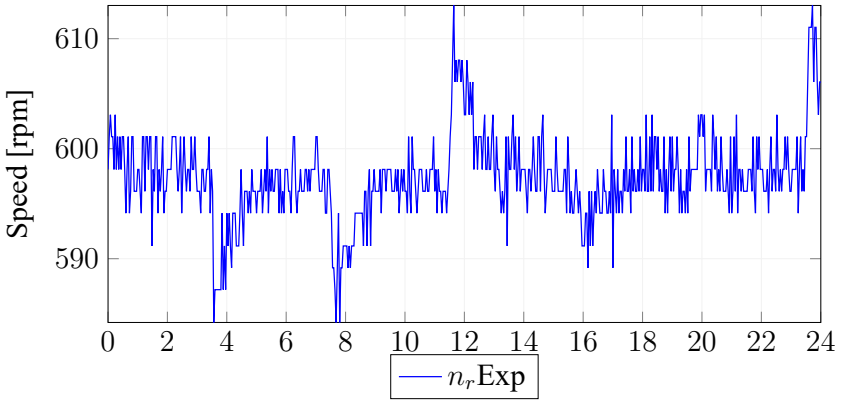

Figure 5.14: Generator rotational Speed fixed to 600 rpm by a 22kW prime mover induction motor

5.8.1 Controller Comparison

The prime mover is set to maintain a natural speed of 600rpm. Naturally during the control phase of the BDFIG torque will be drawn from and supplied to the prime mover, which will at all times attempt to return to natural speed with slight increases in slip, accordingly applying a load to the BDFIG which results in a power output tracking the reference power output. The speed variations during this phase is shown in Figure 5.14. In all the figures to follow, similarly as before the subscripts $3b, 4c$ and $5c$ refer to control typologies from table A.3. During the first 12 seconds of control step changes in active power are made, where the generator delivers between 0 kW and 1 kW into the grid. This is then followed by step changes in reactive power of equivalent magnitude while maintaining constant power output at 0.5 kW. It can be seen in Figures 5.15(a) and 5.15(b) that all three controllers perform very similarly, with the reduced PI model showing marginally more noise between all three controllers. The controller with two cascaded PIs show the best response, with low noise and good stability as can be seen in Figure 5.16 where the generator $d-$axis currents of the reactive power control loop are shown.

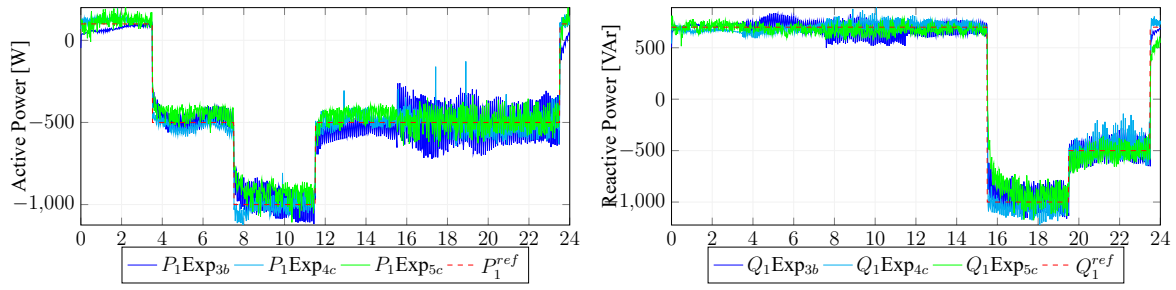

(a) Generator active power **(b)** Generator reactive power

Figure 5.15: Generator control while being fixed to a rotational speed of 600rpm

Stellenbosch University https://scholar.sun.ac.za

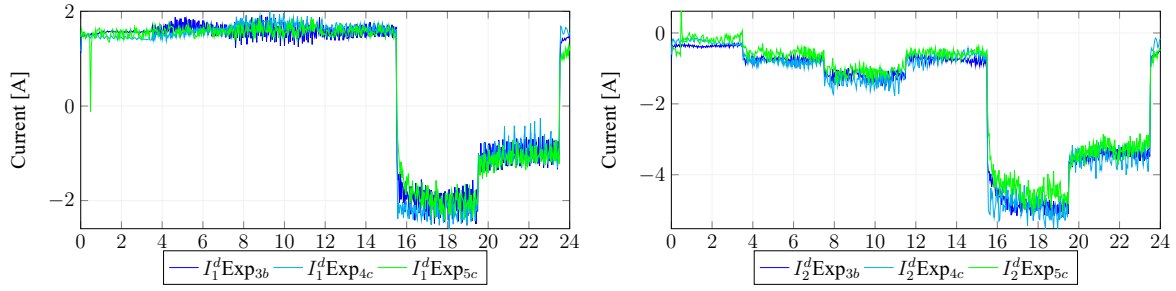

(a) d-axis current primary winding **(b)** d-axis current secondary winding

Figure 5.16: Generator control while being fixed to a rotational speed of 600rpm with step changes in power

5.8.2 Generator transition between generation and motoring modes

In Figure 5.17 the active and reactive power of the machine while transitioning between generation and motoring modes can be observed. Mechanical power is being drawn from the prime mover and supplied primary winding. Conversely when active power is being drawn from the grid then mechanical power is being supplied to the prime mover, which dissipates it through heat or power on its' stator windings.

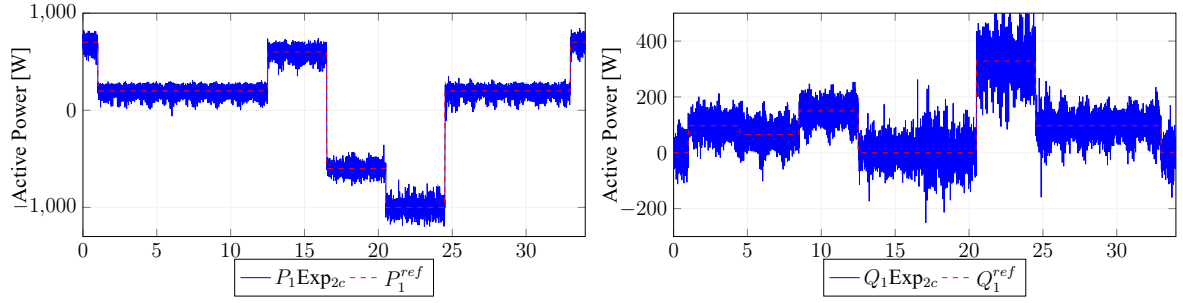

(a) Generator active power **(b)** Generator reactive power

Figure 5.17: Generator control while transitioning between motoring and generation

Stellenbosch University https://scholar.sun.ac.za

5.8.3 Generator operation in sub- and super-synchronous speed

During sub- and super-synchronous operation the machine has two modes of power flow. In sub-synchronous operation the machine is in motoring mode. In this mode power is being drawn from the control winding. When in super-synchronous mode the machine is in generation mode, where power is being supplied to the grid from the control windings. When connected using a back-to-back converter that allows for the secondary winding

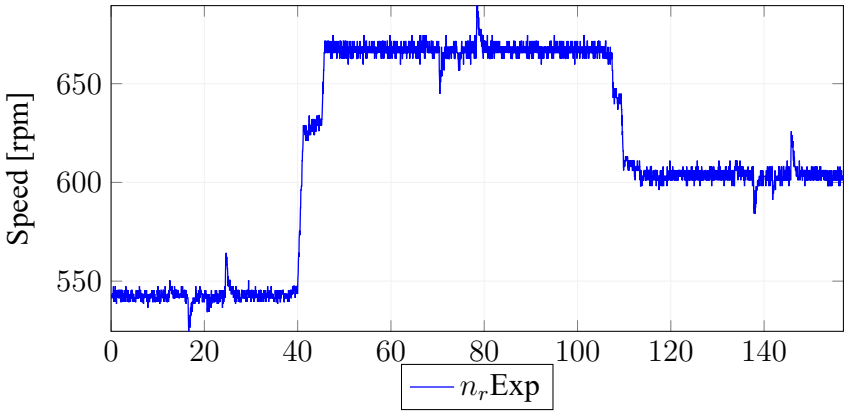

Figure 5.18: Generator rotational Speed transitioning from sub-synchronous to super-synchronous speeds by a 22 kW prime mover induction motor

power to be converted back to grid frequency and is resupplied to the grid. In the setup used however, a back-to-back converter without the GSC was used. Instead a rectifier bridge supplied the DC-bus. This does not allow for bi-directional power flow and as such a load should be added to the DC-bus when in motoring to avoid increases in the DC-bus voltage. To reduce the effects of this the apparent power drawn from the grid was limited to 450 VA. In Figure 5.18 the machine can be seen to transition between sub-synchronous, super-synchronous and synchronous operation.

In Figure 5.17(a) the active power can be seen to draw from the grid and then supply to the grid. In Figure 5.17(b) the reactive power adjusts accordingly to maintain a varying power factor between 0.95 and 0.8 lagging.

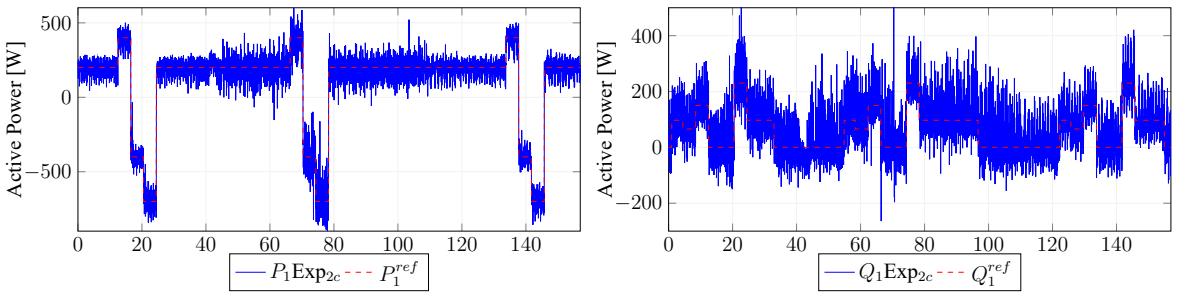

(a) Generator active power **(b)** Generator reactive power

Figure 5.19: Generator control while in sub- and super-synchronous operation

Stellenbosch University https://scholar.sun.ac.za

5.9 Conclusion

For the BDFIM model to be verified reliably as well as the control theory to be confirmed, a practical implementation thereof was implemented. A National Instruments controller in addition to Labview was used to peFrform real time control of the machine and obtain high speed measurement results. These results were then presented and compared, allowing for a direct comparison into the viability of using reduction techniques for state estimators to predict the response of the controller on a theoretical machine. To match the mechanical characteristics of the machine, a process of curve fitting was followed, ensuring that the machine dynamics are similar to that of the practical one. Thereafter the output power and currents were analyzed and compared, showing that the derived parameters are within reasonable accuracy.

The experimental machine was operated in cascade induction mode to show the accuracy of the theoretical model. It was found that the stator currents had a standard deviation and mean of as low as 8.71 and 3.06% respectively. Current control was then performed to show the response of the controller when step references were given to the dq-axis primary and secondary winding currents. This was followed by a comparison of different control methods, where the machine was run in motoring mode and generation modes at sub- and super synchronous speeds.

During all of these tests it can be concluded that good control response and robustness can be obtained using the control reduction methods shown in chapter 4. Additionally it was also shown that fairly accurate current state estimations could be made, when using the appropriate transformation techniques.

Stellenbosch University https://scholar.sun.ac.za

Chapter 6

Conclusions and Future Recommendations

Various methods for modeling the brushless doubly fed induction machine are presented in this dissertation. A parameter reduction technique presented in [15] was applied to a bar-cage rotor, showing its' validity as a general solution for rotors of differing types. It was decided to use a model presented in [48] to simulate the machine responses for control. To ensure accurate simulation results, the full expanded 23-state BDFIM model was used and compared to actual experimental measurements performed using a National Instruments controller in conjunction with Labview. The control performed covered various versions of the ideal theoretical controller - simplified and reduced in order to increase robustness while maintaining accuracy and detailed control. This was observed in real-time while the control philosophy was applied to an experimental bar cage brushless doubly fed induction machine. It was found that various portions of the controller, such as certain cross compensation terms were negligible and could at times be detrimental to the control system, causing instability if noisy / inaccurate measurements were observed.

6.1 Conclusion

In this thesis the modeling of the whole BDFIM, including the wind energy conversion system, filter, wind turbine, back-to-back converter, GSC and CWSC was presented. An in depth review of a suitable reduction technique was presented and applied to a physical machine. It was noted that the reduction technique would be suitable for general types of rotor structures, however only results for nested loop type rotors have been shown and as such it was important to show that the procedure followed remains suitable for rotors of other types, such as the bar-cage rotor used in this experiment. It was found that both the full state and reduced order models showed satisfactory resemblance to that of the physical machine during free acceleration. A control strategy of the grid-side converter based on an L-filter was developed and implemented in Matlab Simulink. Furthermoer a control strategy of the control-winding side converter was presented. This was followed with various conditions under which the controller could be simplified. The controllers showed good stability and similar response accuracy to that of the original controller. At times promising to be less prone to sensor noise and disturbances.

Different modes of control were performed and shown to be very responsive. Starting with current control of the primary and secondary windings up to speed, active- and reactive-power regulation. All of these were performed on a physical machine and showed

Stellenbosch University https://scholar.sun.ac.za

satisfactory performance and great similarity to that of the simulated predictions. Control under different modes of operation were performed, showing the machine response under synchronous, sub- and super-synchronous speeds. In doing so power was drawn and transferred to the grid using both the primary and secondary windings.

The controller of the proposed control strategy on the BDFIM was implemented in the laboratory using LabVIEW. Through the various operating conditions and control strategies performed, it was shown that the implemented controller had good performance and the reduction techniques presented allowed for accurate approximations of the machines current states.

6.2 Future Recommendations

There are many aspects of the control of BDFIG that can be further investigated. However, a few recommendations are as follows:

- The addition of physical and digital filters to reduce sensor noise. It was seen throughout that inaccurate sensor measurements can cause the controller to respond incorrectly, adding increased noise to the system.
- Sensor-less vector control by implementing an encoder-less controller. By estimating the rotor speed and position, further improvements to the machines robustness can be made.
- The automation of grid synchronization can be explored, allowing for a seamless control system that automatically locks with the grid and is easily engaged.
- Stand-alone operation of the BDFIM where voltage and frequency control is necessary can open the BDFIM to wider markets

Stellenbosch University https://scholar.sun.ac.za

List of References

[1] Downtime reduction via predictive maintenance. oct 2021.
Available at: https://www.jungle.ai/post/downtime-reduction-via-predictive-maintenance

[2] Lamme, B.G.: The story of the induction motor. *J. Am. Inst. Electr. Eng.*, vol. 40, no. 3, pp. 203–223, 1921.

[3] Cotton, H.: Rheostatic speed control of a motor working against a torque which is a function of the speed. *J. Inst. Electr. Eng.*, vol. 66, no. 379, pp. 790–794, 1928.

[4] Gabriel, R., Leonhard, W. and Nordby, C.J.: Field-oriented control of a standard ac motor using microprocessors. *IEEE Trans. Ind. Appl.*, vol. 1, no. 2, pp. 186–192, 1980.

[5] Bozhko, S.V., Blasco-Gimenez, R., Li, R., Clare, J.C. and Asher, G.M.: Control of offshore DFIG-based wind farm grid with line-commutated HVDC connection. *IEEE Trans. Energy Convers.*, vol. 22, no. 1, pp. 71–78, 2007.

[6] Bozhko, S., Asher, G., Li, R., Clare, J. and Yao, L.: Large offshore DFIG-based wind farm with line-commutated HVDC connection to the main grid: Engineering studies. *IEEE Trans. energy Convers.*, vol. 23, no. 1, pp. 119–127, 2008.

[7] Rampion Wind Farm.

[8] Walney Wind Farm.

[9] Löhdefink, P., Dietz, A. and Möckel, A.: Direct drive concept for heavy-duty traction applications with the brushless doubly-fed induction machine. In: *2018 Thirteen. Int. Conf. Ecol. Veh. Renew. Energies*, pp. 1–6. 2018.

[10] Rothenhagen, K. and Fuchs, F.W.: Doubly fed induction generator model-based sensor fault detection and control loop reconfiguration. *IEEE Trans. Ind. Electron.*, vol. 56, no. 10, pp. 4229–4238, 2009.

[11] Ramchandran, A.: *Frequency domain, parameter estimation for a brushless, doubly-fed machine*. Ph.D. thesis, Oregon State University, 1995.

[12] Su, J., Chen, Y., Sun, L., Liu, X. and Kang, Y.: Parameter estimation of brushless doubly-fed induction generator based on steady experimental results. In: *2015 IEEE Energy Convers. Congr. Expo.*, pp. 2800–2804. IEEE, 2015.

[13] Flack, T.J.: Equivalent circuit for the brushless doubly fed machine (BDFM) including parameter estimation and experimental verification. *IEE Proc. - Electr. Power Appl.*, vol. 152, no. 4, pp. 933–942(9), jul 2005. ISSN 1350-2352.
Available at: https://digital-library.theiet.org/content/journals/10.1049/ip-epa{_}20045106

Stellenbosch University https://scholar.sun.ac.za

[14] Boger, M.S.: Aspects of brushless doubly-fed induction machines. *Apollo - Univ. Cambridge Repos.*, oct 2015.
Available at: `https://www.repository.cam.ac.uk/handle/1810/251627`

[15] Roberts, P.C.: Study of brushless doubly-fed (induction) machines: contributions in machine analysis, design and control. *Apollo - Univ. Cambridge Repos.*, oct 2015.
Available at: `https://www.repository.cam.ac.uk/handle/1810/251955`

[16] Honório, D.A., Diniz, E.C., de Souza, A.B., Almeida, O.M. and Barreto, L.H.S.C.: Comparison between sliding model control and vector control for a DSP-based position control applied to squirrel-cage induction motor. In: *2010 9th IEEE/IAS Int. Conf. Ind. Appl. - INDUSCON 2010*, pp. 1–6. 2010.

[17] Poza, J., Oyarbide, E. and Roye, D.: New vector control algorithm for brushless doubly-fed machines. In: *IEEE 2002 28th Annu. Conf. Ind. Electron. Soc. IECON 02*, vol. 2, pp. 1138–1143 vol.2. 2002.

[18] Hutton, T. and Gule, N.: Simplified Vector Control of a Nested-Loop Rotor Brush-less Doubly Fed Induction Motor. In: *2020 Int. Symp. Power Electron. Electr. Drives, Autom. Motion*, pp. 53–58. IEEE, 2020.

[19] Gorginpour, H., Oraee, H. and McMahon, R.A.: Performance Description of Brushless Doubly-Fed Induction Machine in Its Asynchronous and Variable Speed Synchronous Modes. *J. Electromagn. Anal. Appl.*, vol. 03, no. 12, pp. 490–511, 2011.
Available at: `https://doi.org/10.4236/jemaa.2011.312077`

[20] Wallace, A.K., Spee, R. and Lauw, H.K.: The potential of brushless doubly-fed machines for adjustable speed drives. In: *Annu. Tech. Conf. Pulp Pap. Ind.*, pp. 45–50. 1990.

[21] Brune, C., Spe, R. and Wallace, A.K.: Experimental evaluation of a variable-speed, doubly-fed wind-power generation system. In: *Conf. Rec. 1993 IEEE Ind. Appl. Conf. Twenty-Eighth IAS Annu. Meet.*, pp. 480–487 vol.1. 1993.

[22] Thompson, S.P.: *Polyphase Electric Currents and Alternate-current Motors.* Finsbury technical manuals. Spon, 1895.
Available at: `https://books.google.co.za/books?id=TvwHAAAAMAAJ`

[23] Ferraris, G.: Sulle differenze di fase delle correnti, sul ritardo dell{\textquotesingle}induzione e sulla dissipazione di energia nei trasformatori. *Nuovo Cim. Ser. 3*, vol. 23, no. 1, pp. 138–158, dec 1888.
Available at: `https://doi.org/10.1007/bf02730236`

[24] Chapman, S.J.: *Electric Machinery Fundamentals (Power & energy).* Power & energy, 4th edn. McGraw Hill Higher Education, 2004. ISBN 9780071151559,0071151559.
Available at: `http://gen.lib.rus.ec/book/index.php?md5=13fb26e59c12418a13736d89a6c61d87`

[25] Donald Fink, H.B.: *Standard Handbook For Electrical Engineers.* 15th edn. McGraw-Hill Professional, 2006. ISBN 9780071441469,0071441468.
Available at: `http://gen.lib.rus.ec/book/index.php?md5=2452bdba02ebf70217bc07eff506f536`

[26] A. E. Fitzgerald Charles Kingsley Jr., S.U.: *Electric Machinery.* 6th edn. McGraw-Hill Science/Engineering/Math, 2002. ISBN 9780073660097,0073660094.
Available at: `http://gen.lib.rus.ec/book/index.php?md5=b125eb9978ec48037cdacbdfac249833`

Stellenbosch University https://scholar.sun.ac.za

[27] Pena, R.S., Asher, G.M., Clare, J.C. and Cardenas, R.: A constant frequency constant voltage variable speed stand alone wound rotor induction generator. In: *Int. Conf. Oppor. Adv. Int. Electr. Power Gener. (Conf. Publ. No. 419)*, pp. 111–114. 1996.

[28] Artigao, E., Sapena-Bano, A., Honrubia-Escribano, A., Martinez-Roman, J., Puche-Panadero, R. and Gómez-Lázaro, E.: Long-Term Operational Data Analysis of an In-Service Wind Turbine DFIG. *IEEE Access*, vol. 7, pp. 17896–17906, 2019.

[29] Hunt, L.J.: A new type of induction motor. *J. Inst. Electr. Eng.*, vol. 39, pp. 648–667, 1907.

[30] Creedy, F.: Some developments in multi-speed cascade induction motors. *J. Inst. Electr. Eng.*, vol. 59, no. 301, pp. 511–532(21), may 1921. ISSN 0099-2887.
Available at: `https://digital-library.theiet.org/content/journals/10.1049/jiee-1.1921.0036`

[31] Munoz, A.R. and Lipo, T.A.: Dual stator winding induction machine drive. *IEEE Trans. Ind. Appl.*, vol. 36, no. 5, pp. 1369–1379, 2000.

[32] Ojo, O.: Coupled-circuit-model simulation and airgap-field calculation of a dual-stator-winding induction machine. *IEE Proc. - Electr. Power Appl.*, vol. 153, no. 3, pp. 387–400(13), may 2006. ISSN 1350-2352.
Available at: `https://digital-library.theiet.org/content/journals/10.1049/ip-epa{_}20050466`

[33] Troncoso, P.E., Battaiotto, P.E. and Mantz, R.J.: Active and reactive power control capability in wind generation based on BDFIG machine. In: *2015 IEEE PES Innov. Smart Grid Technol. Lat. Am. (ISGT LATAM)*, pp. 546–551. 2015.

[34] Spee, R., Wallace, A.K. and Lauw, H.K.: Performance simulation of brushless doubly-fed adjustable speed drives. In: *Conf. Rec. IEEE Ind. Appl. Soc. Annu. Meet.*, pp. 738–743 vol.1. 1989.

[35] Long, T., Shao, S., Malliband, P., Abdi, E. and McMahon, R.A.: Crowbarless Fault Ride-Through of the Brushless Doubly Fed Induction Generator in a Wind Turbine Under Symmetrical Voltage Dips. *IEEE Trans. Ind. Electron.*, vol. 60, no. 7, pp. 2833–2841, 2013.

[36] Tavner, P.J., Mcmahon, R.A., Roberts, P., Wang, X., Jagieła, M. and Chick, T.: Rotor Design & Performance for a BDFM. *Power*, pp. 2–6, 2006.

[37] Burbridge, L.: Self-cascaded machine: a low-speed motor or high-frequency brushless alternator. *Proc. Inst. Electr. Eng.*, vol. 117, no. 7, pp. 1277–1290(13), jul 1970. ISSN 0020-3270.
Available at: `https://digital-library.theiet.org/content/journals/10.1049/piee.1970.0247`

[38] Wang, X., Liu, D., Polinder, H., Lahaye, D. and Ferreira, J.A.: Comparison of nested-loop rotors in brushless doubly-fed induction machines. In: *2016 19th Int. Conf. Electr. Mach. Syst.*, pp. 1–6. 2016.

[39] Logan, T.G., McMahon, R.A., Tavner, P.J. and Tohidi, S.: A comparison of cage and nested-loop BDFM rotors. In: *6th IET Int. Conf. Power Electron. Mach. Drives (PEMD 2012)*, pp. 1–6. 2012.

Stellenbosch University https://scholar.sun.ac.za

[40] Liu, Y., Xu, W., Zhu, J. and Blaabjerg, F.: Sensorless Control of Standalone Brushless Doubly Fed Induction Generator Feeding Unbalanced Loads in a Ship Shaft Power Generation System. *IEEE Trans. Ind. Electron.*, vol. 66, no. 1, pp. 739–749, 2019.

[41] Carlson, R., Voltolini, H., Runcos, F. and Kuo-Peng, P.: A performance comparision between brush and brushless doubly fed asynchronous generators for wind power systems. *Renew. Energy Power Qual. J.*, vol. 1, no. 04, pp. 258–262, apr 2006.
Available at: `https://doi.org/10.24084/repqj04.405`

[42] Renewable {Independent} {Power} {Producer} {Programme} {\textbar} {South} {African} {Government}. .
Available at: `https://www.gov.za/about-government/government-programmes/renewable-independent-power-producer-programme{#}:{~}:text=RenewableIndependentPowerProducerProgramme(REIPPP)isaimedatbringing,132jobssinceitsinception.`

[43] {IPP} {Renewables}. .
Available at: `https://www.ipp-renewables.co.za/`

[44] Joos, G.: Wind turbine generator low voltage ride through requirements and solutions. In: *2008 IEEE Power Energy Soc. Gen. Meet. - Convers. Deliv. Electr. Energy 21st Century*, pp. 1–7. 2008.

[45] Alizadeh, M., Ghazi, R., Haghani, E.E. and Rad, M.E.: Improving Analysis of Low Voltage Ride Through Capability in Turbines Connected to The Brushless Doubly Fed Induction Generator (BDFIG) under Fault Conditions. In: *2019 Int. Power Syst. Conf.*, pp. 655–661. 2019.

[46] Long, T., Shao, S., Abdi, E., McMahon, R.A. and Liu, S.: Asymmetrical Low-Voltage Ride Through of Brushless Doubly Fed Induction Generators for the Wind Power Generation. *IEEE Trans. Energy Convers.*, vol. 28, no. 3, pp. 502–511, 2013.

[47] Barati, F., McMahon, R., Shao, S., Abdi, E. and Oraee, H.: Generalized vector control for brushless doubly fed machines with nested-loop rotor. *IEEE Trans. Ind. Electron.*, vol. 60, no. 6, pp. 2477–2485, 2013. ISSN 02780046.

[48] Rodriguez, M.: Unified reference frame dq model of the brushless doubly fed machine. *IEE Proc. - Electr. Power Appl.*, vol. 153, no. 5, pp. 726–734(8), sep 2006. ISSN 1350-2352.
Available at: `https://digital-library.theiet.org/content/journals/10.1049/ip-epa{_}20050404`

[49] Li, R., Spee, R., Wallace, A.K. and Alexander, G.C.: Synchronous drive performance of brushless doubly-fed motors. *IEEE Trans. Ind. Appl.*, vol. 30, no. 4, pp. 963–970, 1994.

[50] Wallace, A.K.: Generalised theory of the brushless doubly-fed machine. Part 1: Analysis. *IEE Proc. - Electr. Power Appl.*, vol. 144, no. 2, pp. 111–122(11), mar 1997. ISSN 1350-2352.
Available at: `https://digital-library.theiet.org/content/journals/10.1049/ip-epa{_}19971051`

[51] Ferreira, A.C.: Generalised theory of the brushless doubly-fed machine. Part 2: Model verification and performance. *IEE Proc. - Electr. Power Appl.*, vol. 144, no. 2, pp. 123–129(6), mar 1997. ISSN 1350-2352.
Available at: `https://digital-library.theiet.org/content/journals/10.1049/ip-epa{_}19971052`

Stellenbosch University https://scholar.sun.ac.za

[52] Jovanovic, M.: Sensored and sensorless speed control methods for brushless doubly fed reluctance motors. *IET Electr. Power Appl.*, vol. 3, no. 6, pp. 503–513(10), nov 2009. ISSN 1751-8660.
Available at: `https://digital-library.theiet.org/content/journals/10.1049/iet-epa.2008.0227`

[53] Shao, S., Abdi, E. and McMahon, R.: Low-Cost Variable Speed Drive Based on a Brushless Doubly-Fed Motor and a Fractional Unidirectional Converter. *IEEE Trans. Ind. Electron.*, vol. 59, no. 1, pp. 317–325, 2012.

[54] Takahashi, I. and Noguchi, T.: A New Quick-Response and High-Efficiency Control Strategy of an Induction Motor. *IEEE Trans. Ind. Appl.*, vol. IA-22, no. 5, pp. 820–827, 1986.

[55] Depenbrock, M.: Direct self-control (DSC) of inverter-fed induction machine. *IEEE Trans. Power Electron.*, vol. 3, no. 4, pp. 420–429, 1988.

[56] Ghaffarpour, A., Barati, F. and Oraee, H.: Implementation of drirect torque control method on brushless doubly fed induction machines in unbalenced situations. In: *2016 7th Power Electron. Drive Syst. Technol. Conf.*, pp. 70–75. 2016.

[57] Mosaddegh, H.R. and Zarchi, H.A.: Maximum torque per ampere control of brushless doubly fed induction machine using variable structure approach. In: *2014 22nd Iran. Conf. Electr. Eng.*, pp. 677–682. 2014.

[58] Zhou, D., Spee, R. and Alexander, G.C.: Experimental evaluation of a rotor flux oriented control algorithm for brushless doubly-fed machines. *IEEE Trans. Power Electron.*, vol. 12, no. 1, pp. 72–78, 1997.

[59] Munoz, A.R. and Lipo, T.A.: Complex vector model of the squirrel-cage induction machine including instantaneous rotor bar currents. *IEEE Trans. Ind. Appl.*, vol. 35, no. 6, pp. 1332–1340, 1999.

[60] Barati, F., Oraee, H., Abdi, E., Shao, S. and McMahon, R.: The Brushless Doubly-Fed Machine Vector Model in the rotor flux oriented reference frame. In: *2008 34th Annu. Conf. IEEE Ind. Electron.*, pp. 1415–1420. 2008.

[61] Poza, J., Oyarbide, E., Sarasola, I. and Rodriguez, M.: Vector control design and experimental evaluation for the brushless doubly fed machine. *IET Electr. Power Appl.*, vol. 3, no. 4, pp. 247–256, 2009. ISSN 17518660.

[62] Shao, S., Abdi, E., Barati, F. and McMahon, R.: Stator-Flux-Oriented Vector Control for Brushless Doubly Fed Induction Generator. *IEEE Trans. Ind. Electron.*, vol. 56, no. 10, pp. 4220–4228, 2009.

[63] Barati, F., Oraee, H., Abdi, E. and McMahon, R.: Derivation of a vector model for a Brushless Doubly-Fed Machine with multiple loops per nest. In: *2008 IEEE Int. Symp. Ind. Electron.*, pp. 606–611. 2008.

[64] Barati, F. and Oraee, H.: Vector model utilization for nested-loop rotor Brushless Doubly-Fed Machine analysis, control and simulation. In: *2010 1st Power Electron. Drive Syst. Technol. Conf.*, pp. 295–301. 2010.

[65] Barati, F., Shao, S., Abdi, E., Oraee, H. and McMahon, R.: Synchronous operation control of the Brushless Doubly-Fed Machine. In: *2010 IEEE Int. Symp. Ind. Electron.*, pp. 1510–1516. 2010.

Stellenbosch University https://scholar.sun.ac.za

[66] Mosaddegh, H.R. and Zarchi, H.A.: Variable structure direct torque control of brushless doubly fed induction generator for wind turbine applications. In: *2014 22nd Iran. Conf. Electr. Eng.*, pp. 671–676. IEEE, 2014.

[67] Voltolini, H. and Carlson, R.: Grid synchronization and Maximum Power Point Tracking for wind energy generation system with Brushless Doubly Fed Induction Generator. pp. 2173–2177. 2008.

[68] Cai, S. and Wen, H.: Modeling and MPPT control of DFIG wind energy system. In: *Int. Conf. Renew. Power Gener. (RPG 2015)*, pp. 1–6. 2015.

[69] Bossoufi, B., Aroussi, H.A., Ziani, E.M., Karim, M., Lagrioui, A., Derouich, A. and Taoussi, M.: Robust adaptive Backstepping control approach of DFIG generators for wind turbines variable-speed. In: *2014 Int. Renew. Sustain. Energy Conf.*, pp. 791–797. 2014.

[70] Bakouri, A., Mahmoudi, H., Barara, M., Abbou, A., Bennassar, A. and Moutchou, M.: A complete control startegy of DFIG connected to the grid for wind energy conversion systems. In: *2015 3rd Int. Renew. Sustain. Energy Conf.*, pp. 1–6. 2015.

[71] Zamzoum, O., Mourabit, Y.E., Derouich, A. and Ghzizal, A.E.: Study and implementation of the {MPPT} strategy applied to a variable speed wind system based on {DFIG} with {PWM}-vector control. In: *2016 Int. Conf. Electr. Sci. Technol. Maghreb*, pp. 1–6. IEEE, oct 2016.

[72] Zheng, X., Li, L., Xu, D. and Platts, J.: Sliding Mode {MPPT} Control of Variable Speed Wind Power System. In: *2009 Asia-Pacific Power Energy Eng. Conf.*, pp. 1–4. IEEE, mar 2009.
Available at: `https://doi.org/10.1109/appeec.2009.4918770`

[73] Ferreira, A.C. and Williamson, S.: Time-stepping finite-element analysis of brushless doubly fed machine taking iron loss and saturation into account. *IEEE Trans. Ind. Appl.*, vol. 35, no. 3, pp. 583–588, 1999.

[74] Strous, T.D., Wang, X., Polinder, H. and Ferreira, J.A.B.: Brushless Doubly Fed Induction Machines: Magnetic Field Analysis. *IEEE Trans. Magn.*, vol. 52, no. 11, pp. 1–10, 2016.

[75] Gorginpour, H., Jandaghi, B., Saket, M.A., Oraee, A. and Oraee, H.: Magnetic Field Harmonic Analysis in brushless doubly fed machine. In: *Proc. 2011 3rd Int. Youth Conf. Energ.*, pp. 1–7. 2011.

[76] Zhang, J., Wang, X., Wu, T., Xiong, F. and Kan, C.: The principle and harmonic analysis of a new BDFM with tooth harmonic wound rotor using as a generator. In: *2008 Int. Conf. Electr. Mach. Syst.*, pp. 3622–3626. 2008.

[77] Wallace, A.K., Spee, R. and Lauw, H.K.: Dynamic modeling of brushless doubly-fed machines. In: *Conf. Rec. IEEE Ind. Appl. Soc. Annu. Meet.*, pp. 329–334 vol.1. 1989.

[78] Boger, M.S., Wallace, A.K., Spee, R. and Li, R.: General pole number model of the brushless doubly-fed machine. *IEEE Trans. Ind. Appl.*, vol. 31, no. 5, pp. 1022–1028, 1995.

[79] Li, R., Wallace, A. and Spee, R.: Dynamic simulation of brushless doubly-fed machines. *IEEE Trans. Energy Convers.*, vol. 6, no. 3, pp. 445–452, 1991.

Stellenbosch University https://scholar.sun.ac.za

[80] Li, R., Wallace, A., Spee, R. and Wang, Y.: Two-axis model development of cage-rotor brushless doubly-fed machines. *IEEE Trans. Energy Convers.*, vol. 6, no. 3, pp. 453–460, 1991.

[81] Olubamiwa, O., Gule, N. and Kamper, M.: Coupled circuit analysis of the brushlessdoubly fed machine using the windingfunction theory. *IET Electr. Power Appl.*, vol. 14, 2020.

[82] Beres, R.N., Wang, X., Liserre, M., Blaabjerg, F. and Bak, C.L.: A review of passive power filters for three-phase grid-connected voltage-source converters. *IEEE J. Emerg. Sel. Top. Power Electron.*, vol. 4, no. 1, pp. 54–69, 2015.

[83] Sen, S., Yenduri, K. and Sensarma, P.: Step-by-step design and control of LCL filter based three phase grid-connected inverter. In: *2014 IEEE Int. Conf. Ind. Technol.*, pp. 503–508. IEEE, 2014.

[84] Liserre, M., Blaabjerg, F. and Hansen, S.: Design and control of an LCL-filter-based three-phase active rectifier. *IEEE Trans. Ind. Appl.*, vol. 41, no. 5, pp. 1281–1291, 2005.

[85] Piasecki, S., Szmurlo, R. and Jasinski, M.: Design of Grid Connected AC-DC Converter using Multi-Objective Optimization. *Sci. J. Riga Tech. Univ. Control Commun. Eng.*, vol. 5, no. 1, pp. 11–19, 2014.

[86] Tang, Y., Yao, W., Loh, P.C. and Blaabjerg, F.: Design of LCL filters with LCL resonance frequencies beyond the Nyquist frequency for grid-connected converters. *IEEE J. Emerg. Sel. Top. Power Electron.*, vol. 4, no. 1, pp. 3–14, 2015.

[87] Mbukani, M. and Gule, N.: Analysis and control of a grid-connected three-phase PWM voltage-source converter based LCL filter. In: *South. African Univ. Power Eng. Conf.*, p. 853. 2017.

[88] McMahon, R.A., Wan, X., Abdi-Jalebi, E., Tavner, P.J., Roberts, P.C. and Jagiela, M.: The BDFM as a Generator in Wind Turbines. In: *2006 12th Int. Power Electron. Motion Control Conf.*, pp. 1859–1865. 2006.

[89] Asher, G.M.: Doubly fed induction generator using back-to-back PWM converters and its application to variable-speed wind-energy generation. *IEE Proc. - Electr. Power Appl.*, vol. 143, no. 3, pp. 231–241(10), may 1996. ISSN 1350-2352.
Available at: `https://digital-library.theiet.org/content/journals/10.1049/ip-epa{_}19960288`

[90] Reznik, A.: *Analysis and design of a smart-inverter for renewable energy interconnection to the grid*. Colorado School of Mines, 2013.

[91] Teodorescu, R., Liserre, M. and Rodriguez, P.: *Grid converters for photovoltaic and wind power systems*, vol. 29. John Wiley & Sons, 2011.

[92] Barbosa, A., Júnior, G.A., Barros, P. and Grande, C.: Symmetrical optimum based PI control redesign. In: *An. do XX Congr. Bras. Automática*, pp. 1143–1149. 2014.

[93] Mitchell, J.C.: *The control of a back-to-back power converter for small-scale reluctance synchronous generators in grid-connectedwind turbine systems*. Ph.D. thesis, Stellenbosch: Stellenbosch University, 2017.

[94] Mahmoodabadi, M., Taherkhorsandi, M., Castillo-Villar, K., Janaghaei, F. and Mortazavi Yazdi, S.M.: *Optimal Sliding and Decoupled Sliding Mode Tracking Control by Multi-objective Particle Swarm Optimization and Genetic Algorithms*, vol. 576, pp. 43–78. Springer, 2015. ISBN 978-3-319-11173-5.

Stellenbosch University https://scholar.sun.ac.za

[95] Sadeghi, R., Madani, S.M., Ataei, M., Kashkooli, M.R.A. and Ademi, S.: Super-Twisting Sliding Mode Direct Power Control of a Brushless Doubly Fed Induction Generator. *IEEE Trans. Ind. Electron.*, vol. 65, no. 11, pp. 9147–9156, nov 2018.
Available at: `https://doi.org/10.1109/tie.2018.2818672`

[96] Ji, K., Long, W. and He, J.: A Direct Control for Stand-Alone Operation Brushless Doubly Fed Induction Generator Using Sliding-Mode Control Approach. In: *2019 22nd Int. Conf. Electr. Mach. Syst.*, pp. 1–6. IEEE, aug 2019.
Available at: `https://doi.org/10.1109/icems.2019.8922197`

[97] Zhang, W.-F. and Yu, Y.-H.: Comparison of three SVPWM strategies. *J. Electron. Sci. Technol.*, vol. 5, no. 3, pp. 283–287, 2007.

[98] Kumar, K.V., Michael, P.A., John, J.P. and Kumar, S.S.: Simulation and comparison of SPWM and SVPWM control for three phase inverter. *ARPN J. Eng. Appl. Sci.*, vol. 5, no. 7, pp. 61–74, 2010.

[99] Haitham Abu?Rub Atif Iqbal, J.G.: *High Performance Control of AC Drives with MATLAB/Simulink Models*. John Wiley \& Sons, 2012. ISBN 9780470978290,9781119969242.
Available at: `http://gen.lib.rus.ec/book/index.php?md5=dc437f6918dd72536855f0efb40aba45`

[100] Lobo, F.J.P.: *Modélisation, conception et commande d'une machine asynchrone sans balais doublement alimentée pour la génération à vitesse variable*. Ph.D. thesis, Institut National Polytechnique de Grenoble-INPG, 2003.

[101] Emami-Naeini, G.F.F.J.D.P.A.: *Feedback Control of Dynamic Systems*. 7th edn. Pearson, 2014. ISBN 0133496597,9780133496598.
Available at: `http://gen.lib.rus.ec/book/index.php?md5=8690f2db3552e1e7c76ef585253afde8`

[102] Ho, S.L., Niu, S. and Fu, W.N.: A Novel Solid-Rotor Induction Motor With Skewed Slits in Radial and Axial Directions and Its Performance Analysis Using Finite Element Method. *IEEE Trans. Appl. Supercond.*, vol. 20, no. 3, pp. 1089–1092, 2010.

[103] Chiba, A. and Asama, J.: Influence of Rotor Skew in Induction Type Bearingless Motor. *IEEE Trans. Magn.*, vol. 48, no. 11, pp. 4646–4649, 2012.

Stellenbosch University https://scholar.sun.ac.za

Appendices

Stellenbosch University https://scholar.sun.ac.za

Appendix A

Vector Control and Transformations

Table A.1: cwsc gains

	Controller					
	1		2		3	
	Kp	***Ti***	***Kp***	***Ti***	***Kp***	***Ti***
CW Current Loop	9.64	0.036	9.64	0.036	9.64	0.036
PW Current Loop	66.134	0.098	-	-	-	-
Reactive Power Loop	0.0011	0.055	0.0019	0.04	0.0019	0.04
Torque Loop	0.079	0.054	0.18	0.046	-	-
Speed Loop	0.23	0.47	0.25	0.53	0.0746	0.3

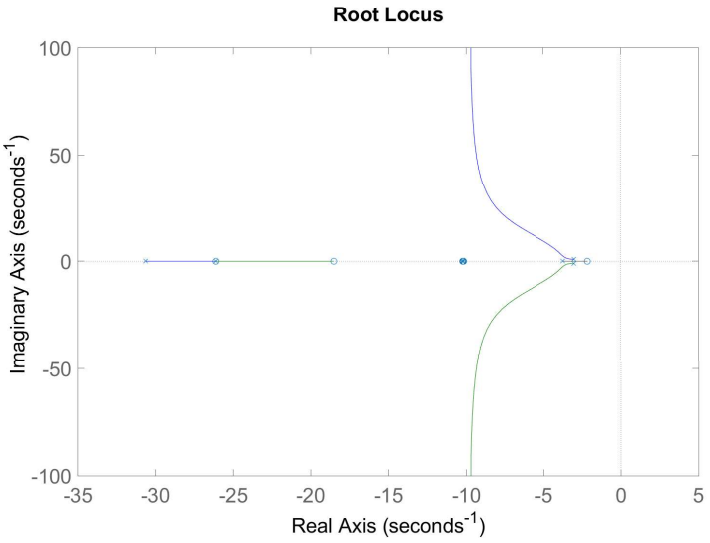

Figure A.1: Root locus for BDFIM presented in [61]

Stellenbosch University https://scholar.sun.ac.za

A.1 Tables of control methods and reductions performed

Table A.2: Table of experimental control simplifications performed

	Id	Subtest Approximation Assumptions
Category 0	Exp_{0a}	$V^d_{c-comp} \approx 0$
	Exp_{0b}	$V^q_{c-comp} \approx 0$
	Exp_{0c}	Exp_{0a}, Exp_{0b}
	Exp_{0d}	PI $\not{i^d_c}$
	Exp_{0e}	PI $\not{i^q_c}$
	Exp_{0f}	Exp_{0d}, Exp_{0e}
	Exp_{0g}	Exp_{0c}, Exp_{0f}
Category 1	Exp_{1a}	$\frac{dI^d_c}{dt} = I^d_c$
	Exp_{1b}	$\frac{dI^q_c}{dt} = I^q_c$
	Exp_{1c}	Exp_{1a}, Exp_{1b}
	Exp_{1d}	$\text{U}^q_{p-comp} \approx 0$
	Exp_{1e}	$\text{U}^d_{p-comp} \approx 0$
	Exp_{1f}	Exp_{1d}, Exp_{1e}
	Exp_{1g}	Exp_{1c}, Exp_{1f}
Category 2	Exp_{2a}	PI $\not{i^d_p}$
	Exp_{2b}	PI $\not{i^q_p}$ (see 4.40)
	Exp_{2c}	Exp_{2a}, Exp_{2b}

Table A.3: Table of experimental controllers

	Id	Subtest Removed	Description
Controller 1	Exp_{3a}	Exp_{0g},Exp_{1g},Exp_{2c}	Single PI, no cross compensation
	Exp_{3b}	Exp_{0f},Exp_{1g},Exp_{2c}	Single PI, V_c cross compensation
	Exp_{3c}	Exp_{0f},Exp_{1c},Exp_{2c}	Single PI, V_c,U_p cross compensation
Controller 2	Exp_{4a}	Exp_{0c},Exp_{1g},Exp_{2c}	Dual PI, no cross compensation
	Exp_{4b}	Exp_{1g},Exp_{2c}	Dual PI, V_c cross compensation
	Exp_{4c}	Exp_{1c},Exp_{2c}	Dual PI, V_c,U_p cross compensation
Controller 3	Exp_{5a}	Exp_{0c},Exp_{1g}	Three PI, no cross compensation
	Exp_{5b}	Exp_{1g}	Three PI, V_c cross compensation
	Exp_{5c}	Exp_{1c}	Three PI, V_c,U_p cross compensation
	Exp_{5d}		Three PI, V_c,U_p cross compensation, Integrator

Stellenbosch University https://scholar.sun.ac.za

A.2 Rotor reference frame sub-matrices

$$\boldsymbol{Q}^{dq0} = \begin{bmatrix} Q_{s1}^{dq0} & 0 & Q_{sr1}^{dq0} \\ 0 & Q_{s2}^{dq0} & Q_{sr2}^{dq0} \\ 0 & 0 & 0 \end{bmatrix}, \qquad \boldsymbol{M}^{dq0} = \begin{bmatrix} M_{s1}^{dq0} & 0 & M_{sr1}^{dq0} \\ 0 & M_{s2}^{dq0} & M_{sr2}^{dq0} \\ (M_{sr1}^{dq0})^T & (M_{sr2}^{dq0})^T & M_r^{dq0} \end{bmatrix}$$
$$\boldsymbol{R}^{dq0} = \begin{bmatrix} R_{s1}^{dq0} & 0 & 0 \\ 0 & R_{s2}^{dq0} & 0 \\ 0 & 0 & R_r^{dq0} \end{bmatrix} \tag{A.1}$$

$$T_e = \frac{1}{2} i^T \frac{d\boldsymbol{M}}{d\theta_r} i \tag{A.2}$$

A.3 Synchronous reference frame sub-matrices

$$\begin{bmatrix} v_{s1}^{dq0} \\ v_{s2}^{dq0} \\ 0 \end{bmatrix} = \left(\boldsymbol{T}_{sync}\boldsymbol{R}_{dq}\boldsymbol{T}_{sync}^{-1} + \omega_r \boldsymbol{T}_{sync}\boldsymbol{Q}_{dq}\boldsymbol{T}_{sync}^{-1} + \boldsymbol{T}_{sync}\boldsymbol{M}_{dq}\tfrac{d}{dt}\boldsymbol{T}_{sync}^{-1}\right) \begin{bmatrix} i_{s1}^{dq0} \\ i_{s2}^{dq0} \\ i_r^{dqr} \end{bmatrix}$$
$$+\boldsymbol{T}_{sync}\boldsymbol{M}_{dq}\boldsymbol{T}_{sync}^{-1}\frac{d}{dt} \begin{bmatrix} i_{s1}^{dq0} \\ i_{s2}^{dq0} \\ i_r^{dqr} \end{bmatrix} \tag{A.3}$$

$$T_e = \frac{1}{2} \begin{bmatrix} i_{s1}^{dq0} \\ i_{s2}^{dq0} \\ i_r^{dqr} \end{bmatrix}^T \boldsymbol{T}_{sync} \begin{bmatrix} 0 & 0 & \boldsymbol{Q}_{sr1}^{dq0} \\ 0 & 0 & \boldsymbol{Q}_{sr2}^{dq0} \\ (\boldsymbol{Q}_{sr1}^{dq0})^T & (\boldsymbol{Q}_{sr2}^{dq0})^T & 0 \end{bmatrix} \boldsymbol{T}_{sync}^{-1} \begin{bmatrix} i_{s1}^{dq0} \\ i_{s2}^{dq0} \\ i_r^{dqr} \end{bmatrix} \tag{A.4}$$

Equivalently...

$$\begin{bmatrix} v_{s1}^{dq0} \\ v_{s2}^{dq0} \\ 0 \end{bmatrix} = \left(\boldsymbol{R}_{sync} + \boldsymbol{Q}_{sync}\right) \begin{bmatrix} i_{s1}^{dq0} \\ i_{s2}^{dq0} \\ i_r^{dqr} \end{bmatrix} + \boldsymbol{M}_{sync}\frac{d}{dt} \begin{bmatrix} i_{s1}^{dq0} \\ i_{s2}^{dq0} \\ i_r^{dqr} \end{bmatrix} \tag{A.5}$$

$$T_e = \frac{1}{2} \begin{bmatrix} i_{s1}^{dq0} \\ i_{s2}^{dq0} \\ i_r^{dqr} \end{bmatrix}^T \boldsymbol{S}_{sync} \begin{bmatrix} i_{s1}^{dq0} \\ i_{s2}^{dq0} \\ i_r^{dqr} \end{bmatrix} \tag{A.6}$$

where...

$$\boldsymbol{R}_{sync} \triangleq \boldsymbol{T}_{sync}\boldsymbol{R}_{dq}\boldsymbol{T}_{sync}^{-1} \tag{A.7}$$

$$\boldsymbol{Q}_{sync}(\omega_1, \omega_r) \triangleq \omega_r \boldsymbol{T}_{sync}\boldsymbol{Q}_{dq}\boldsymbol{T}_{sync}^{-1} + \boldsymbol{T}_{sync}\boldsymbol{M}_{dq}\frac{d}{dt}\boldsymbol{T}_{sync}^{-1} \tag{A.8}$$

$$\boldsymbol{M}_{sync} \triangleq \boldsymbol{T}_{sync}\boldsymbol{M}_{dq}\boldsymbol{T}_{sync}^{-1} \tag{A.9}$$

$$\boldsymbol{S}_{sync} \triangleq \boldsymbol{T}_{sync} \begin{bmatrix} 0 & 0 & \boldsymbol{Q}_{sr1}^{dq0} \\ 0 & 0 & \boldsymbol{Q}_{sr2}^{dq0} \\ (\boldsymbol{Q}_{sr1}^{dq0})^T & (\boldsymbol{Q}_{sr2}^{dq0})^T & 0 \end{bmatrix} \boldsymbol{T}_{sync}^{-1} \tag{A.10}$$

Stellenbosch University https://scholar.sun.ac.za

Appendix B

Machine Specifications and results after simplification

B.1 Experimental Machine Parameters

Table B.1: Experimental Machine Parameters

Item	Symbol	Unit	Value
Rated PW & CW Voltage	V_{LL}	V_{rms}	381
Rated PW Current	I	I_{rms}	6.56
Rated CW Current	I	I_{rms}	5.6
Grid frequency	f_p	Hz	50
PW pole pairs	p_p	-	2
CW pole pairs	p_c	-	3
Natural speed	n_r	rpm	600
Moment of inertia	J	$kg.m^2$	0.154
Rotor friction coefficient	b	-	0.022
Rotor Bar resistance	R_b	$\mu\Omega$	26
Rotor lower end ring segment resistance	R_e	$\mu\Omega$	2.89
Rotor upper end ring segment resistance	R_{er}	$\mu\Omega$	14.5
Rotor loop 2 resistance	R_{r2}	$\mu\Omega$	60.7
Rotor loop 3 resistance	R_{r3}	$\mu\Omega$	54.9
Rotor Bar Inductance	L_b	μH	1.22
Rotor lower end ring segment inductance	L_e	μH	0.169
Rotor upper end ring segment inductance	L_{er}	μH	0.845
Rotor mutual inductance between the bar and loop 2	L_{12}	μH	2.95
Rotor mutual inductance between the bar and loop 3	L_{13}	μH	2.61

Stellenbosch University https://scholar.sun.ac.za

B.2 Full state machine paramaters

For a detailed breakdown on how the equivalent rotor bar matrices are calculated see [81]

$$R_s = \begin{bmatrix} 4.1 & 0 & 0 & 0 & 0 & 0 \\ 0 & 4.1 & 0 & 0 & 0 & 0 \\ 0 & 0 & 4.1 & 0 & 0 & 0 \\ 0 & 0 & 0 & 6.1 & 0 & 0 \\ 0 & 0 & 0 & 0 & 6.1 & 0 \\ 0 & 0 & 0 & 0 & 0 & 6.1 \end{bmatrix}$$

$$L_s = \begin{bmatrix} 1,503 & -0,627 & -0,627 & 0,000 & 0,000 & 0,000 \\ -0,627 & 1,503 & -0,627 & 0,000 & 0,000 & 0,000 \\ -0,627 & -0,627 & 1,503 & 0,000 & 0,000 & 0,000 \\ 0,000 & 0,000 & 0,000 & 1,602 & -0,633 & -0,633 \\ 0,000 & 0,000 & 0,000 & -0,633 & 1,602 & -0,633 \\ 0,000 & 0,000 & 0,000 & -0,633 & -0,633 & 1,602 \end{bmatrix}$$

$$R_{rr} = \begin{bmatrix} R_{r_{11}} & R_{r_{12}} & R_{r_{13}} \\ R_{r_{12}}^T & R_{r_{22}} & R_{r_{23}} \\ R_{r_{13}}^T & R_{r_{23}}^T & R_{r_{33}} \end{bmatrix}, L_{rr} = \begin{bmatrix} L_{r_{11}} & L_{r_{12}} & L_{r_{13}} \\ L_{r_{12}}^T & L_{r_{22}} & L_{r_{23}} \\ L_{r_{13}}^T & L_{r_{23}}^T & L_{r_{33}} \end{bmatrix}$$

$$R_{r_{11}} = \begin{bmatrix} 80.972 & -26.045 & 0.000 & 0.000 & -26.045 \\ -26.045 & 80.972 & -26.045 & 0.000 & 0.000 \\ 0.000 & -26.045 & 80.972 & -26.045 & 0.000 \\ 0.000 & 0.000 & -26.045 & 80.972 & -26.045 \\ -26.045 & 0.000 & 0.000 & -26.045 & 80.972 \end{bmatrix} \mu\Omega$$

$$R_{r_{22}} = \begin{bmatrix} 69.420 & 0.000 & 0.000 & 0.000 & 0.000 \\ 0.000 & 69.420 & 0.000 & 0.000 & 0.000 \\ 0.000 & 0.000 & 69.420 & 0.000 & 0.000 \\ 0.000 & 0.000 & 0.000 & 69.420 & 0.000 \\ 0.000 & 0.000 & 0.000 & 0.000 & 69.420 \end{bmatrix} \mu\Omega$$

$$R_{r_{33}} = \begin{bmatrix} 57.867 & 0.000 & 0.000 & 0.000 & 0.000 \\ 0.000 & 57.867 & 0.000 & 0.000 & 0.000 \\ 0.000 & 0.000 & 57.867 & 0.000 & 0.000 \\ 0.000 & 0.000 & 0.000 & 57.867 & 0.000 \\ 0.000 & 0.000 & 0.000 & 0.000 & 57.867 \end{bmatrix} \mu\Omega$$

Stellenbosch University https://scholar.sun.ac.za

$$R_{r_{12}} = \begin{bmatrix} 8.664 & 0.000 & 0.000 & 0.000 & 0.000 \\ 0.000 & 8.664 & 0.000 & 0.000 & 0.000 \\ 0.000 & 0.000 & 8.664 & 0.000 & 0.000 \\ 0.000 & 0.000 & 0.000 & 8.664 & 0.000 \\ 0.000 & 0.000 & 0.000 & 0.000 & 8.664 \end{bmatrix} \mu\Omega$$

$$R_{r_{13}} = \begin{bmatrix} 2.888 & 0.000 & 0.000 & 0.000 & 0.000 \\ 0.000 & 2.888 & 0.000 & 0.000 & 0.000 \\ 0.000 & 0.000 & 2.888 & 0.000 & 0.000 \\ 0.000 & 0.000 & 0.000 & 2.888 & 0.000 \\ 0.000 & 0.000 & 0.000 & 0.000 & 2.888 \end{bmatrix} \mu\Omega$$

$$R_{r_{23}} = \begin{bmatrix} 2.888 & 0.000 & 0.000 & 0.000 & 0.000 \\ 0.000 & 2.888 & 0.000 & 0.000 & 0.000 \\ 0.000 & 0.000 & 2.888 & 0.000 & 0.000 \\ 0.000 & 0.000 & 0.000 & 2.888 & 0.000 \\ 0.000 & 0.000 & 0.000 & 0.000 & 2.888 \end{bmatrix} \mu\Omega$$

$$L_{r_{11}} = \begin{bmatrix} 64.046 & -16.198 & -14.979 & -14.979 & -16.198 \\ -16.198 & 64.046 & -16.198 & -14.979 & -14.979 \\ -14.979 & -16.198 & 64.046 & -16.198 & -14.979 \\ -14.979 & -14.979 & -16.198 & 64.046 & -16.198 \\ -16.198 & -14.979 & -14.979 & -16.198 & 64.046 \end{bmatrix} \mu H$$

$$L_{r_{22}} = \begin{bmatrix} 42.998 & -5.393 & -5.393 & -5.393 & -5.393 \\ -5.393 & 42.998 & -5.393 & -5.393 & -5.393 \\ -5.393 & -5.393 & 42.998 & -5.393 & -5.393 \\ -5.393 & -5.393 & -5.393 & 42.998 & -5.393 \\ -5.393 & -5.393 & -5.393 & -5.393 & 42.998 \end{bmatrix} \mu H$$

$$L_{r_{33}} = \begin{bmatrix} 17.156 & -0.599 & -0.599 & -0.599 & -0.599 \\ -0.599 & 17.156 & -0.599 & -0.599 & -0.599 \\ -0.599 & -0.599 & 17.156 & -0.599 & -0.599 \\ -0.599 & -0.599 & -0.599 & 17.156 & -0.599 \\ -0.599 & -0.599 & -0.599 & -0.599 & 17.156 \end{bmatrix} \mu H$$

$$L_{r_{12}} = \begin{bmatrix} 36.458 & -8.988 & -8.988 & -8.988 & -8.988 \\ -8.988 & 36.458 & -8.988 & -8.988 & -8.988 \\ -8.988 & -8.988 & 36.458 & -8.988 & -8.988 \\ -8.988 & -8.988 & -8.988 & 36.458 & -8.988 \\ -8.988 & -8.988 & -8.988 & -8.988 & 36.458 \end{bmatrix} \mu H$$

$$L_{r_{13}} = \begin{bmatrix} 12.153 & -2.996 & -2.996 & -2.996 & -2.996 \\ -2.996 & 12.153 & -2.996 & -2.996 & -2.996 \\ -2.996 & -2.996 & 12.153 & -2.996 & -2.996 \\ -2.996 & -2.996 & -2.996 & 12.153 & -2.996 \\ -2.996 & -2.996 & -2.996 & -2.996 & 12.153 \end{bmatrix} \mu H$$

$$L_{r_{23}} = \begin{bmatrix} 13.351 & -1.798 & -1.798 & -1.798 & -1.798 \\ -1.798 & 13.351 & -1.798 & -1.798 & -1.798 \\ -1.798 & -1.798 & 13.351 & -1.798 & -1.798 \\ -1.798 & -1.798 & -1.798 & 13.351 & -1.798 \\ -1.798 & -1.798 & -1.798 & -1.798 & 13.351 \end{bmatrix} \mu H$$

Stellenbosch University https://scholar.sun.ac.za

Table B.2: BDFIM reduced model synchronous frame parameters

	Value		
	PW	***CW***	***Rotor***
Resistance(Ω)	4.1	6.1	112.5μ
Self Inductance(H)	2.1299	2.2355	117.56μ
Mutual Inductance(mH)	11.9	9	

Stellenbosch University https://scholar.sun.ac.za

B.3 Parameter Derivation

2021/11/07 7:10 PM C:\Users\taint\Google Drive (em... 1 of 8

```
clear all;sympref('FloatingPointOutput',true); digits(18)
%% Variables
syms B1 B2 phi thr t p1 p2
%% Assumptions
assumeAlso(thr, 'real'); assumeAlso(B1, 'real'); assumeAlso(B2, 'real'); assumeAlso
(phi, 'real'); assumeAlso(p1,'real');assumeAlso(p2,'real');
%% Machine Parameters
poles = {2 3};
S = p1+p2; S = subs(S,{p1 p2},poles);
N = 3;
%B1 = 0; B2 = 32*180/pi; phi = 0;

n = 1:S; %rotor nests
m = 1:3; %phases

Rs1 = (diag([4.1;4.1;4.1]));
Rs2 = (diag([6.1;6.1;6.1]));

Ls1 =  ([   1.5033   -0.6266   -0.6266;...
                  -0.6266    1.5033   -0.6266;...
                  -0.6266   -0.6266    1.5033]);
Ls2 =   ([      1.6022   -0.6333   -0.6333;...
                       -0.6333    1.6022   -0.6333;...
                       -0.6333   -0.6333    1.6022]);

Rss = ([Rs1,zeros(3,3);...
        zeros(3,3),Rs2]);
Mss = ([Ls1,zeros(3,3);...
        zeros(3,3),Ls2]);

M = sym('M%d%d',[2,3]); assumeAlso(M,'real');
% M =    ([   0.0049    0.0035    0.0013;...
%             0.0033    0.0031    0.0013]);

% % For simplified model (1 rotor loop)
% Rrr = 1.0e-04*[ 0.7982   -0.2604         0         0   -0.2604;...
%                -0.2604    0.7982   -0.2604         0         0;...
%                      0   -0.2604    0.7982   -0.2604         0;...
%                      0         0   -0.2604    0.7982   -0.2604;...
%                -0.2604         0         0   -0.2604    0.7982]
%
% Mrr = 1.0e-03*[  0.2444   -0.0508   -0.0495   -0.0495   -0.0508;...
%                -0.0508    0.2444   -0.0508   -0.0495   -0.0495;...
%                -0.0495   -0.0508    0.2444   -0.0508   -0.0495;...
%                -0.0495   -0.0495   -0.0508    0.2444   -0.0508;...
%                -0.0508   -0.0495   -0.0495   -0.0508    0.2444]

%% For expanded model (3 loops 5 nests)
Rrr = 1.0e-04*[ 0.8100   -0.2600         0         0   -0.2600    0.0866         0
0         0         0    0.0289         0         0         0         0
               -0.2600    0.8100   -0.2600         0         0         0    0.0866
0         0         0         0    0.0289         0         0         0
                     0   -0.2600    0.8100   -0.2600         0         0         0
```

Stellenbosch University https://scholar.sun.ac.za


```
0.0866         0         0         0         0    0.0289         0         0
                     0         0   -0.2600    0.8100   -0.2600         0         0
0    0.0866         0         0         0         0    0.0289         0
               -0.2600         0         0   -0.2600    0.8100         0         0
0         0    0.0866         0         0         0         0    0.0289
                0.0866         0         0         0         0    0.6940         0
0         0         0    0.0289         0         0         0         0
                     0    0.0866         0         0         0         0    0.6940
0         0         0         0    0.0289         0         0         0
                     0         0    0.0866         0         0         0         0
0.6940         0         0         0         0    0.0289         0         0
                     0         0         0    0.0866         0         0         0
0    0.6940         0         0         0         0    0.0289         0
                     0         0         0         0    0.0866         0         0
0         0    0.6940         0         0         0         0    0.0289
                0.0289         0         0         0         0    0.0289         0
0         0         0    0.5790         0         0         0         0
                     0    0.0289         0         0         0         0    0.0289
0         0         0         0    0.5790         0         0         0
                     0         0    0.0289         0         0         0         0
0.0289         0         0         0         0    0.5790         0         0
                     0         0         0    0.0289         0         0         0
0    0.0289         0         0         0         0    0.5790         0
                     0         0         0         0    0.0289         0         0
0         0    0.0289         0         0         0         0    0.5790]

Mrr = 1.0e-04*[ 0.6405   -0.1620   -0.1498   -0.1498   -0.1620    0.3646   -0.0899
-0.0899   -0.0899   -0.0899    0.1220   -0.0300   -0.0300   -0.0300   -0.0300
               -0.1620    0.6405   -0.1620   -0.1498   -0.1498   -0.0899    0.3646
-0.0899   -0.0899   -0.0899   -0.0300    0.1220   -0.0300   -0.0300   -0.0300
               -0.1498   -0.1620    0.6405   -0.1620   -0.1498   -0.0899   -0.0899
0.3646   -0.0899   -0.0899   -0.0300   -0.0300    0.1220   -0.0300   -0.0300
               -0.1498   -0.1498   -0.1620    0.6405   -0.1620   -0.0899   -0.0899
-0.0899    0.3646   -0.0899   -0.0300   -0.0300   -0.0300    0.1220   -0.0300
               -0.1620   -0.1498   -0.1498   -0.1620    0.6405   -0.0899   -0.0899
-0.0899   -0.0899    0.3646   -0.0300   -0.0300   -0.0300   -0.0300    0.1220
                0.3650   -0.0899   -0.0899   -0.0899   -0.0899    0.4300   -0.0539
-0.0539   -0.0539   -0.0539    0.1340   -0.0180   -0.0180   -0.0180   -0.0180
               -0.0899    0.3650   -0.0899   -0.0899   -0.0899   -0.0539    0.4300
-0.0539   -0.0539   -0.0539   -0.0180    0.1340   -0.0180   -0.0180   -0.0180
               -0.0899   -0.0899    0.3650   -0.0899   -0.0899   -0.0539   -0.0539
0.4300   -0.0539   -0.0539   -0.0180   -0.0180    0.1340   -0.0180   -0.0180
               -0.0899   -0.0899   -0.0899    0.3650   -0.0899   -0.0539   -0.0539
-0.0539    0.4300   -0.0539   -0.0180   -0.0180   -0.0180    0.1340   -0.0180
               -0.0899   -0.0899   -0.0899   -0.0899    0.3650   -0.0539   -0.0539
-0.0539   -0.0539    0.4300   -0.0180   -0.0180   -0.0180   -0.0180    0.1340
                0.1220   -0.0300   -0.0300   -0.0300   -0.0300    0.1340   -0.0180
-0.0180   -0.0180   -0.0180    0.1716   -0.0060   -0.0060   -0.0060   -0.0060
               -0.0300    0.1220   -0.0300   -0.0300   -0.0300   -0.0180    0.1340
-0.0180   -0.0180   -0.0180   -0.0060    0.1716   -0.0060   -0.0060   -0.0060
               -0.0300   -0.0300    0.1220   -0.0300   -0.0300   -0.0180   -0.0180
0.1340   -0.0180   -0.0180   -0.0060   -0.0060    0.1716   -0.0060   -0.0060
               -0.0300   -0.0300   -0.0300    0.1220   -0.0300   -0.0180   -0.0180
```

Stellenbosch University https://scholar.sun.ac.za


```
-0.0180    0.1340   -0.0180   -0.0060   -0.0060   -0.0060    0.1716   -0.0060
              -0.0300   -0.0300   -0.0300   -0.0300    0.1220   -0.0180   -0.0180
-0.0180   -0.0180    0.1340   -0.0060   -0.0060   -0.0060   -0.0060    0.1716];
Msr = [];
for k = 1:size(m,2)
    Msr = [Msr, [M(1,k)*cos(p1*(thr-(n(:)-1)*2*pi/S-B1))';...
                 M(1,k)*cos(p1*(thr-(n(:)-1)*2*pi/S-B1-2*pi/(3*p1)))';...
                 M(1,k)*cos(p1*(thr-(n(:)-1)*2*pi/S-B1-4*pi/(3*p1)))';...
                 M(2,k)*cos(p2*(thr-(n(:)-1)*2*pi/S-B2))';...
                 M(2,k)*cos(p2*(thr-(n(:)-1)*2*pi/S-B2-2*pi/(3*p2)))';...
                 M(2,k)*cos(p2*(thr-(n(:)-1)*2*pi/S-B2-4*pi/(3*p2)))']];
end
Msr
%% Rotor plane transformation matrix's
Cs1 = [];
for i = 1:3
    tmp1 = [cos(p1*(thr-(i-1)*2*pi/(3*p1)))];
    tmp1 = [tmp1;sin(p1*(thr-(i-1)*2*pi/(3*p1)))];
    tmp1 = [tmp1;1/sqrt(2)];
    Cs1 = [Cs1,tmp1];
end
Cs1 = sqrt(2/3)*Cs1;

Cs2 = [];
for i = 1:3
    tmp1 = [cos(p2*(thr-(i-1)*2*pi/(3*p2)))];
    tmp1 = [tmp1;sin(p2*(thr-(i-1)*2*pi/(3*p2)))];
    tmp1 = [tmp1;1/sqrt(2)];
    Cs2 = [Cs2,tmp1];
end
Cs2 = sqrt(2/3)*Cs2;

Cr1 = [];
for i = 1:S
    tmp1 = [cos(2*pi*(i-1)*p1/(p1+p2))];
    tmp1 = [tmp1;sin(2*pi*(i-1)*p1/(p1+p2))];
    tmp1 = [tmp1;1/sqrt(2)];
    Cr1 = [Cr1,tmp1];
end
Cr1 = sqrt(2/(p1+p2))*Cr1;

% Subsitute p1 and p2 with actual pole numbers,
% don't do this for Cs1 and Cs2 as they are already inversable (so simple)
% clear thr; syms thr
% Cs1 = simplify(subs(Cs1, int(wr(t), t), thr))
% Cs2 = simplify(subs(Cs2, int(wr(t), t), thr))
Cs1 = simplify(Cs1); Cs2 = simplify(Cs2);
Cr1 = (double(simplify(subs(Cr1,{p1 p2}, poles))));


Crorth = null(Cr1)';
Cr_temp = [Cr1;Crorth];
```

Stellenbosch University https://scholar.sun.ac.za


```
order = size(Cr_temp);

Cr = (  [Cr_temp,zeros(order),zeros(order);...
                zeros(order),Cr_temp,zeros(order);...
                zeros(order),zeros(order),Cr_temp]);
Cs = [Cs1,zeros(3,3);...
      zeros(3,3),Cs2]
C = [Cs1,zeros(3,3),zeros(3,15);...
     zeros(3,3),Cs2,zeros(3,15);...
     zeros(15,3),zeros(15,3),Cr];

Cr = double(Cr); Mss = double(Mss);

% Resistance matrices in rotor reference frame
Rsdqr = simplify(Cs*Rss*Cs')
Rrdqr = Cr*Rrr*Cr' %(This may be slightly incorrect, we expect a multiple of an↙
identity matrix here)
% Inductance matrices in rotor reference frame
Msdqr = simplify(Cs*Mss*Cs')
Mrdqr = Cr*Mrr*Cr'
% Mutual inductance matrices in rotor reference frame
Msrdqr = simplify(simplify(Cs*Msr)*Cr')
Msrdqr_transp = simplify(simplify(Cr*Msr')*Cs')
%-------------------------------------------------------------------------
clear thr; syms wr(t);
thr(t) = int(wr(t),t); assumeAlso(wr(t),'real'); assumeAlso(thr(t),'real');
Cs = subs(Cs,sym('thr'),thr); Msr = subs(Msr,sym('thr'),thr);

% Derivative Inductance matrices in rotor reference frame
dMsdqr = simplify(simplify(Cs*Mss)*diff(Cs'))/wr;
Qsdqr = dMsdqr

dMrdqr = diff(Cr*Mrr*Cr',t);
Qrdqr = dMrdqr
% Derivative mutual inductance matrices in rotor reference frame
dMsrdqr = simplify(simplify(Cs*diff(Msr))*Cr')/wr;
Qsrdqr  = dMsrdqr
dMsrdqr_transp = simplify(Cr*simplify(diff(Msr'*Cs')/wr));
Qsrdqr_transp = dMsrdqr_transp

%% Equivalent matrices in rotor reference frame after removing unobservable parts
% Resistance matrices in rotor reference frame
Rrdqr = [Rrdqr([1:3,6:8,11:13,4:5,9:10,14:15],:)];  %rearrange rows
Rrdqr = [Rrdqr(:,[1:3,6:8,11:13,4:5,9:10,14:15])];  %rearrange columns
Rrdqr_obs = Rrdqr(1:9,1:9)
Rrdqr_unobs = Rrdqr(10:size(Rrdqr,1),10:size(Rrdqr,2)); %Remove unobservable↙
components
% Inductance matrices in rotor reference frame
Mrdqr = [Mrdqr([1:3,6:8,11:13,4:5,9:10,14:15],:)];  %rearrange rows
Mrdqr = [Mrdqr(:,[1:3,6:8,11:13,4:5,9:10,14:15])];  %rearrange columns
Mrdqr_obs = Mrdqr(1:9,1:9)
Mrdqr_unobs = Mrdqr(10:size(Mrdqr,1),10:size(Mrdqr,2)); %Remove unobservable↙
components
```

Stellenbosch University https://scholar.sun.ac.za


```
% Mutual inductance matrices in rotor reference frame
Msrdqr = [Msrdqr(:,[1:3,6:8,11:13,4:5,9:10,14:15])]; %rearrange columns
Msrdqr_obs = Msrdqr(:,1:9)
Msrdqr_unobs = Msrdqr(:,10:size(Msrdqr,2)); %Remove unobservable components

Msrdqr_transp = [Msrdqr_transp([1:3,6:8,11:13,4:5,9:10,14:15],:)]; %rearrange↙
columns
Msrdqr_transp_obs = Msrdqr_transp(1:9,:)
Msrdqr_transp_unobs = Msrdqr_transp(10:size(Msrdqr_transp,2),:); %Remove↙
unobservable components
% Derivative mutual inductance matrices in rotor reference frame
Qsrdqr = formula(Qsrdqr);
Qsrdqr = [Qsrdqr(:,[1:3,6:8,11:13,4:5,9:10,14:15])]; %rearrange columns
Qsrdqr_obs = Qsrdqr(:,1:9)
Qsrdqr_unobs = Qsrdqr(:,10:size(Qsrdqr,2)); %Remove unobservable components

Qsrdqr_transp = formula(Qsrdqr_transp);
Qsrdqr_transp = [Qsrdqr_transp([1:3,6:8,11:13,4:5,9:10,14:15],:)]; %rearrange↙
columns
Qsrdqr_transp_obs = Qsrdqr_transp(1:9,:)
Qsrdqr_transp_unobs = Qsrdqr_transp(10:size(Qsrdqr_transp,2),:); %Remove↙
unobservable components

Qrdqr = [Qrdqr([1:3,6:8,11:13,4:5,9:10,14:15],:)];
Qrdqr = [Qrdqr(:,[1:3,6:8,11:13,4:5,9:10,14:15])];
Qrdqr_obs = Qrdqr(1:9,1:9)
Qrdqr_unobs = Qrdqr(10:size(Qrdqr,1),10:size(Qrdqr,2)); %Remove unobservable↙
components
% Final Matrices
Qdqr = [Qsdqr,Qsrdqr;...
       Qsrdqr_transp,Qrdqr]
Mdqr = [Msdqr,Msrdqr;...
     Msrdqr_transp,Mrdqr]

Qdqr_obs = [Qsdqr,Qsrdqr_obs;...
           Qsrdqr_transp_obs,Qrdqr_obs]
Mdqr_obs = [Msdqr,Msrdqr_obs;...
     Msrdqr_transp_obs,Mrdqr_obs]
Rdqr_obs = [Rsdqr,zeros(6,size(Rrdqr_obs,2));...
           zeros(6,size(Rrdqr_obs,2))',Rrdqr_obs]
%Convert to formula equivalent
Qdqr = formula(Qdqr); Mdqr = formula(Mdqr); Qdqr_obs = formula(Qdqr_obs); Mdqr_obs↙
= formula(Mdqr_obs); Rdqr_obs = formula(Rdqr_obs);
Qsdqr = formula(Qsdqr);
% size(Qdqr), size(Mdqr), size(Qdqr_obs), size(Mdqr_obs), size(Rdqr_obs)

%% New BDFM Rotor State Reduction Technique
% First remove 0 vectors
Rrdqr_eq = Rrdqr_obs(1:9,:);
Rrdqr_eq = Rrdqr_eq(:,1:9)

Mrdqr_eq = Mrdqr_obs(1:9,:); %Reduce Mrr to just dq order
Mrdqr_eq = Mrdqr_eq(:,1:9) %Reduce Mrr to just dq order
```

Stellenbosch University https://scholar.sun.ac.za


```
Qrdqr_eq = Qrdqr_obs(1:9,:); %Reduce Mrr to just dq order
Qrdqr_eq = Qrdqr_eq(:,1:9) %Reduce Mrr to just dq order

Msrdqr_eq = Msrdqr_obs(1:6,:);
Msrdqr_eq = Msrdqr_eq(:,1:9)
Qsrdqr_eq = Qsrdqr_obs(1:6,:);
Qsrdqr_eq = Qsrdqr_eq(:,1:9)

Msrdqr_transp_eq = Msrdqr_transp_obs(1:9,:);
Msrdqr_transp_eq = Msrdqr_transp_eq(:,1:6)
Qsrdqr_transp_eq = Qsrdqr_transp_obs(1:9,:);
Qsrdqr_transp_eq = Qsrdqr_transp_eq(:,1:6)
% Calculate eigen values and vectors in decending order of Mrdqr_eq
[u,v] = eig(double(Mrdqr_eq))
T1 = [      0.7954   -0.0000   -0.0000    0.5693   -0.0000   -0.0000    0.2080 ↙
-0.0000   -0.0000
           -0.0000   -0.7954   -0.0000   -0.0000   -0.5693   -0.0000   -0.0000 ↙
-0.2080    0.0000
           -0.0001    0.0000   -0.0227    0.0001   -0.0000   -0.8584    0.0001 ↙
-0.0000   -0.5124] %By inspection of u with v sorted descending left to right

% The simplified equivalent model parameters in the rotor reference frame are:
Rsdqr_eq = Rsdqr(1:6,1:6)
Msdqr_eq = Msdqr(1:6,1:6)
Qsdqr_eq = Qsdqr(1:6,1:6)

Msrdqr_eq = eye(6)*Msrdqr_eq*T1';
Msrdqr_eq = collect(simplify(Msrdqr_eq),{'sin' 'cos'})
Qsrdqr_eq = eye(6)*Qsrdqr_eq*T1';
Qsrdqr_eq = collect(simplify(Qsrdqr_eq),{'sin' 'cos'})
Msrdqr_transp_eq = T1*Msrdqr_transp_eq*eye(6)';
Msrtrtransp_eq = collect(simplify(Msrdqr_transp_eq),{'sin' 'cos'})
Qsrdqr_transp_eq = T1*Qsrdqr_transp_eq*eye(6)';
Qsrtrtransp_eq = collect(simplify(Qsrdqr_transp_eq),{'sin' 'cos'})
Mrdqr_eq = T1*Mrdqr_eq*T1'
Qrdqr_eq = T1*Qrdqr_eq*T1'
Rrdqr_eq = T1*Rrdqr_eq*T1'

% Final simplified matrices
Rsrdqr_eq = zeros(size(Msrdqr_eq))
Rsrtrtransp_eq = zeros(size(Msrtrtransp_eq))
Qdqr_eq = [Qsdqr_eq,Qsrdqr_eq;...
       Qsrdqr_transp_eq,Qrdqr_eq]
Mdqr_eq = [Msdqr_eq,Msrdqr_eq;...
     Msrtrtransp_eq,Mrdqr_eq]
Rdqr_eq = [Rsdqr_eq,Rsrdqr_eq;...
     Rsrtrtransp_eq,Rrdqr_eq]

%% Primary Stator reference frame equivalent
syms w1 w2 % p1 p2% phi1 phi2
assumeAlso(w1,'real'); assumeAlso(w2,'real'); assumeAlso(t,'real');
phi1 = B1*p1; phi2 = -B2*p2 %Choose opposite direction to earlier definition
Tsync1 = [cos(p1*thr-w1*t+phi1), sin(p1*thr-w1*t+phi1), 0;...
```

Stellenbosch University https://scholar.sun.ac.za


```
         -sin(p1*thr-w1*t+phi1), cos(p1*thr-w1*t+phi1), 0;...
                                0,                     0, 1];

Tsync2 = [cos(p1*thr-w1*t+phi2),-sin(p1*thr-w1*t+phi2), 0;...
          sin(p1*thr-w1*t+phi2), cos(p1*thr-w1*t+phi2), 0;...
                                0,                     0, 1];

Tsyncr = [cos(p1*thr-w1*t), sin(p1*thr-w1*t), 0;...
         -sin(p1*thr-w1*t), cos(p1*thr-w1*t), 0;...
                                0,                     0, 1];
% Tsync2 = simplify(inv(subs(Tsync1,phi1,phi2))); %or Tsync1'
% Tsyncr = subs(Tsync1,phi1,0);

Tsync = formula([Tsync1,Tsync2,repmat(Tsyncr,1,1)]);

temp  = []
k = 0
for i = 1:3:size(Tsync,2)
    temp = [temp;zeros(3,i-1),Tsync(:,i:i+2),zeros(3,size(Tsync,2)-i-2)];
    size(temp);
end
Tsync = simplify(temp)
% Tsync = Tsync(1:end-1,1:end-1)
dTsync = simplify(diff(inv(Tsync),t))

Rsync = simplify(Tsync*Rdqr_eq*inv(Tsync)) % Re-organise this

Msr_sync = collect(simplify(Tsync(1:6,1:6)*Mdqr_eq(1:6,7:end)*Tsync(7:end,7:end)'), ↙
{'sin' 'cos'})
Msync = collect(simplify(Tsync*Mdqr_eq*inv(Tsync)),{'sin' 'cos'})
Qsync = simplify(wr*Tsync*Qdqr_eq*inv(Tsync)+Tsync*Mdqr_eq*diff(inv(Tsync),t)) %↙
verify this
Qdqsr1_eq = Qdqr_eq(1:3,7:end)
Qdqsr2_eq = Qdqr_eq(4:6,7:end)
Ssync = simplify(Tsync*[zeros(size(Qdqsr1_eq,1)),zeros(size(Qdqsr2_eq,1)), ↙
Qdqsr1_eq;...
                        zeros(size(Qdqsr1_eq',2)),zeros(size(Qdqsr2_eq',2)), ↙
Qdqsr2_eq;...
                        Qdqsr1_eq',Qdqsr2_eq', zeros(size(Qdqsr1_eq,2))]*inv ↙
(Tsync))

% Subsitude values
Msr_sync = subs(Msr_sync,{p1 p2 B1},{2 3 0})
Msync = simplify(subs(Msync,{p1 p2 B1},{2 3 0}))
Qsync = formula(simplify(subs(Qsync,{p1 p2 B1},{2 3 0})))
Ssync = simplify(subs(Ssync,{p1 p2 B1},{2 3 0}))

% Controlled test / confirmation of above result
% Qsync_confirm = formula(simplify(subs(subs(diag([1,2,0,0,0]),{1,2},{p1*wr*[0,1,0; ↙
-1,0,0;0,0,0],p2*wr*[0,1,0;-1,0,0;0,0,0]})*Tsync*Mdqr_obs*inv(Tsync)+(-p1*wr+w1) ↙
*Tsync*Mdqr_obs*inv(Tsync)*subs(diag([1,2,1,1,1]),{1,2},{[0,1,0;-1,0,0;0,0,0],[0, ↙
-1,0;1,0,0;0,0,0]}),{p1 p2 B1},{2 3 0})));
%Ssync_confirm = formula(simplify(subs(subs(subs(diag([1,2,0,0,0]),{1,2},{p1* ↙
```

Stellenbosch University https://scholar.sun.ac.za


```
[0,1,0;-1,0,0;0,0,0],p2*[0,1,0;-1,0,0;0,0,0]}))*Tsync*Mdqr_obs*inv(Tsync) ↙
+Tsync*Mdqr_obs*inv(Tsync)*subs(diag([1,2,0,0,0]),{1,2},{p1*[0,-1,0;1,0,0;0,0,0], ↙
p2*[0,-1,0;1,0,0;0,0,0]}),{p1 p2 B1},{2 3 0}))))
```

Stellenbosch University https://scholar.sun.ac.za

B.4 Model overview

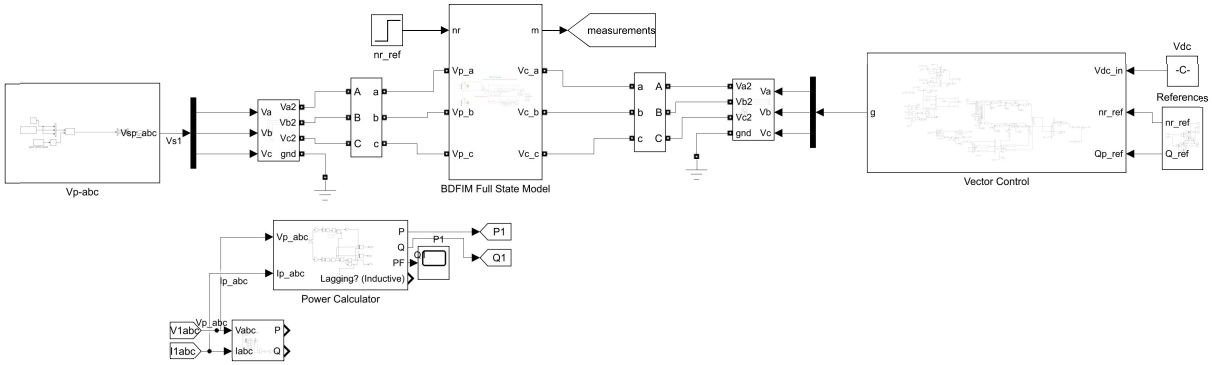

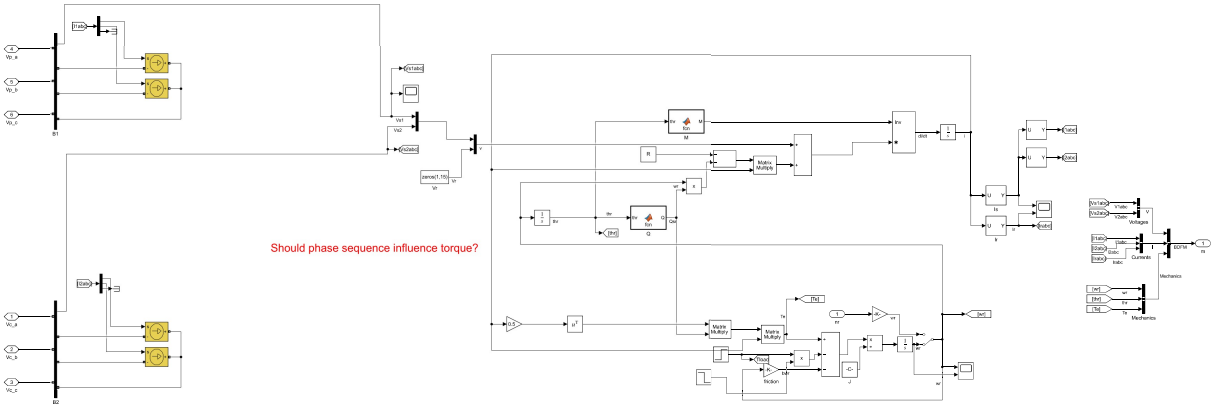

B.5 Vector control

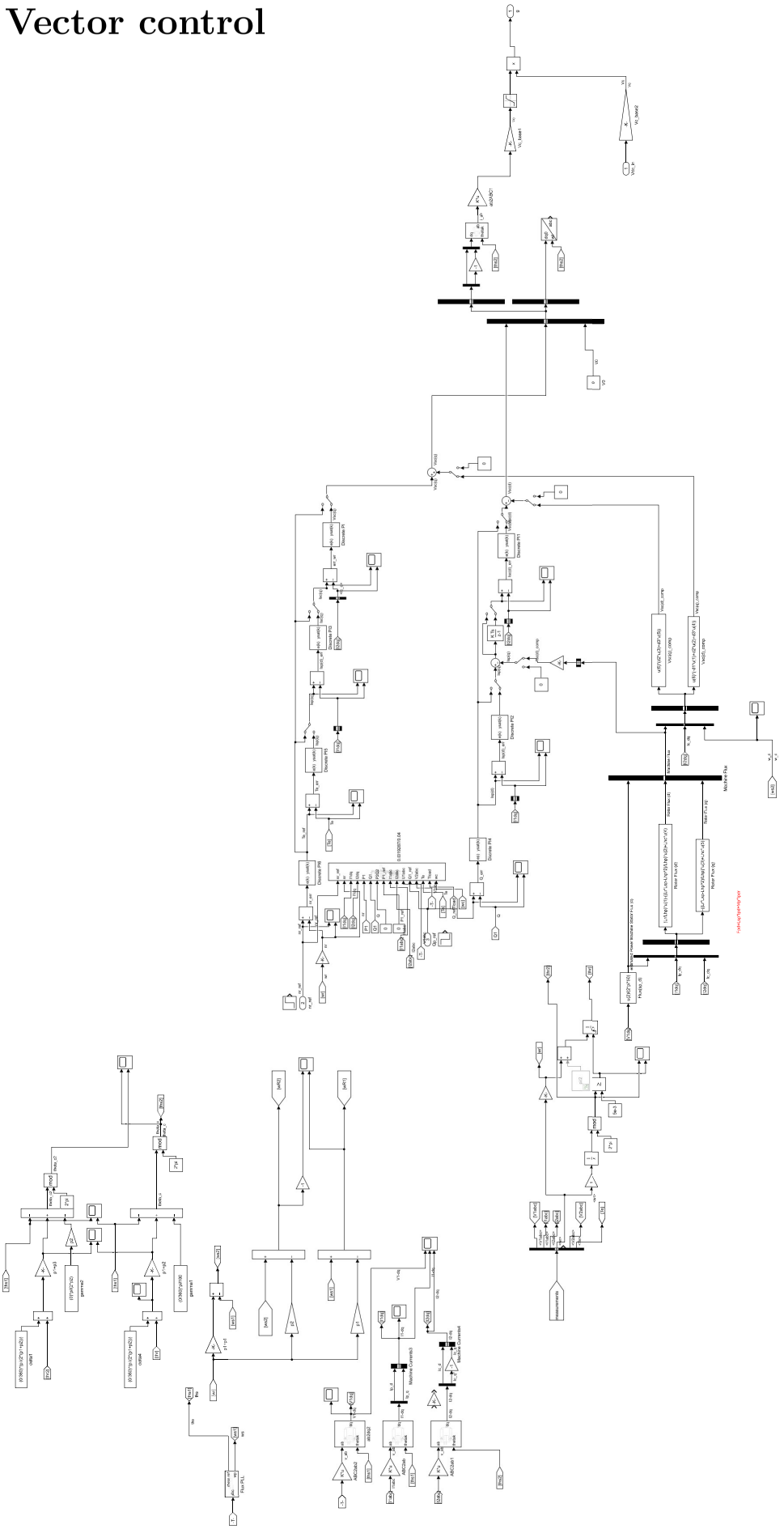

Stellenbosch University https://scholar.sun.ac.za

Stellenbosch University https://scholar.sun.ac.za

B.6 Mutual Inductance calculation

```
function M = fcn(thr)
M =[[                          1.5033,                         -0.6266,                         -0.6266,                               0,
[                         -0.6266,                          1.5033,                         -0.6266,                               0,
[                         -0.6266,                         -0.6266,                          1.5033,                               0,
[                               0,                               0,                               0,                          1.6022,                         -0
[                               0,                               0,                               0,                         -0.6333,                          1
[                               0,                               0,                               0,                         -0.6333,                         -0
[           0.0049*cos(2*thr),  0.0049*cos(2*thr - 2.0944),  0.0049*cos(2*thr - 4.1888),           0.0033*cos(3*thr),  0.0033*cos(3*thr - 2.
[  0.0049*cos(2*thr - 2.5133),  0.0049*cos(2*thr - 4.6077),  0.0049*cos(2*thr - 6.7021),  0.0033*cos(3*thr - 3.7699),  0.0033*cos(3*thr - 5.
[  0.0049*cos(2*thr - 5.0265),  0.0049*cos(2*thr - 7.1209),  0.0049*cos(2*thr - 9.2153),  0.0033*cos(3*thr - 7.5398),  0.0033*cos(3*thr - 9.
[  0.0049*cos(2*thr - 7.5398),  0.0049*cos(2*thr - 9.6342), 0.0049*cos(2*thr - 11.7286), 0.0033*cos(3*thr - 11.3097), 0.0033*cos(3*thr - 13.
[ 0.0049*cos(2*thr - 10.0531), 0.0049*cos(2*thr - 12.1475), 0.0049*cos(2*thr - 14.2419), 0.0033*cos(3*thr - 15.0796), 0.0033*cos(3*thr - 17.
[           0.0035*cos(2*thr),  0.0035*cos(2*thr - 2.0944),  0.0035*cos(2*thr - 4.1888),           0.0031*cos(3*thr),  0.0031*cos(3*thr - 2.
[  0.0035*cos(2*thr - 2.5133),  0.0035*cos(2*thr - 4.6077),  0.0035*cos(2*thr - 6.7021),  0.0031*cos(3*thr - 3.7699),  0.0031*cos(3*thr - 5.
[  0.0035*cos(2*thr - 5.0265),  0.0035*cos(2*thr - 7.1209),  0.0035*cos(2*thr - 9.2153),  0.0031*cos(3*thr - 7.5398),  0.0031*cos(3*thr - 9.
[  0.0035*cos(2*thr - 7.5398),  0.0035*cos(2*thr - 9.6342), 0.0035*cos(2*thr - 11.7286), 0.0031*cos(3*thr - 11.3097), 0.0031*cos(3*thr - 13.
[ 0.0035*cos(2*thr - 10.0531), 0.0035*cos(2*thr - 12.1475), 0.0035*cos(2*thr - 14.2419), 0.0031*cos(3*thr - 15.0796), 0.0031*cos(3*thr - 17.
[           0.0013*cos(2*thr),  0.0013*cos(2*thr - 2.0944),  0.0013*cos(2*thr - 4.1888),           0.0013*cos(3*thr),  0.0013*cos(3*thr - 2.
[  0.0013*cos(2*thr - 2.5133),  0.0013*cos(2*thr - 4.6077),  0.0013*cos(2*thr - 6.7021),  0.0013*cos(3*thr - 3.7699),  0.0013*cos(3*thr - 5.
[  0.0013*cos(2*thr - 5.0265),  0.0013*cos(2*thr - 7.1209),  0.0013*cos(2*thr - 9.2153),  0.0013*cos(3*thr - 7.5398),  0.0013*cos(3*thr - 9.
[  0.0013*cos(2*thr - 7.5398),  0.0013*cos(2*thr - 9.6342), 0.0013*cos(2*thr - 11.7286), 0.0013*cos(3*thr - 11.3097), 0.0013*cos(3*thr - 13.
[ 0.0013*cos(2*thr - 10.0531), 0.0013*cos(2*thr - 12.1475), 0.0013*cos(2*thr - 14.2419), 0.0013*cos(3*thr - 15.0796), 0.0013*cos(3*thr - 17.
```

```
function Q = fcn(thr)
Q =[[                          0,                               0,                               0,                               0,
[                         0,                               0,                               0,                               0,
[                         0,                               0,                               0,                               0,
[                         0,                               0,                               0,                               0,
[                         0,                               0,                               0,                               0,
[                         0,                               0,                               0,                               0,
[          -0.0098*sin(2*thr),  0.0098*sin(2*thr + 1.0472), -0.0098*cos(2*thr + 0.5236),          -0.0099*sin(3*thr),  0.0099*sin(3*thr + 1.
[  0.0098*sin(2*thr + 0.6283), -0.0098*cos(2*thr + 0.1047),  0.0098*cos(2*thr + 1.1519), -0.0099*sin(3*thr - 3.7699), -0.0099*sin(3*thr + 0.
[ -0.0098*sin(2*thr + 1.2566),  0.0098*cos(2*thr + 0.7330),  0.0098*sin(2*thr + 0.2094),  0.0099*cos(3*thr + 0.3142), -0.0099*cos(3*thr + 1.
[  0.0098*cos(2*thr + 0.3142), -0.0098*cos(2*thr + 1.3614), -0.0098*sin(2*thr + 0.8378), -0.0099*sin(3*thr + 1.2566),  0.0099*cos(3*thr + 0.
[ -0.0098*cos(2*thr + 0.9425), -0.0098*sin(2*thr + 0.4189),  0.0098*sin(2*thr + 1.4661),  0.0099*sin(3*thr + 0.6283), -0.0099*cos(3*thr + 0.
[          -0.0070*sin(2*thr),  0.0070*sin(2*thr + 1.0472), -0.0070*cos(2*thr + 0.5236),          -0.0093*sin(3*thr),  0.0093*sin(3*thr + 1.
[  0.0070*sin(2*thr + 0.6283), -0.0070*cos(2*thr + 0.1047),  0.0070*cos(2*thr + 1.1519), -0.0093*sin(3*thr - 3.7699), -0.0093*sin(3*thr + 0.
[ -0.0070*sin(2*thr + 1.2566),  0.0070*cos(2*thr + 0.7330),  0.0070*sin(2*thr + 0.2094),  0.0093*cos(3*thr + 0.3142), -0.0093*cos(3*thr + 1.
[  0.0070*cos(2*thr + 0.3142), -0.0070*cos(2*thr + 1.3614), -0.0070*sin(2*thr + 0.8378), -0.0093*sin(3*thr + 1.2566),  0.0093*cos(3*thr + 0.
[ -0.0070*cos(2*thr + 0.9425), -0.0070*sin(2*thr + 0.4189),  0.0070*sin(2*thr + 1.4661),  0.0093*sin(3*thr + 0.6283), -0.0093*cos(3*thr + 0.
[          -0.0026*sin(2*thr),  0.0026*sin(2*thr + 1.0472), -0.0026*cos(2*thr + 0.5236),          -0.0039*sin(3*thr),  0.0039*sin(3*thr + 1.
[  0.0026*sin(2*thr + 0.6283), -0.0026*cos(2*thr + 0.1047),  0.0026*cos(2*thr + 1.1519), -0.0039*sin(3*thr - 3.7699), -0.0039*sin(3*thr + 0.
[ -0.0026*sin(2*thr + 1.2566),  0.0026*cos(2*thr + 0.7330),  0.0026*sin(2*thr + 0.2094),  0.0039*cos(3*thr + 0.3142), -0.0039*cos(3*thr + 1.
[  0.0026*cos(2*thr + 0.3142), -0.0026*cos(2*thr + 1.3614), -0.0026*sin(2*thr + 0.8378), -0.0039*sin(3*thr + 1.2566),  0.0039*cos(3*thr + 0.
[ -0.0026*cos(2*thr + 0.9425), -0.0026*sin(2*thr + 0.4189),  0.0026*sin(2*thr + 1.4661),  0.0039*sin(3*thr + 0.6283), -0.0039*cos(3*thr + 0.
```

B.7 Labview Control Panel

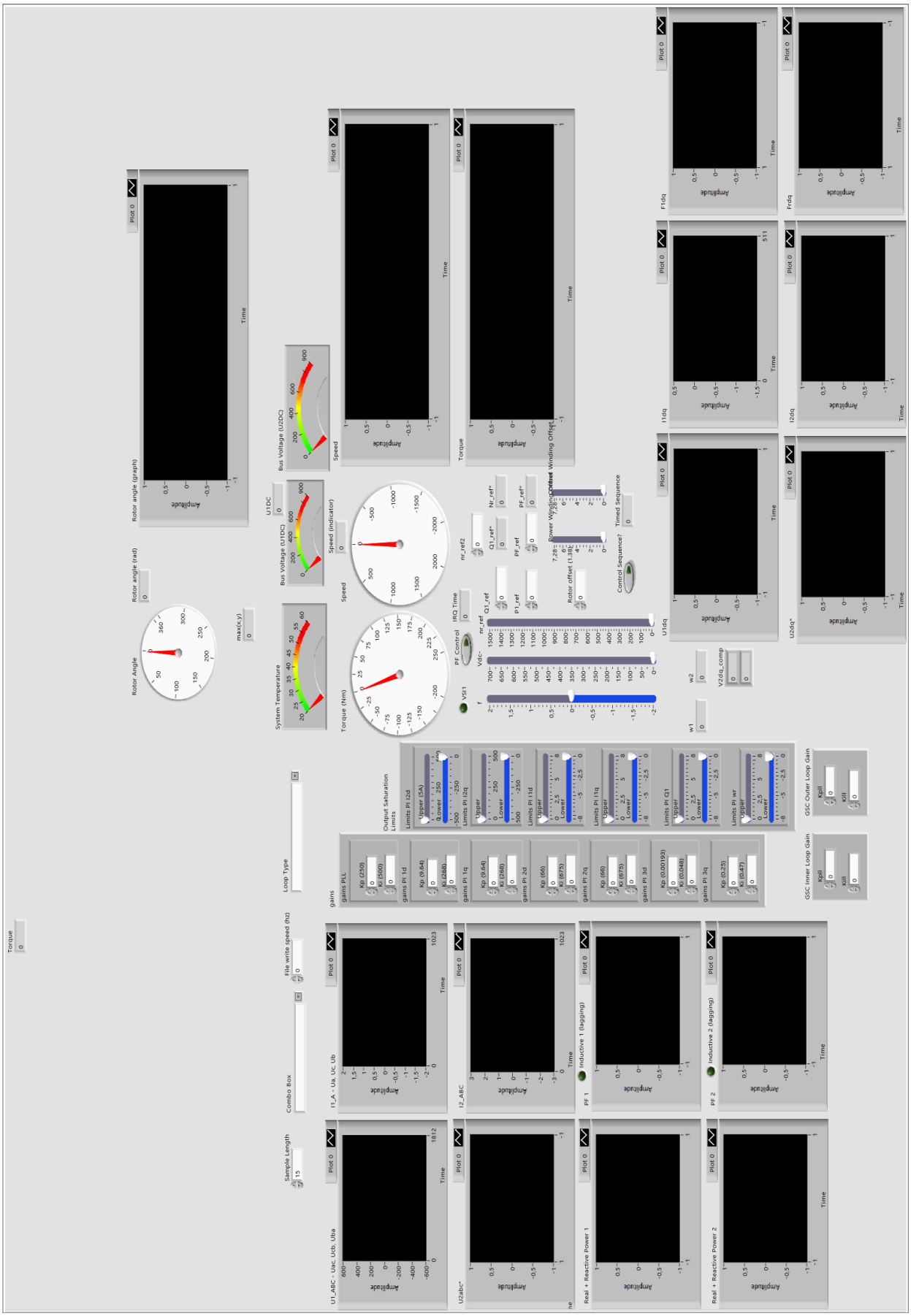

Stellenbosch University https://scholar.sun.ac.za

Stellenbosch University https://scholar.sun.ac.za

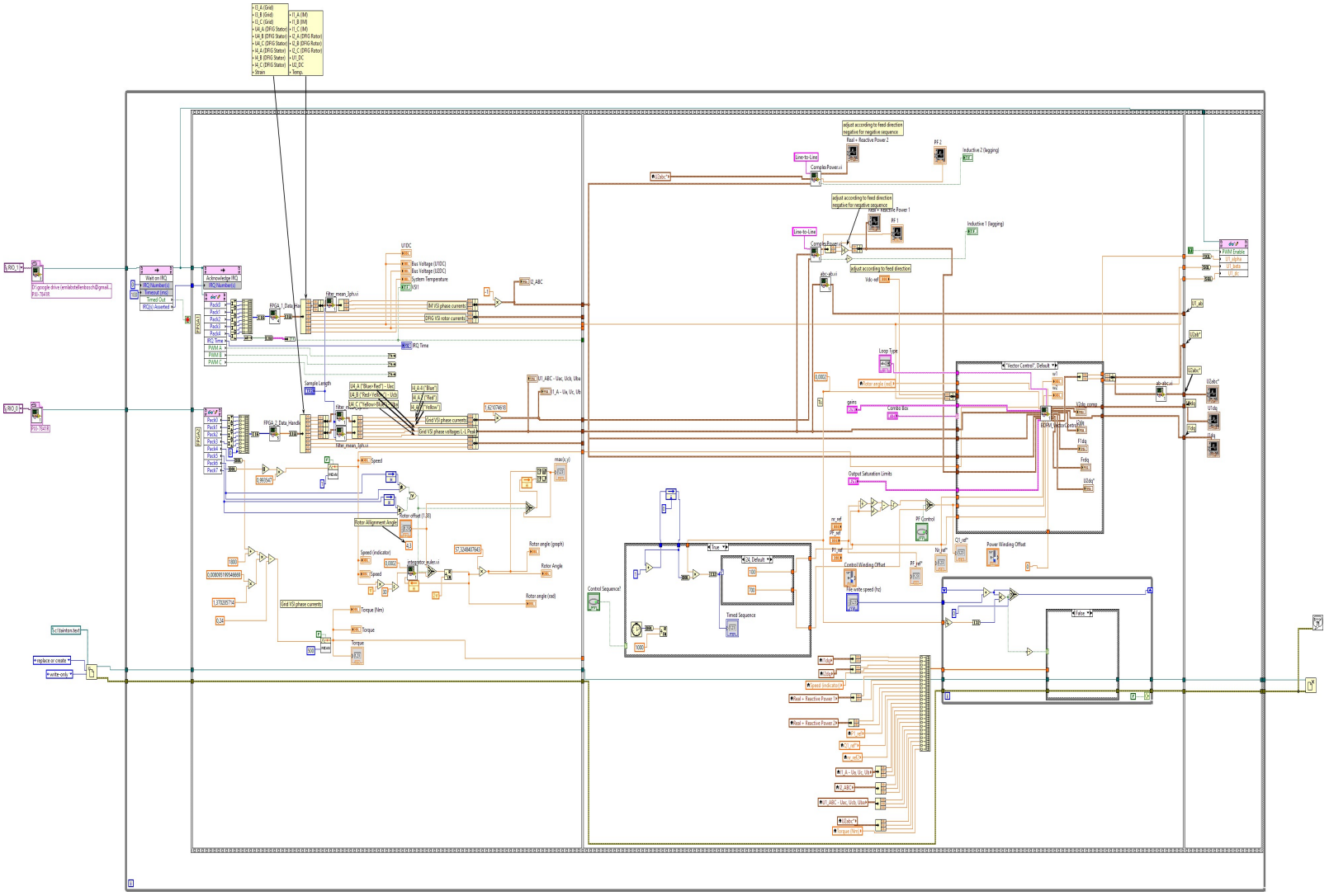

Stellenbosch University https://scholar.sun.ac.za

B.8 Labview Vector Controller